International Pacific Research Center

APRIL 2007–MARCH 2008 REPORT

School of Ocean and Earth Science and Technology
University of Hawai'i at Mānoa

CONTENTS

Editor: Gisela E. Speidel, PhD
Consulting Editor: Zuojun Yu, PhD
Japanese Translator: Keiko Tokinaga

Design: Susan Yamamoto
Printer: Hagadone Printing Company

RECYCLED PAPER ECO-FRIENDLY INKS PrintGreen

THE INTERNATIONAL PACIFIC RESEARCH CENTER

The International Pacific Research Center (IPRC) at the University of Hawai‘i conducts climate research with a focus on the Asia-Pacific region. Conceived under the “U.S.–Japan Common Agenda for Cooperation in Global Perspective,” the center was established in October 1997 at the Mānoa Campus of the University of Hawai‘i. The center’s mission is “to provide an international, state-of-the-art research environment to improve understanding of the nature and predictability of climate variability in the Asia-Pacific sector, including regional aspects of global environmental change.” The international group of scientists at the IPRC is guided by the following broad research themes and goals of the IPRC Science Plan.

Indo-Pacific Ocean Climate: To understand climate variations in the Pacific and Indian oceans on interannual-to-interdecadal timescales.

Regional Ocean Influences: To determine the influences on Asia-Pacific climate of western-boundary currents, the Kuroshio-Oyashio Extension system, marginal seas, and the Indonesian Throughflow.

Asian-Australian Monsoon System: To understand the processes responsible for climatic variability and predictability of the Asian-Australian monsoon system and its hydrological cycle at intraseasonal through interdecadal timescales.

Impacts of Global Environmental Change: To identify the relationships between global environmental change and Asia-Pacific climate.

The Asia-Pacific Data-Research Center (APDRC): To provide the international research community with easy access to climate data.

The IPRC research strategy is to carry out diagnostic analyses and modeling studies of the atmosphere, ocean, and coupled ocean–atmosphere–land system, rather than to conduct field research. Data assimilation, allowing optimal incorporation of observed data into models, is an integral part of this effort.

The IPRC continues to be funded by Japan through the Japan Agency for Marine-Earth Science and Technology (JAMSTEC) and through U.S. sources, which include the State of Hawai‘i, NASA, NOAA, NSF, DOE, and ONR.

国際太平洋研究センター

ハワイ大学国際太平洋研究センター(IPRC)は、アジア・太平洋地域を中心に地球環境とその変動に関する研究を行っています。当センターは、「地球的展望に立った協力のための日米共通課題」の下、1997年10月にハワイ大学マノア地区の海洋地球科学技術学部内に設立されました。その使命は、「最新鋭の研究環境を、アジア・太平洋地域における自然現象、気候変動予測可能性および地球規模の変動の地域的側面についての研究を促進するために提供すること」です。

IPRCの研究は、以下に示すように、大きく5つの研究テーマに分けることができます。

インド洋・太平洋地域の気候：太平洋およびインド洋における数年から数十年規模での気候変動を理解する。

局地的海洋現象の影響：西岸境界流、黒潮・親潮続流系、縁辺海、インドネシア通過流などが、アジア・太平洋地域の気候に及ぼす影響を解明する。

アジア・オーストラリアモンスーンシステム：水循環を含めたアジア・オーストラリアモンスーンシステムの気候変動特性および予測可能性を、季節内から数十年の時間規模で理解する。

地球規模環境変化の影響：地球規模の環境変化とアジア・太平洋地域の気候の関係を明らかにする。

アジア太平洋データ研究センター：世界中の研究者たちに気候データを使いやすい形で提供する。

IPRCの研究戦略は、観測研究というよりは、診断解析およびモデリングによって、大気、海洋、大気海洋陸面結合系の研究を行うことです。観測データを最適な形でモデルに取り込むという意味で、データ同化もこの取り組みに含まれています。

IPRCは、海洋研究開発機構を通して、引き続き日本から研究費をいただいております。また、ハワイ州、航空宇宙局、海洋大気庁、国立科学財団、エネルギー省、海軍研究局等、米国各種機関から研究助成を受けております。

FOREWORD

The IPRC performs research to enhance understanding of the nature and mechanisms of climate variability and change, and to improve the tools for modeling and forecasting the climate system. The widespread public concern about anthropogenic alteration of climate over the next century provides much of the ultimate impetus for our research. Progress on producing more detailed and confident climate change projections depends on improving understanding of basic processes as well as on advances in model development and evaluation. The impressive portfolio of research outlined in this report is IPRC's response to the scientific challenges presented by the climate system, and to the practical urgency to contribute to the improvement of environmental forecasting capabilities. While the range of work is broad in terms of space and time scales of the phenomena studied, the main focus of our activity exploits IPRC's particular expertise in climate diagnostics and modeling of the Asia-Pacific region. The scope of activities at IPRC also reflects an understanding that the study of natural variability, from intraseasonal to millennial or even longer time scales, plays a critical role in advancing knowledge of the climate system and underpins efforts to improve both short-term and long-term environmental prediction.

This report summarizes the principal activities at IPRC from April 2007 to March 2008. Included are activities involving external collaborations, and indeed the reader will see that a very large portion of our research projects involves colleagues at other institutions throughout the world. Such collaborations greatly enhance the scope and depth of our activities. In addition, most of our research projects involve graduate students and/or postdoctoral fellows and thus contribute directly to education and development of the next generation of climate scientists. Here I will briefly mention just a few of the many highlights of the year's activities.

Comprehensive global models with fine numerical resolution can explicitly represent a wide range of scales of motion. Such models are a valuable resource for understanding many complex phenomena in the atmosphere and ocean, notably phenomena involving strong coupling of motions over a wide range of space and time scales. Collaborations with JAMSTEC colleagues on high-resolution global oceanic and atmospheric modeling have been an important component of IPRC's activities for several years, and a number of significant findings were obtained in the last year. Notably the narrow, nearly-zonal, bands in the geostrophic current in simulations with the JAMSTEC Ocean GCM for the Earth Simulator (OFES) have been compared with similar features inferred from observations. Some overall properties of the velocity bands in observations and in OFES results are similar, although the locations, orientations and scales of individual jets differ somewhat in the model and in observations. A version of OFES that is being applied in a study of the maintenance of the Arabian Sea oxygen minimum zone includes CFC-11 as a tracer. The modeled salinity and CFC-11 in the Arabian Sea have been compared with observations and results suggest that the outflow of the high-salinity water from the Red Sea is much weaker in the model than in the real world. A more detailed analysis is underway to understand the pathways of the water from the Red Sea in the OFES simulation.

The development of the Non-hydrostatic ICosahedral Atmospheric Model (NICAM) by JAMSTEC scientists has opened new possibilities in high-resolution atmospheric simulation. Currently NICAM can be run globally with as fine as 3.5-km horizontal grid spacing, and is run without any subgrid-scale convective parameterizations. At IPRC we are analyzing several aspects of NICAM simulations. It has been particularly exciting to see the mechanisms involved in the early stages of tropical cyclone formation, notably the formation and merger of vortical hot towers, appearing in the NICAM simulation.

Several IPRC projects completed in the last year concern the atmospheric effects of oceanic fronts. The results of all these studies suggest that the effects penetrate much higher in the atmosphere than previously recognized. Notably satellite analysis shows that the subtropical front of the Northwest Pacific anchors a deep convective rainband during April–May, leaving a distinct surface signature including positive wind curls. A series of idealized global atmospheric model experiments show a pronounced influence of mid-latitude ocean fronts on the storm tracks, the surface westerlies, and the annular mode of atmospheric variation. Finally a wide-ranging study that synthesized satellite observations, atmospheric reanalysis data and global atmospheric model experiments reveals clearly that the Gulf

Stream influence penetrates significantly into the upper troposphere, a surprising finding that has important implications for understanding the role of extratropical ocean surface temperature anomalies in driving large-scale atmospheric variability.

A JAMSTEC-IPRC collaboration has explored the interesting period between about 18,000–14,600 years before present, which was characterized by major reorganizations of the global ocean circulation. Colleagues at the JAMSTEC Institute of Observational Research for Global Change have recently produced evidence for rapid changes in the North Pacific oxygen concentrations at intermediate depths during this period. Analysis of a suite of simulations conducted with a number of global coupled ocean–atmosphere models showed that a collapse of the Atlantic Meridional Overturning that occurred between 17,000 and 15,000 years before present led to a substantial cooling of the North Pacific and an increase in surface salinities. The simulations suggest that the resulting higher surface density triggered deep winter-time mixing in the Gulf of Alaska and the Bering Sea. The reduction in stratification in these regions then can lead to adjustments in the North Pacific circulation that are consistent with proxy observations from this period.

An extensive ensemble of hindcasts using the IPRC hybrid coupled atmosphere-ocean model was produced. The ensemble mean of the hindcasts displayed considerable skill in representing the actual behavior of the Madden-Julian Oscillation and associated rainfall for more than a month, a very encouraging result for the prospects of practical extended-range weather forecasting in the tropics.

Through the Asia-Pacific Data-Research Center (APDRC) the IPRC operates a web-based data-server system that makes data resources readily accessible to, and usable by, IPRC researchers, the international climate community and the general public. Over the last year the APDRC continued to expand its data holdings and server capabilities. The APDRC has taken the lead in producing new surface and subsurface ocean current data derived from extensive ARGO in situ float observations.

The IPRC was established in October 1997 and so the period covered by this report marked the completion of a full decade of research activities. The IPRC has become a center of excellence in climate research with a scientific staff of over 40 and an enviable international reputation for its accomplishments in diagnostics and modeling of the climate system. While there have been many changes over the last decade, IPRC has consistently maintained its commitment to excellent science and its broad international outlook.

The study of the climate system combines some of the most exciting intellectual challenges in science with the opportunity to contribute to the solution of some of humankind's most pressing practical problems. IPRC scientists are privileged to devote their working lives to this very meaningful activity. We greatly appreciate the support of the University of Hawai'i and the agencies who fund our research, and also are grateful to the wider public for their support and interest in our work. We look forward to an exciting and productive second decade.

Kevin P. Hamilton, PhD
Interim Director

はじめに

国際太平洋研究センター(IPRC)では、気候変動の性質とそのメカニズムに対する理解を深め、気候系のモデル化と予測に必要な道具を改良するという目的の下、研究活動を行っています。次世紀にかけて起こるであろう人為起源の気候変動に対する一般の方々の関心が、IPRCの研究活動の最大の推進力となっています。より詳細で信頼性の高い気候変動予測を実現するには、基本物理過程の理解を深めること、また、モデルの開発と評価を向上させることが不可欠です。本報告で紹介する研究成果は、気候系が挑戦に値する研究対象であることだけでなく、環境予測性能の向上が差し迫った実世界の要求であることも反映しています。対象となる現象の時空間規模が多様であるため研究領域は広大ですが、IPRCの得意分野であるところのアジア・太平洋地域の気候診断とモデル化を中心に、研究活動を行っています。また、季節内から千年規模、さらにそれより長い時間規模の自然変動の研究は、気候系の理解を向上させる上で重要な役割を担い、短期・長期環境予測改善への取り組みの裏付けとなります。IPRCの研究活動の範囲は、このことを反映させたものとなっています。

本報告では、2007年4月から2008年3月までのIPRCにおける主な活動をまとめています。中には、他機関との共同研究も含まれていますが、実は、IPRCの研究活動のかなりの部分は世界中の研究者との協力により実施されているのです。このような研究協力によって、IPRCの活動は大いに広がりと奥行きを持つことができます。さらに、IPRCの研究活動は、その大半に大学院生やポストドクトラル研究員が関与しており、次世代の気候学研究者の育成に直接貢献しています。本年度も目立った研究成果が多々ありますが、その中から幾つか、以下に簡単に紹介します。

高解像度全球大循環モデルでは、広い時空間規模に渡る現象を陽に表現することが可能です。このようなモデルは、大気海洋の数々の複雑な現象、とりわけ広範囲の時空間規模が結合する現象を理解する上で、重要な手段です。ここ何年にもわたってIPRCの活動において重要な位置を占めてきたのは、海洋研究開発機構(JAMSTEC)の研究者たちと進めている高解像度全球大気海洋モデルに関する共同研究です。例えば、海洋大循環モデルOFESによる再現実験結果の中に、ほぼ東西方向に延びる細長い地衡流の帯が数多く見られ、観測にも、比較できるような同様の現象があることが分かりました。この細長い帯の全体的な特徴は観測とモデルで似ていますが、個々の流れの位置・方向・スケールはやや異なっています。また、OFESの、CFC-11をトレーサとして含む再現実験が、アラビア海における酸素極小域の維持のメカニズムの研究にも利用されています。モデルで再現されたアラビア海の塩分とCFC-11を観測と比較した結果、紅海からの高塩分水の流出が現実よりも弱いのではないかということが分かりました。モデルの中で紅海から流出する水の流路を理解するために、より詳細な解析が現在行われています。

JAMSTECの研究者たちは、非静力正二十面体大気モデルNICAMを開発し、高解像度大気シミュレーションに新しい可能性を開きました。現在NICAMでは全球3.5kmもの高解像度化が可能で、サブグリッドスケールの対流パラメタリゼーションは使用されていません。IPRCでは、NICAMによる再現実験を様々な角度から解析しています。熱帯低気圧の形成の初期段階に関わるメカニズム、とりわけ多数の対流に伴う渦の形成と融合がNICAMでの再現実験に現れたのは、大変な成果です。

昨年は、海面水温前線の大気への影響に関わる研究がいくつか完了しました。いずれの研究結果も、海面水温前線の影響がこれまでに考えられていた以上に上空にまで及んでいることを示しています。例えば、北西太平洋における亜熱帯海面水温前線が、深い対流性降水帯を留めていることが、人工衛星データの解析によって明らかになりました。この降水帯は4月から5月にかけて形成され、それに伴い、低気圧性回転をもつ明瞭な海上風のパターンが生じます。また、大気大循環モデルを用いて一連の理想化実験を行い、中緯度の海面水

温前線がストームトラック・海上偏西風・環状モードに顕著な影響を及ぼしていることを示しました。さらに、衛星観測・大気再解析データ・全球大気モデル実験を統合した広範囲にわたる研究は、メキシコ湾流の影響が対流圏上層にまで到達していることを明瞭に示しており、中緯度の大規模大気変動を引き起こす海面水温偏差の役割を理解する上で重要な意味を持つ、驚くべき発見となりました。

JAMSTECとIPRCの共同研究の一つとして、今から18000年前から14600年前にかけての時代を研究しました。この期間は、海洋大循環が大規模に再構成された興味深い時期として特徴づけられます。JAMSTEC地球環境観測研究センターの研究者は、先頃、この時期の北太平洋中深層の酸素濃度に急激な変化があったことを示唆する新たな証拠をつかみました。数々の全球大気海洋結合モデルを使った一連の再現実験の解析からは、今から17000年前から15000年前に起きた大西洋の子午面循環の衰退が、北太平洋の大幅な冷却と海面塩分の増加をもたらしたことがわかりました。さらに、この海面密度の上昇により、冬季にアラスカ湾とベーリング海に深い対流が引き起こされたことが示唆されました。対流によってこの海域における成層が弱まったことが、この時期の代替指標にも見られる北太平洋循環の変化を招いたと考えられます。

IPRCのハイブリッド結合大気海洋モデルを用いて過去の再現実験を行い、大きなアンサンブルを得ました。アンサンブル平均は、マデン・ジュリアン振動の実際の振る舞いとそれに伴う降水をひと月以上に渡って再現するという高い能力を示しました。熱帯において数ヶ月先の天気を実用的に予報することができそうだという、大変期待の持てる結果です。

IPRC附置のアジア太平洋データ研究センター（APDRC）では、ウェブ上にデータサーバを運用しており、IPRCや世界中の気候研究者たち、さらに広く一般の人が容易に使えるような形でデータを提供しています。昨年も、APDRCは保有データとサーバ性能の拡張を続けました。APDRCが主導して、アルゴフロートによる大規模な現場観測から、海面と中層における流速場のデータを新たに作成しました。

IPRCの設立は1997年10月ですので、本報告で扱っている期間は、十年間の研究活動の締めくくりであったとも言えます。IPRCは、四十名以上の研究スタッフを抱える卓越した気候研究の拠点に成長し、気候系の診断とモデル化における成果に対して、国際的な評価も高まっています。この十年で大きな変革をとげながらも、IPRCは一貫して、優れた科学に対する献身と国際的な広い視野を維持し続けています。

気候研究は、科学における最も刺激的な知的挑戦であると同時に、人類が直面している現実的な問題の解決に貢献する機会でもあります。IPRCの研究者は、研究生活をこの大変意義のある活動に捧げるという幸運に恵まれています。ハワイ大学および研究資金を提供くださる内外の機関に深く感謝すると同時に、一般の皆様の支援と関心に心から感謝いたします。これからも、活気に満ち創造性に富んだ時代が続くでしょう。

国際太平洋研究センター
所長　ケビン P. ハミルトン

Participants at the IPRC Tenth Anniversary Symposium held in Spring 2008 at the East-West Center.

INDO-PACIFIC OCEAN CLIMATE (THEME 1)

Research under *Indo-Pacific Ocean Climate* seeks to determine the role of the oceans in the climate system—particularly the role of the Indian and Pacific Oceans—by conducting studies on air–sea interaction, ocean processes, and climate variability. Accomplishments for the past year (April 2007–March 2008) span all three areas. Selected highlights of this research are described below.

Air–Sea Interaction

An emerging research field is the study of the impact of small-scale ocean–atmosphere interactions at oceanic fronts on the large-scale circulation. This past year, IPRC scientists and their colleagues at other institutions have conducted three studies that have greatly advanced our knowledge on how midlatitude weather systems are organized into "storm tracks" near oceanic frontal zones with pronounced sea surface temperature (SST) gradients. Each study shows that the atmospheric effects of oceanic fronts reach a much higher altitude than previously realized.

Annual cycle of air–sea interaction in the western North Pacific subtropical front. The western North Pacific subtropical front around 25ºN shows a sharp sea surface temperature (SST) gradient that is most pronounced in spring. The effects of this front on the atmosphere were investigated in satellite observations. Against mean annual anticyclonic wind stress curl, the April–May surface wind stress curl turns slightly cyclonic along the front. During these months, the atmospheric column-integrated water vapor reaches a meridional maximum along the surface low pressure over the front, suggesting the atmospheric response has a deep vertical structure there. Cyclonic wind curl occurs intermittently every few days along the front in small-scale low-pressure systems that accompany broader-scale high-pressure systems in the main storm track to the north of the front. The sub-synoptic-scale surface lows produce convective rainfall

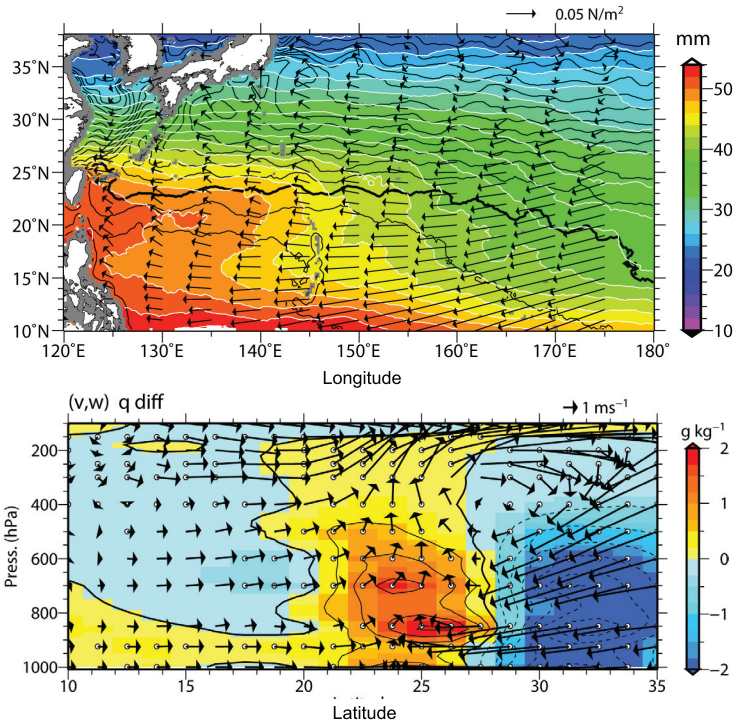

Figure 1.1. (top) May climatology of satellite observations: wind stress vector, columnar water vapor (color shades), and sea surface temperature (black contours at intervals of 1°C). A thick black contour marks the 27°C isotherm. (bottom) Latitude-height section at 142.875°E of cyclonic-anticyclonic curl composite differences of meridional and vertical winds (vectors) and specific humidity (color shades). The vertical wind speed is multiplied by 100. Open circles show grid points with significant differences in specific humidity at >95% confidence level. Results are based on the JRA-25 reanalysis.

with strong upward motion that moistens the entire troposphere. The resulting condensational heating reinforces the lows, leading to the weak cyclonic wind curl along the front. The low-pressure systems display vertical structures that are characteristic of baroclinic instability, suggesting they are triggered by the passage of synoptic highs and grow on the baroclinic conditions over the SST front. The cyclonic wind curls tend to occur during the cloudy, rainband season in May before the Baiu/Meiyu front has formed. [F. Kobashi (Tokyo University of Marine Science and Technology), S.-P. Xie (IPRC), N. Iwasaka (Tokyo University of Marine Science and Technology), and T. Sakamoto (JAMSTEC FRCGC)]

Effect of thermal gradient on air-sea interaction. Two experiments were conducted with the Atmospheric General Circulation Model for the Earth Simulator (AFES), in which the sea surface temperature (SST) profiles were uniform in the east-west direction. The experiments showed that the observed collocation of the front and storm track does not happen by chance. In the *control* experiment, which kept the midlatitude SST front with its north–south thermal gradients, the front anchored a storm track with energetic eddies that produced a well-defined polar-front jet (PFJ) along the oceanic front, even during winter when the subtropical jet stream intensified. The *no-front* experiment removed the north–south thermal gradients. This weakened the eddy activity and the PFJ considerably, especially in winter (Figure 1.2a and b). The removal also weakened the annular mode —the dominant mode of westerly-jet variability— and its notable structural distortion in winter (Figure 1.2c and d). Though idealized, the experiments indicate that midlatitude oceanic fronts impact the tropospheric circulation and its variability. [H. Nakamura (U. of Tokyo), T. Sampe (IPRC), A. Goto (JMA), W. Ohfuchi (JAMSTEC-ESC), and S.-P. Xie (IPRC)]

The Gulf Stream's signature on the atmosphere. A combination of satellite data, reanalysis data and experiments with the Atmospheric General Circulation Model for the Earth Simulator (AFES) shows that surface winds, flowing across the SST front generated by the warm Gulf Stream in the cold North

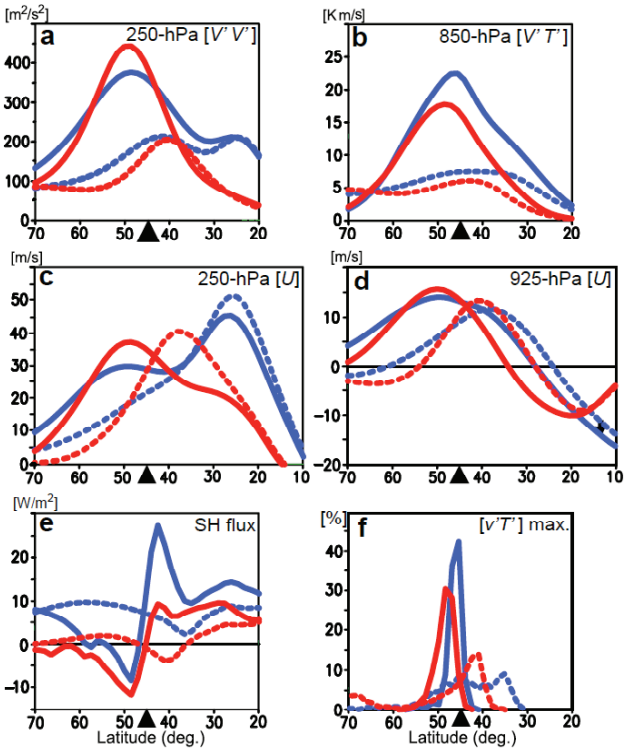

Figure 1.2. Meridional profiles of the mean states of (a) longitudinal variance of 250-hPa meridional wind fluctuations (m^2/s^2), (b) 850-hPa poleward eddy heat flux (K m/s), both associated with disturbances shorter than one week, (c) 250-hPa zonally-averaged westerly wind velocity [U] (m/s), (d) 925-hPa [U] (m/s; negative: easterly), (e) turbulent sensible heat flux (W/m^2) from the surface (positive: upward), and (f) probability density of 850-hPa storm-track axis (maximum eddy heat flux), based on the 60-month AGCM integrations with (solid, *control*) and without (dotted, *no-front*) SST fronts (triangle) for the summer (red) and winter (blue) hemispheres. The differences between solid (control) and dashed lines (no-front) in (a) and (b) show how the oceanic front increases storm activity; (c) and (d) show how the oceanic front increases westerly wind speed by 7–15 m/s around 50° latitude; (e) shows the prominent contrast in sensible heat from the model ocean that keeps atmospheric temperature gradient above the oceanic front; (f) shows the storm tracks stay close to the oceanic front and they tend to wobble if the oceanic front is removed.

Atlantic, warm and rise to form a rainband that follows the Gulf Stream front. This rainband has upward motions and cloud formations that reach up to 7 miles high and penetrate the upper troposphere. In the upper troposphere, the winds branch out and form planetary waves that travel eastward toward Europe and could have far-reaching weather/climate impacts. [The study was published as the cover article in *Nature* in 2008 and received wide media coverage in Japan, US and Europe: S. Minobe (Hokkaido University); A. Kuwano-Yoshida and N. Komori (JAMSTEC-ESC); S.-P. Xie and R. J. Small (IPRC); S. Minobe et al., 2008: Influence of the Gulf Stream on the troposphere, *Nature*, **452**, 206–209]

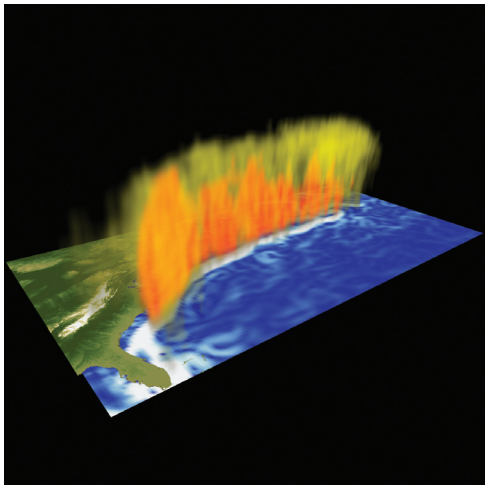

Figure 1.3. The graphic shows the land-surface topography of eastern North America and the Gulf Stream processes that give rise to its climate impact: surface current speeds in blue-white colors (white is the fastest) and upward wind velocities in yellow-red (red for stronger winds).

Climate change in the Atlantic impacts the tropical Pacific across the Central American Isthmus. The IPRC high-resolution regional ocean–atmosphere model (iROAM) implemented for the eastern tropical Pacific was used to investigate the processes by which a cooling of the North Atlantic sea surface can affect tropical Pacific climate across the Central American atmospheric bridge. The simulation shows that the Atlantic cooling increases sea level pressure in the Caribbean, driving anomalous northeasterly wind across the Isthmus year round. While the atmospheric response is most pronounced during boreal summer and fall when the tropical North Atlantic is warm and conducive to deep convection, the Pacific SST response is strongest in winter and spring when the climatological northeast trade winds prevail across the Isthmus (Figure 1.4). During winter, the northeasterly cross-Isthmus winds intensify in response to the Atlantic cooling. This in turn cools the Gulf of Panama by advecting cool and dry air from the Atlantic and by enhancing surface turbulent heat flux and mixing. This Gulf of Panama cooling reaches the equator and is amplified by the Bjerknes feedback during boreal spring. The equatorial anomalies of SST and zonal winds dissipate quickly in early summer when the seasonal development of the cold tongue increases the stratification of the atmospheric boundary layer and shields the surface from the Atlantic influence, which propagates into the Pacific as tropospheric Rossby waves. The climatological winds over the far-eastern Pacific warm pool turn southwesterly in summer and fall, and the superimposed anomalous northeasterlies induce a weak SST warming there.

The iROAM results were compared with global model water-hosing runs to shed light on inter-model consistency and differences in response to a shutdown of the Atlantic meridional overturning circulation, and the implications for interpreting paleoclimate changes due to Heinrich events discussed. The results also help to understand current climate phenomena, such as the Central American mid-summer drought and the Atlantic multi-decadal oscillation. [S.-P. Xie (IPRC), Y. Okumura (NCAR), T. Miyama (JAMSTEC-FRCGC), and A. Timmermann (IPRC); S.-P. Xie et al.: Influences of Atlantic climate change on the tropical Pacific via the Central American Isthmus. *J. Climate*, in press]

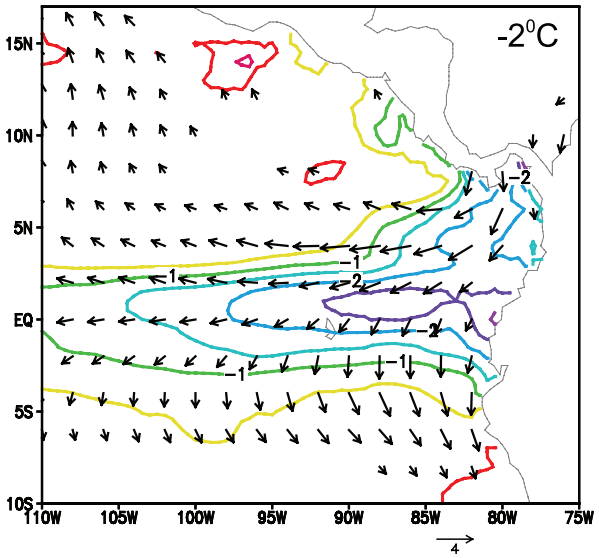

Figure 1.4. SST (contours) and surface wind (m/s) response to a 2°C cooling over the tropical North Atlantic in iROAM during January–March. The Panama wind jet intensifies, inducing a decrease in SST both locally and in the equatorial Pacific. In the latter region, the Bjerknes feedback between the SST cooling and strengthened easterly trades amplifies the coupled response.

Climate Variability

Year-to-year natural fluctuations in weather and climate can have devastating and costly consequences for society and the economy. A focal point of IPRC research, therefore, is the study of variations in ocean-based climates at seasonal, interannual, and decadal timescales, and the processes that drive these variations.

Unraveling the cause of tropical Indian Ocean warming. The tropical Indian Ocean has warmed steadily since the 1950s by about 0.5°C, according to observations. Somewhat puzzling is that the observed net surface heat flux has changed little during the warming. To pinpoint the reason for this lack of change, a study examined changes in the various surface heat flux components in 11 models of the World Climate Research Program's Third Coupled Model Intercomparison multimodel bank; the models had been driven with observed history of greenhouse gas concentrations and solar radiation. The results, which compare well with observations, show that on average the warming is trapped in the top

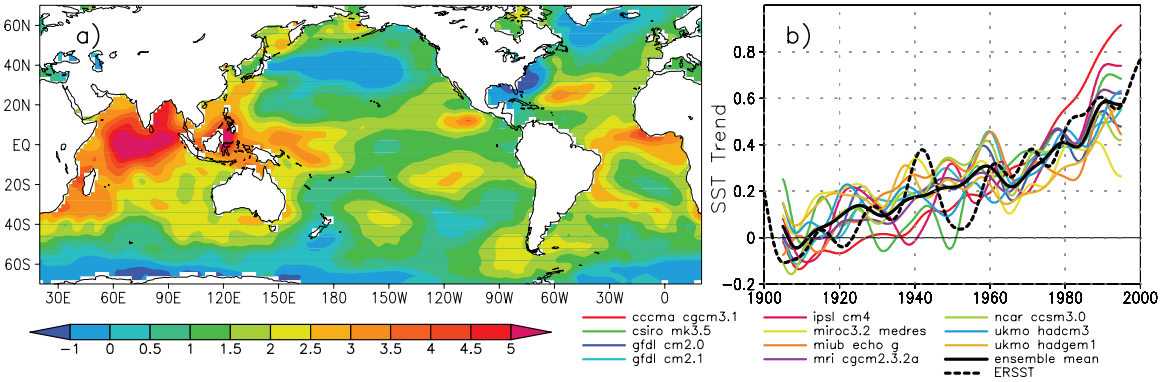

Figure 1.5. SST trend: (a) Ratio of the trend to the standard deviation of the detrended yearly SST in the Extended Reconstructed SST (ERSST) observations from December 1947 to November 2007. (b) SST trend (°C) averaged over the Tropical Indian Ocean basin (40°E–120°E, 20°S–20°N) from the 1900–2004 mean in ERSST and 11 coupled models. For each model, the ensemble mean (10-year low-pass filter) of the CMIP3 20th century runs is shown.

125 m with little change in net surface heat flux. The heat flux analysis shows a series of complicated atmospheric–oceanic adjustments that account for the observed warming and that can be summarized as follows. The rise in greenhouse gas concentrations increases downward longwave radiation, warming the tropical Indian Ocean. The resulting tropospheric moistening amplifies the downward longwave radiation and thus the ocean warming. The increase in evaporation due to the warming dampens the rise in SST, but evaporation itself is dampened because the warming weakens the winds and raises the surface relative humidity. The simulated changes in surface solar radiation vary considerably among models and are highly correlated with variations among models in the sea surface temperature trend. The variations are very likely due to uncertainties in the simulation of clouds [Y. Du and S.-P. Xie (IPRC); Y. Du and S.-P. Xie: Role of atmospheric adjustments in the tropical Indian Ocean warming during the 20th century in climate models. *Geophys. Res. Lett.*, in press].

The capacitor effect of the Indian Ocean. After El Niño has dissipated in spring in the equatorial Pacific, significant climate anomalies persist in the Indian Ocean through June-August. They include increased tropical Indian Ocean sea surface temperature (SST), increased tropical tropospheric temperature, an anomalous anticyclone over the subtropical Northwest Pacific, and increased Meiyu-Baiu rainfall over East Asia (Figure 1.6). IPRC scientists and colleagues at the Chinese Academy of Sciences have investigated the cause of these lingering El Niño effects. Their results indicate that the tropical Indian Ocean warming acts as a capacitor that anchors atmospheric anomalies over the Indo-western Pacific Oceans. This effect causes tropospheric temperature to increase by moist adiabatic adjustment in deep convection, from which a baroclinic, warm Kelvin wave emanates into the Pacific. In the Northwest Pacific, this equatorial Kelvin wave induces northeasterly surface wind anomalies with the help of surface friction, and the resultant divergence in the subtropics suppresses convection and the anomalous anticyclone (Figure 1.6). Their results with a general circulation model (GCM) support this

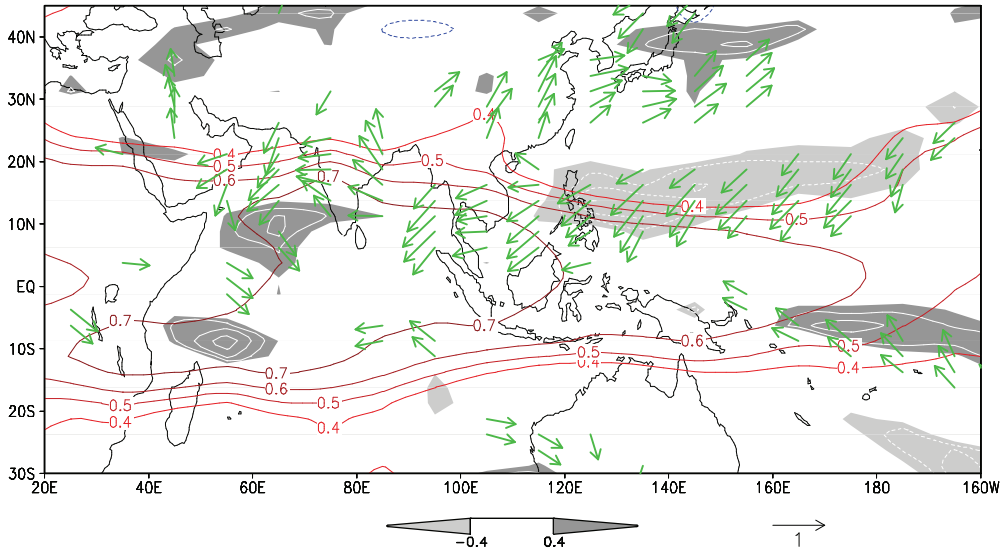

Figure 1.6. Atmospheric anomalies in the summer after El Niño's dissipation, expressed as correlation with an El Niño index in the prior winter: tropospheric (850–250 hPa) temperature (colored contours), precipitation (white contours at intervals of 0.1; dark shade > +0.4; light < –0.4), and surface wind velocity (vectors in m/s). Tropospheric temperature anomalies resemble the so-called Matsuno-Gill pattern, with a warm Kelvin wave penetrating into the western Pacific along the equator. This tropospheric wave induces a series of atmospheric responses with the help of surface friction and convective feedback, forming a large-scale anticyclonic (cyclonic) circulation in the subtropics (over Japan).

Kelvin wave-induced Ekman divergence mechanism. In response to a prescribed SST increase over the tropical Indian Ocean, the GCM simulates the Kelvin wave with low pressure on the equator as well as suppressed convection and the anomalous anticyclone over the subtropical Northwest Pacific. An additional experiment further indicates that the North Indian Ocean warming is critical for the formation of the Kelvin wave and the Northwest Pacific anticyclone, a result corroborated by observations.

The results have important implications for the predictability of Indo-western Pacific summer climate: the spatial distribution and magnitude of the tropical Indian Ocean warming, rather than the occurrence of an El Niño in the preceding winter, affect summer climate anomalies over the Indo-western Pacific and East Asia. [S.-P. Xie (IPRC); K. Hu (CAS); J. Hafner (IPRC); H. Tokinaga and Y. Du (IPRC); G. Huang (CAS); and T. Sampe (IPRC)]

Review of Indian Ocean circulation and climate variability. A major review on a broad range of topics on Indian Ocean circulation and climate variability is being published in *Review of Geophysics*. Until quite recently, it was generally accepted that the Indian Ocean had little appreciable influence on climate variability beyond its impact on the monsoons. This view changed profoundly when in 1997 scientists noted warmer than normal water in the western and cooler than normal water in the eastern equatorial Indian Ocean. This unusual pattern altered not only the local atmospheric circulation but also distant rainfall patterns. The efforts to determine the physical cause of the extraordinary 1997 event led to rapid progress in understanding Indian Ocean air–sea interaction and modes of climate variability. Several reviews of Indian Ocean variability have been published, most of them focusing on the dynamics and impacts of the Indian Ocean dipole (IOD), the sea surface temperature pattern that was so pronounced in 1997. The Schott et al. review goes far beyond the IOD and includes the Indian Ocean basin-warming forced by El Niño. The latest studies show that this basin-warming acts as a capacitor unleashing El Niño's effects after Pacific sea surface temperatures have returned to normal. The review also covers the recent progress made in studying Indian Ocean climate change and its far-reaching effects. [F. A. Schott (U. of Kiel); S.-P. Xie and J. P. McCreary (IPRC)]

The role of weather noise in modeling and predicting ENSO. The effect of westerly wind bursts on the predictability of the El Niño–Southern Oscillation (ENSO) was studied by creating numerical and analytical solutions to the Fokker-Planck equation. The interaction between the westerly wind bursts and ENSO leads to a noise-induced instability for ENSO, not accounted for previously. Moreover, the fact that the climate background state in which ENSO operates is not an equilibrium state leads to a system that may be in any number of states, making it difficult to identify the Hopf bifurcation in parameter space. In addition, the stochastic forcing further impacts the instability boundary of ENSO. These three lines of thought show that the ENSO instability concept is more complicated – and perhaps less useful in the interpretation of observations and even in coupled general circulation model data – than previously assumed. [A. Timmermann (IPRC) and F.F. Jin (UH); A. Timmermann and F.F. Jin: *'Aha Huliko'a* 2007]

The North Pacific Gyre Oscillation. Decadal fluctuations in nutrients, zooplankton, and fish stocks in the Northeast Pacific are poorly correlated with the widely used climate variability index, the Pacific Decadal Oscillation (PDO). IPRC scientists and their colleagues at other institutions have now identified in sea surface height measurements a new pattern of climate variation, which they named the *North Pacific Gyre Oscillation* (NPGO). The NPGO does correlate well with fluctuations in salinity, nutrients and chlorophyll, particularly off the California coast.

The Regional Ocean Modeling System (ROMS), representing a nested configuration of the Northeast Pacific (180ºW–110ºW; 25ºN–62ºN) and driven with NCEP surface wind stresses and heat fluxes from

1950 to 2004, realistically reconstructed the region's oceanic biological and physical conditions. The sea surface height anomalies of the PDO show a single large gyre north of 25ºN and a strong poleward flow along the coast from 25ºN to 55ºN forced by downwelling at the coast; during the positive PDO phase, the Alaskan Gyre is stronger and the California Current weaker than normally. During the positive NPGO phase, a pair of counter-rotating gyres forms: the Alaskan Gyre and the Subtropical Gyre are separated by the North Pacific Current, flowing eastward along 40ºN. The North Pacific Current bifurcates at the coast, flowing northward as the Alaskan Coastal Current and southward as the California Current. The positive NPGO phase strengthens the North Pacific Current and (in contrast to the PDO) the transport of both the Alaska Coastal and the California Current (Figure 1.7). In the model, the Alaskan and Subtropical gyres intensify because of open-ocean wind stress curl anomalies and stronger wind-driven coastal upwelling. Both processes increase salinity and nutrient concentrations, which, in turn, increase phytoplankton concentrations.

The spatial structure of the wind anomalies associated with the NGPO is consistent with the positive phase of the North Pacific Oscillation, an oscillation in atmospheric sea level pressure. The NPGO pattern extends beyond the North Pacific and appears to be part of a global-scale mode of climate variability, evident in global sea level trends and sea surface temperature. The greater NPGO variance noted in recent observations and in global warming simulations suggests the NPGO's role in global-scale changes in marine ecosystems is increasing. [E. Di Lorenzo (Georgia Institute of Technology), N. Schneider (IPRC), K. M. Cobb (Georgia Institute of Technology), et al.; E. Di Lorenzo et al., 2008: North Pacific Gyre Oscillation links ocean climate and ecosystem change. *Geophys. Res. Lett.*, **35**, L08607]

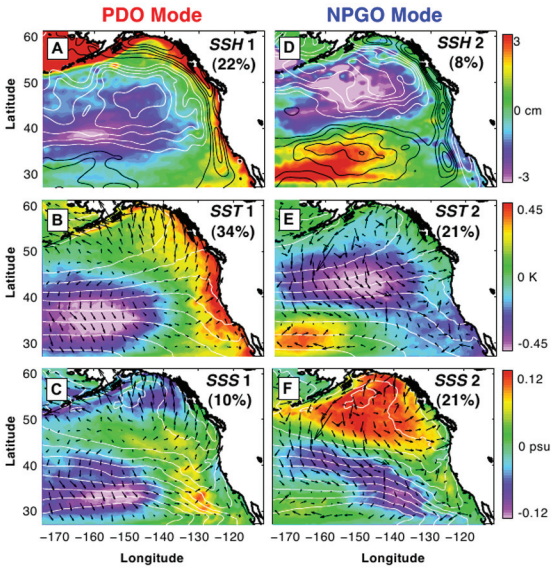

Figure 1.7. Comparison between PDO (left column) and NPGO (right column) patterns in the northeast Pacific for sea surface height (top row), sea surface temperature (middle row) and sea surface salinity (bottom row). Superposed as contour lines are the associated Ekman pumping (top row), mean sea surface temperature (middle) and salinity (bottom). The black arrows denote Ekman advection (middle and bottom rows).

Natural variations in the strength of the South Pacific Gyre. A related study was conducted on the sea-level variability in the South Pacific from 1970 to 2003. The analysis combines the hindcast simulation of the Ocean General Circulation Model for the Earth Simulator (OFES) with tide-gauge observations and satellite altimetry (since 1992) measurements. The model sea level was fairly stable and high until it fell rapidly in the late 1970s, and it remained low until it rose again in the late 1990s. These model results are consistent with tide-gauge and satellite observations. The decadal changes are accompanied by circulation changes of the subtropical gyre at 1000-m depth. The corresponding atmospheric variations are associated with the decadal variability of the El Niño-Southern Oscillation (ENSO). Thus,

decadal sea level variability in the western and central South Pacific in the past three-and-a-half decades and decadal ENSO variability are likely to be connected. The sea level rise in the 1990s attracted much attention in relation to the global warming, but it is more likely associated with the spin up of the South Pacific gyre that is part of the tropical Pacific decadal fluctuations. [Y. N. Sasaki and S. Minobe (Hokkaido University); N. Schneider (IPRC); T. Kagimoto, M. Nonaka, and H. Sasaki (JAMSTEC); Y.N. Sasaki et al.: Decadal sea level variability in the South Pacific in a global eddy-resolving ocean model hindcast. *J. Phys. Oceanogr.*, in press]

Tracking the origin of equatorial thermocline variability. The strength and duration of an El Niño event are thought to depend partly on changes in the subtropical overturning cells (STCs), circulations in the North and South Pacific in which water sinks in the subtropics, flows in the thermocline toward the equator, where it upwells and returns poleward along the surface. These cells are an important mechanism by which heat and salt are transferred poleward in the ocean. Studies on the STCs in the Pacific have focused on the Northern Hemisphere. The South Pacific, until very recently, has lacked good data coverage and the South Pacific STC has, therefore, been poorly studied. First estimates of its transport in the early 1990s revealed an annual subduction rate that was much smaller than that of the North Pacific.

In the past decade, however, a large number of hydrographic observations in this region has become available. IPRC scientists and their colleagues at other institutions set about to obtain a new estimate of the South Pacific subduction rate. They used high-resolution conductivity-temperature-depth profiles, complemented by a large amount of recently available Argo data and a significantly improved climatological dataset on the mixed layer properties from 10°S to 60°S. This calculation produced an estimated annual subduction rate of 48.8 Sv (1 Sv = 10^6 m^3/s). Specifically, the annual subduction rate from 16ºS and 48ºS was found to be 33.2 Sv, about 50% higher than the earlier estimate (21.6 Sv), and comparable to the subduction rate of 31.1 Sv for the North Pacific. This suggests that the South Pacific STC contributes significantly more than suspected to the formation of the equatorial thermocline. The authors expect that future study of South Pacific STC will reveal the degree to which eddies and larger oceanic vortices strengthen or weaken STC cycles, and how such strengthening or weakening influences the equatorial thermocline. [T. Qu and S. Gao (IPRC); I. Fukumori (JPL), R. A. Fine (U. of Miami), and E. J. Lindstrom (NASA); T. Qu et al., 2008: Subduction of South Pacific Waters. *Geophys. Res. Lett.*, **35**, L02610]

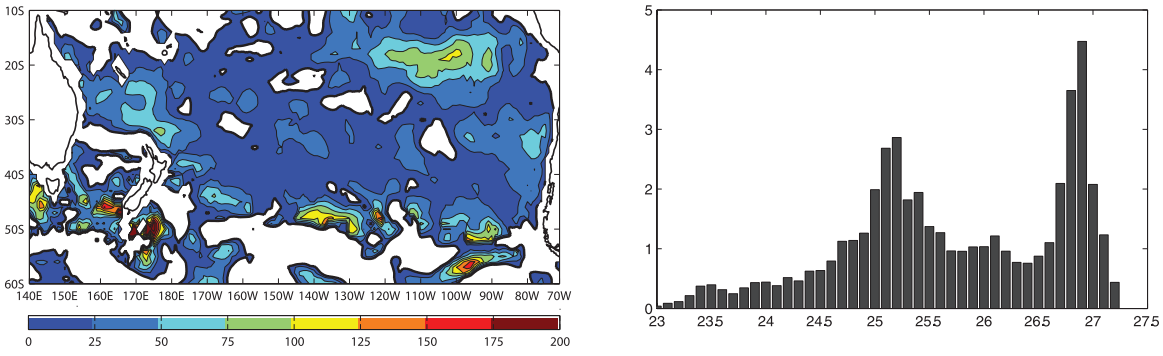

Figure 1.8. (left) Annual subduction rate (m/yr) in the South Pacific, representing the volume flux of mixed layer water entering the thermocline per unit horizontal area. The spatial distribution of the subduction rate clearly demonstrates that the formation of South Pacific waters mainly occurs in the Sub-Antarctic Front and the Eastern Subtropical Gyre (where the subduction rate is largest). The winter surface densities of these two regions are at 25.0–25.5 and 26.6–27.1 σ_θ, corresponding to the two peaks in the right panel, which shows the annual subduction (Sv) per $0.1\sigma_\theta$ as a function of winter mixed layer density in the South Pacific.

Ocean Processes

The ocean with its gyres, upwellings, downwellings, and eddies impacts Earth's climate greatly. For instance, the ocean's large heat capacity and poleward transport of heat greatly dampen the effects of the uneven heating of the atmosphere; its vertical movements bring nutrients to the surface or store them in the abyss.

Maintenance of the Arabian Sea oxygen minimum zone. The Arabian Sea oxygen minimum zone (ASOMZ) is present at depths from 200–1000 m in the central and eastern Arabian Sea. As with all OMZs elsewhere, it is caused by the sinking of surface-produced detritus and its consumption by bacteria at depth. An unusual feature of the ASOMZ, however, is that it is not located in the western Arabian Sea where surface production is largest. A possible physical cause for its eastward shift is the presence of oxygenated Red Sea water (RSW) in the western Arabian Sea.

During the past year, IPRC and JAMSTEC scientists have explored the influence of RSW in the Arabian Sea in OFES and a 6½-layer Indian Ocean model, using salinity as an indicator of RSW. Interestingly, OFES was initialized with the observed high salinity in the northern Arabian Sea, but that feature weakened markedly during the 50-year integration, likely because OFES does not include RSW inflow. In support of this conclusion, high salinity spreads throughout the western Arabian Sea in the 6½-layer model only when there is an inflow of RSW.

Based on these findings, it is expected that RSW will increase oxygen similarly in the western Arabian Sea, causing the eastward shift of the OMZ. During the coming year, solutions will be obtained to coupled, biophysical models that can simulate oxygen distributions, both with and without RSW inflow. Solutions will also be found on both coarse and eddy-resolving grids, in order to determine the role of eddies in spreading oxygen throughout the basin. [J. P. McCreary, Z. Yu, and K. J. Richards (IPRC); A. Ishida, Y. Sasai, and H. Aiki (JAMSTEC)]

Dynamics of near-surface, eastward flow in the South Indian Ocean. An intriguing feature of the near-surface circulation in the tropical and subtropical South Indian Ocean (SIO) is the presence of eastward flow across the basin, which cannot be explained by either Ekman or Sverdrup theory. Figure 1.9 (p. 10) illustrates the horizontal and vertical structures of the flow in observations, a reanalysis product (SODA), and two numerical models (COCO and OFES). The reanalysis and models are able to simulate the observed horizontal structure with varying degrees of success, and COCO is able to reproduce its shallowness.

The eastward flow also tends to divide into separate jets. One prominent jet is the South Indian Countercurrent (SICC), which appears to extend from Madagascar to the southwestern corner of Australia. A possible cause of this jet is the radiation of Rossby waves from Australia along Rossby-wave characteristics that flow both westward and northward due to the background Sverdrup circulation. Furthermore, the SICC is linked to the existence of the Indonesian Throughflow, as it nearly vanishes in a solution without any throughflow. [J. McCreary, J. Potemra, R. Furue and J. Hafner (IPRC); H. Sasaki and M. Nonaka (JAMSTEC)]

Dynamics of the Atlantic meridional overturning circulation. A hierarchy of models [constant-density 2-layer ocean model (CDLOM), variable-density 2-layer ocean model (VDLOM), and an ocean general circulation model (COCO)] is being used to study the large-scale processes that cause water to sink in the North Atlantic. Overturning in the CDLOM solutions is forced by an *externally* specified northern-boundary condition on upper-layer thickness, and the solutions show clearly how the overturning strength (M) is related to the thermocline depth throughout the basin. In VDLOM, the state of the northern-boundary

region is determined *internally* by cooling the surface layer to the north until its temperature reduces to that of the deep ocean. Along the eastern boundary, the surface layer thickens to the north (until the second layer shrinks to zero thickness). This coastal structure subsequently propagates offshore as a Rossby wave, and large-scale overturning, M, is generated when the wave is damped. Similar processes occur in COCO, which shows how the offshore decay of the Rossby wave is determined by mixing. Figure 1.10 shows the structure of the coastal response in COCO, as well as its offshore decay. [J. McCreary, A. Timmermann, R. Furue, and F. Schloesser (IPRC); M. Nonaka and T. Miyama (FRCGC-JAMSTEC)]

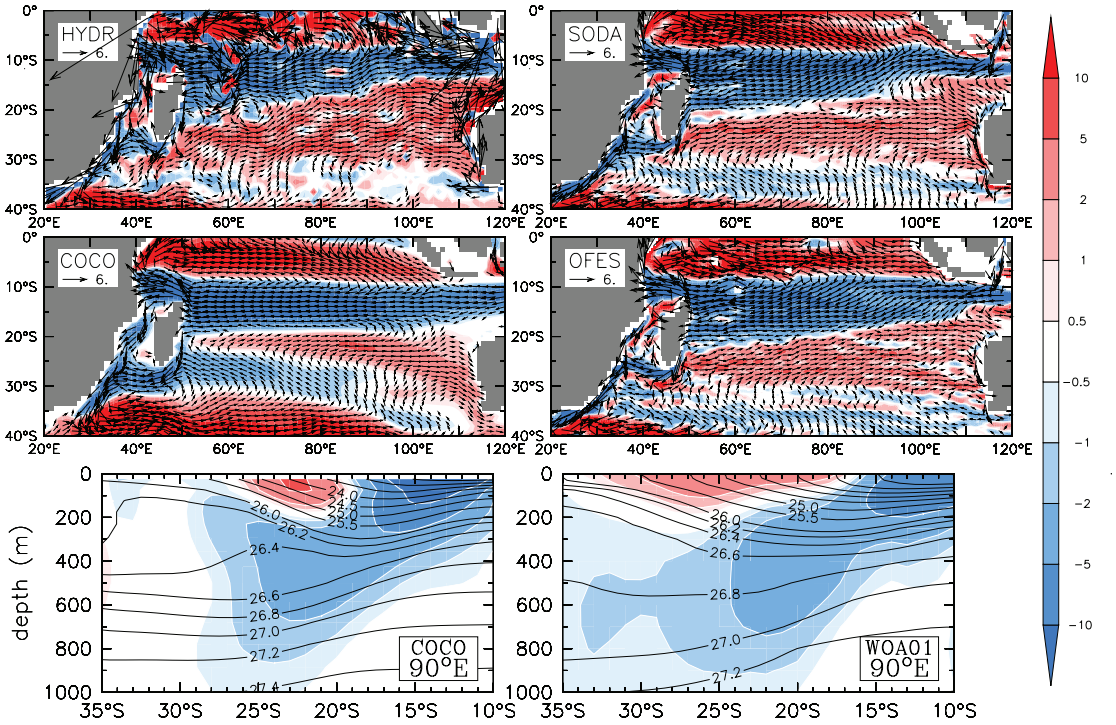

Figure 1.9. Top and middle: Annual-mean, near-surface velocity (cm/s, shading) and velocity vectors (arrows) from Hydrobase2 (geostrophic flow referenced to 2000 db), SODA 2.0.3 reanalysis (1980–1999), COCO, and OFES (last six years of climatological run). Bottom: Zonal velocity (cm/s, shading) and potential density (σ_θ, contours) at 90°E for COCO and for World Ocean Atlas 2001 (geostrophic flow referenced to 2000 db).

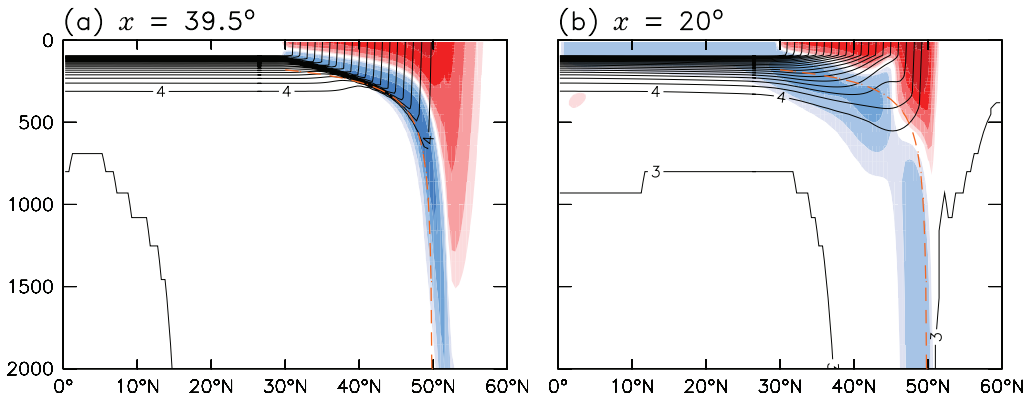

Figure 1.10. Sections of zonal velocity (cm/s) and temperature (°C, contours) at (a) x = 39.5° and (b) x = 20° in a COCO solution using vertical diffusivity 0.1 cm^2/s. The orange dashed curve is an analytic solution for the mixed-layer thickness.

Bands of zonal striations in the ocean and their potential impact on climate. An emerging field is the study of zonal jet-like bands seen in high-resolution observations and outputs of ocean general circulation models. Do the striations really exist, what characteristics do they have, are there different types, and do they impact climate?

In a project spearheaded by IPRC scientists, expendable bathythermograph (XBT) and float data of the World Ocean Database 2005 were used to demonstrate the existence of these nearly stationary jet-like features that had been noted in the high-resolution mean dynamic ocean topography. Two regions in the eastern Pacific that show such striations, but are free of strong currents, were selected for study: one in the North Pacific and one in the South Pacific Subtropical Gyre. The stripes emerge from the background eddy noise when horizontal high-pass filtering is applied to the mean temperature at 100-m depth. The bands are co-located with those seen in the mean dynamic ocean topography. The striations are still clearly visible at the deeper 12°C isotherm, close to the thermocline; they are oriented nearly

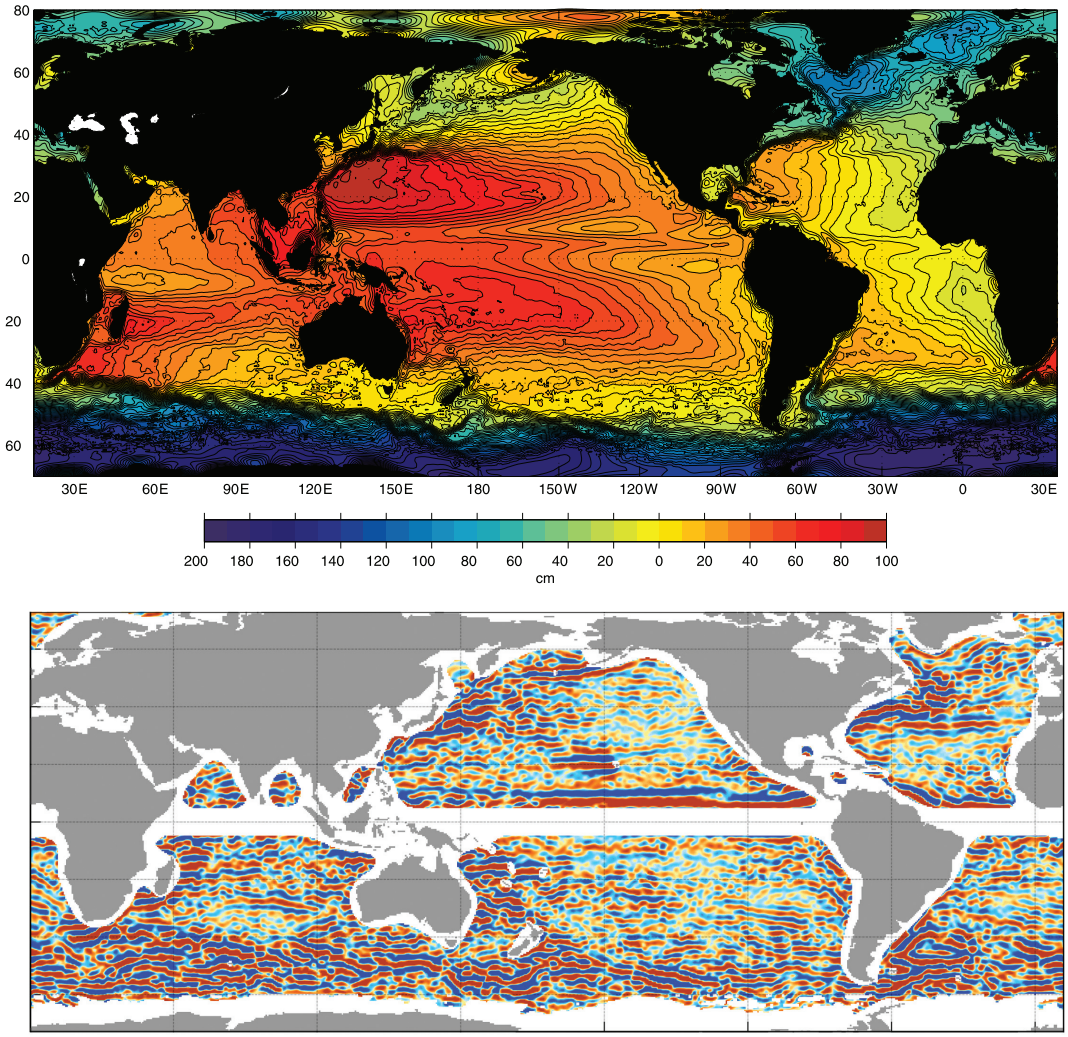

Figure 1.11. 1993–2002 map of mean dynamic topography (i.e., mean sea level due to ocean currents) in cm, contour interval is 5 cm, and isolines represent the pattern of geostrophic currents (top). Zonal geostrophic velocity (bottom) derived from this topography by high-pass filtering with a two-dimensional Hanning filter of 4° half-width. Red (blue) shading denotes eastward (westward) flow.

zonally and coherent vertically to a depth of at least 700 m; their wavelength is approximately 400 km, and the azimuth of wavevector is −13° in the North Pacific and 9° in the South Pacific. Signs of the striations were also detected in satellite observations of ocean color, SST, wind, atmospheric vapor and liquid water. This suggests that these oceanic features may affect the Earth's climate system. [N. Maximenko and O. Melnichenko (IPRC); P. Niiler (SIO); and H. Sasaki (JAMSTEC); N. Maximenko et al., 2008: Stationary mesoscale jet-like features in the ocean. *Geophys. Res. Lett.*, **35**, L08603]

An IPRC-JAMSTEC collaboration is now underway to compare the striations detected in observations with those in the Ocean General Circulation Model for the Earth Simulator (OFES). Preliminary results show that OFES produces features similar to the striped texture noted in the observed ocean circulation. The scales, locations, and orientations of individual jets however differ from those in observations. [O. Melnichenko and N. Maximenko (IPRC); and H. Sasaki (JAMSTEC)]

Early results in a model run on the particle dispersion characteristics of zonal jets in a study of particle trajectories show, as expected, considerably more zonal than meridional dispersion. There are, however, long periods of shear dispersion with anomalous dispersion at long time scales. [K.J. Richards and H. Aiki (IPRC)]

Tracking drifting marine debris by using tracers in a computer ocean circulation model. Drifters are part of marine debris that satellites can track. Statistical analysis of the drifter trajectories, however, is complicated because they are distributed heterogeneously in space and time. To skirt this problem, the probabilistic behavior of drifters was estimated and used as a tracer in a set of numerical experiments to simulate the trajectory of marine debris. Figure 1.12 shows the density distribution of the debris after ten years of advection by realistic currents starting from an initially homogeneous state. Units indicate the relative change in its density. Remarkably, only 30% of the debris was washed onshore during the first decade; 70% remains in the ocean and is largely controlled by convergent, wind-driven Ekman currents. Calculations show that before the diffusion starts dumping the extremes, the maximum density occurs in the five subtropical gyres and varies from 15 times the original density in the North Atlantic and South Indian Ocean to 30 times in the South Atlantic, to 45 times in the North Pacific, and to 150 times in the South Pacific. While the convergence of debris in the North Pacific has been recently identified with a giant patch of floating plastic, the model revealed that the strongest convergence is in the South Pacific. Despite its vicinity to Easter Island, this patch has not yet been detected. [N. Maximenko (IPRC)]

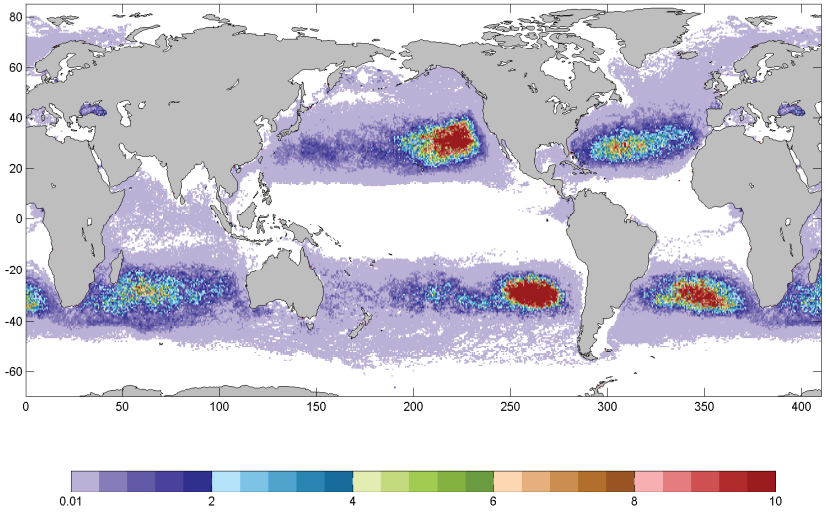

Figure 1.12. Relative change in buoyant tracer density after 10 years of evolution from a homogeneous state.

REGIONAL-OCEAN INFLUENCES (THEME 2)

The research objectives under this theme are aimed at investigating oceanic phenomena in the western Pacific Ocean, its marginal seas, and the connections between the Pacific and Indian oceans, which are known (or believed) to be important in the maintenance and variability of the large-scale oceanic gyres and climate. To address these objectives, during the past year IPRC researchers have analyzed a variety of data sources and model outputs to understand the climate impact of the South China Sea Throughflow and the monsoons of the Indonesian Seas, and they have studied aspects of ocean dynamics, particularly the energetics of flows. The following provides an overview of major activities and accomplishments during the past year.

Marginal Seas, Indonesian Throughflow, and Connections with Adjacent Oceans

Impact of South China Sea Throughflow on Makassar Strait transport. Transporting much heat from the Pacific Ocean to the Indian Ocean, the Indonesian Throughflow modulates the temperature and salinity distribution in the Indian and Pacific oceans with far-reaching impacts on climate. The major pathway of the Indonesian Throughflow, Makassar Strait, has a strong vertical shear, the maximum southward transport occurring at 160-m depth. Two experiments were conducted with the Modular Ocean Model version 3.0, which captures the major features of the Makassar Strait throughflow and the South China Sea Throughflow (SCSTF). In the *Control*, the SCSTF is allowed; in the *No South China Sea*

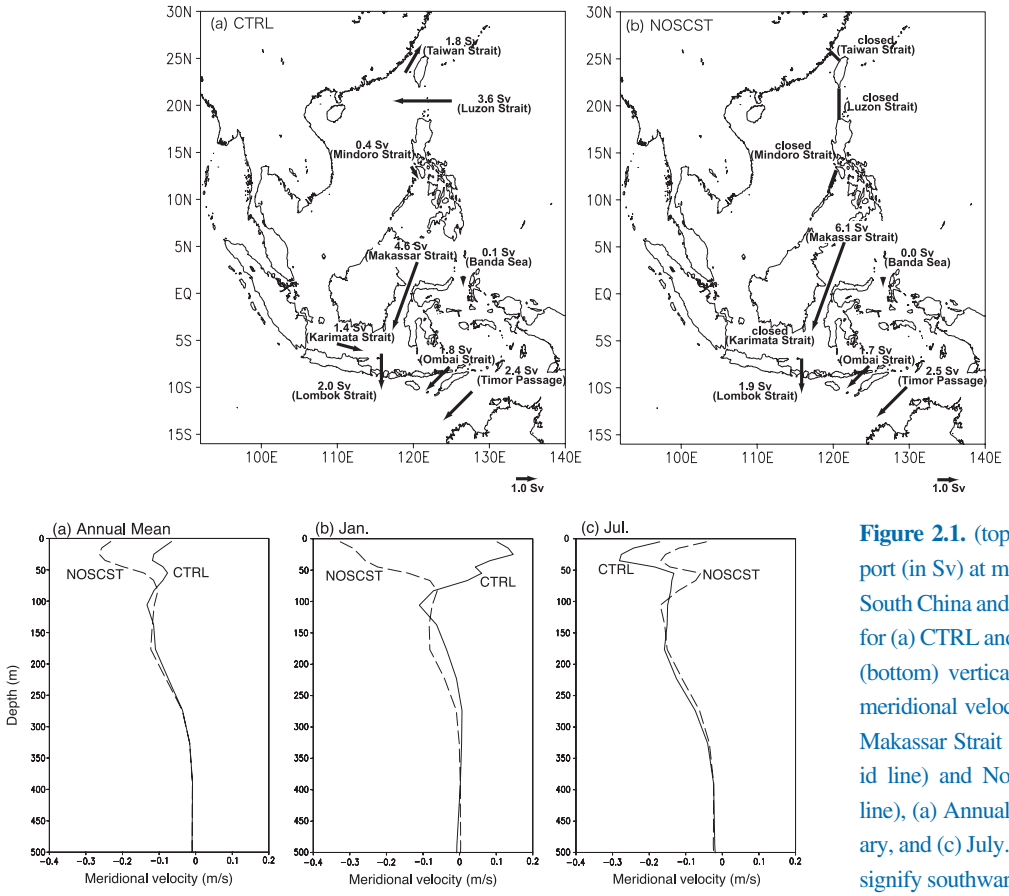

Figure 2.1. (top) Volume transport (in Sv) at major straits in the South China and Indonesian Seas for (a) CTRL and (b) No SCSTF; (bottom) vertical profiles of the meridional velocity at 3°S in the Makassar Strait for Control (solid line) and NoSCSTF (dashed line), (a) Annual mean, (b) January, and (c) July. Negative values signify southward flow.

Throughflow it is absent, the various straits in and out of the South China Sea being blocked. The control run reproduced the Makassar Strait vertical profile of velocity, the southward velocity increasing from the surface to 110-m depth and then decreasing again with depth. When the SCSTF is blocked, however, the maximum southward flow is at the surface and decreases to a negligible flow below 270 m. The experiments demonstrate the SCSTF impact on the Makassar Strait transport and its observed unusual vertical profile with subsurface maximum. When the SCSTF is blocked, the Makassar Strait transport-weighted temperature increases from 19.3°C to 21.4°C and the volume transport from 4.6 Sv to 6.1 Sv. This increase in volume transport and temperature results in a 0.18 petawatts increase in heat transported from the Pacific to the Indian Ocean through Makassar Strait. Furthermore, because the strength of the SCSTF varies with season (being strongest in boreal winter), the SCSTF contributes to seasonal variations in Makassar Strait transport. In summary, the results suggest that the SCSTF plays a more important role in regulating temperature patterns and climate variability in the Indo-Pacific Ocean than previously thought. [T. Tozuka (U. of Tokyo), T. Qu (IPRC), and T. Yamagata (JAMSTEC-FRCGC); T. Tozuka et al., 2007: Dramatic impact of the South China Sea on the Indonesian Throughflow. *Geophys. Res. Lett.*, **34**, L12612]

Monsoons shape the surface temperature patterns of the Indonesian Seas. The surface temperatures of the Indonesian Seas vary with the seasons from an average 27°C to 30.5°C. These seasonal fluctuations and their impact on tropical climate are important because atmospheric upward motions over this very warm body of water are among the strongest on Earth, supplying the large-scale atmospheric circulation with much heat and moisture. Analysis of TRMM observations shows the following annual pattern: temperatures averaged across the Indonesian Seas are near 30°C in November, then drop somewhat to February, rise again to over 30°C in March–April, and then drop to a minimum by August. The temperature changes, moreover, are not uniform: during the cool period temperatures drop more in the eastern half of the seas than in the western half, with a minimum of 25°C in the northeast corner. To understand how these seasonal sea surface temperature (SST) patterns come about, IPRC scientists have studied in a regional ocean model the monsoons' impact on the Indonesian Seas surface temperatures. The model captured the observed SST fluctuations well. Analysis of model results showed that the monsoons contributed to

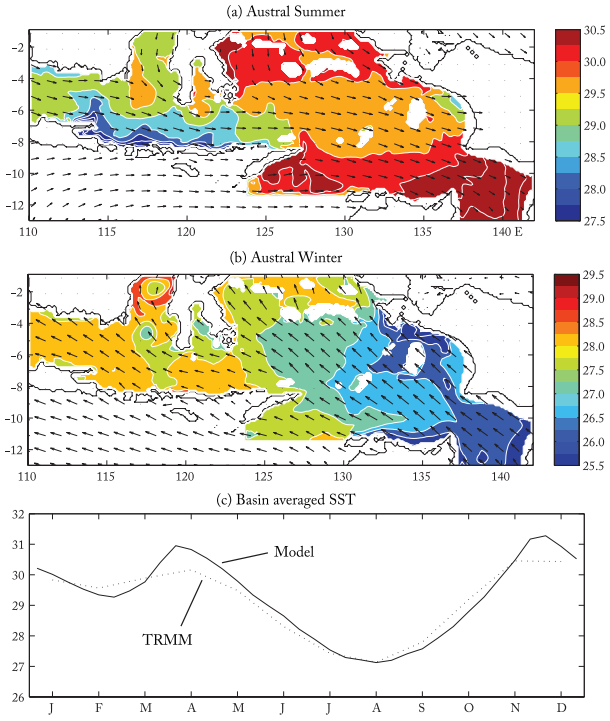

Figure 2.2. The SST simulated in the regional model: (a) Mean SST during January and February contoured every 0.25ºC. A cool SST region is observed north of Lesser Sunda Islands. The northwesterly wind (vectors) is roughly uniform over the basin. (b) Mean SST during July and August contoured every 0.25ºC. A cool SST region is observed to the east of the Indonesian Seas with minimum SST located in the northeast corner. The southeasterly wind has maximum wind speed at the southeast corner that extends northwest. (c) Seasonal variability of the spatially averaged SST (solid line) compares well with TRMM observed SST (dotted line). Largest difference is observed during Austral summer.

roughly half of the basin-averaged annual SST variance. (Seasonal variations in longwave and shortwave radiation and atmospheric temperature and humidity contributed to the remaining variance.) The spatial temperature patterns were traceable to the different behaviors of the southeasterly and northwesterly monsoons. The northwesterly monsoon blows uniformly over the Indonesian Seas, producing rather uniform surface temperatures with some moderate upwelling, and thus cooling, along the northern boundary of the Lesser Sunda Islands. (This upwelling may be partly responsible for the secondary SST minimum during February). The strength of the southeasterly monsoon, on the other hand, varies greatly with geography: it is strongest in the middle of the basin with its axis running from the southeast to the northwest. This pattern causes Ekman upwelling in the northern and downwelling in the southern regions, creating the observed SST pattern during June–August. The model furthermore showed that without the shallow shelf in the eastern region, the advection of the warm water from the west would trap the cold SST region only along the eastern boundary. [S. Kida and K. J. Richards (IPRC)]

Ocean Dynamics

Variability in circulation and mixing in the western equatorial Pacific. A predominant feature in the upper equatorial Pacific Ocean is the interleaving of water masses across the equator. Interleaving is thought to promote lateral mixing and impact the basin-wide dynamics of the equatorial ocean. To determine the impact of interleaving on the circulation, the velocity fields associated with interleaving structures are now being directly measured on two *R/V Mirai* cruises to the western equatorial Pacific. Analysis of data from the first cruise shows a clear signature of small-scale structures in the velocity field associated with similar sized structures in salinity. [K. J. Richards and A. Natarov (IPRC); Y. Kashino (JAMSTEC-IORGC)]

The next step is to study interleaving and its impact on tropical basin flows in the Ocean General Circulation Model for the Earth Simulator (OFES), where inertial instabilities have been found to induce small vertical scale features similar to interleaving [K.J. Richards and A. Natarov (IPRC); H. Sasaki (JAMSTEC-ESC)]. The OFES results will be compared with observations obtained on the cruise. In related work, the circulation patterns in OFES show considerable seasonal-to-interannual variations. These variations have a large impact on the heat budget of the mixed layer. [B. Taguchi and H. Sasaki (JAMSTEC- ESC); and K. J. Richards (IPRC)].

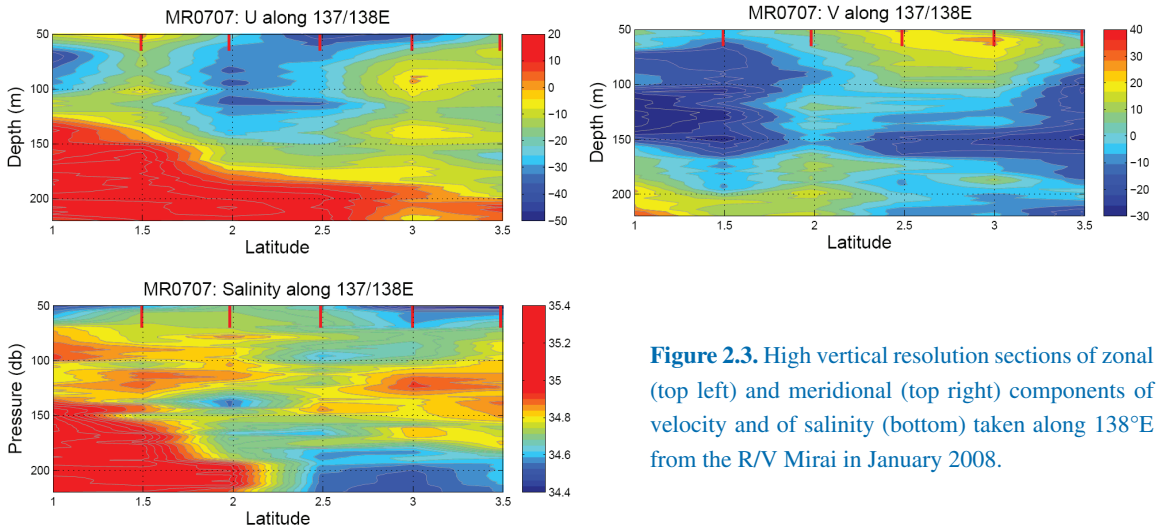

Figure 2.3. High vertical resolution sections of zonal (top left) and meridional (top right) components of velocity and of salinity (bottom) taken along 138°E from the R/V Mirai in January 2008.

The effect of mesoscale eddies on the energetics of ocean circulation. To understand the impact of mesoscale eddies on the strength of the global ocean circulation, the energy conversion due to layer-thickness form drag – the vertical redistribution of the geostrophic momentum by the residual effects of pressure perturbations – was calculated in outputs from the Ocean General Circulation Model for the Earth Simulator (OFES) at 0.1°× 0.1° resolution. While classical analysis of the energetics of flows has not captured the role of layer-thickness form drag, the use of equations in density space in this study enabled for the first time the determination of the global oceanic distribution of layer-thickness form drag. The analysis in density space resolves a debate on the dynamics of the Antarctic Circumpolar Current: results show that the layer-thickness form drag reduces (and thereby cancels) the vertical shear resulting from the eddy-induced overturning circulation rather than the vertical shear resulting from the surface wind stress. This finding rejects the hypothesis presented in previous studies that form drag transfers the wind-induced momentum at the sea surface to bottom layers. The finding also provides direct evidence of some characteristics of layer-thickness form drag that had been proposed by Aiki et al. *GRL*, 2004 in their parameterization of mesoscale eddies for coarse resolution ocean general circulation models. This improved understanding of layer-thickness form drag has led to the inclusion of this parameterization scheme as an option in the latest version of Geophysical Fluid Dynamics Laboratory's Modular Ocean Model [H. Aiki and K. J. Richards (IPRC); H. Aiki and K. J. Richards: Energetics of the global ocean: The role of layer-thickness form drag. *J. Phys. Oceanogr.*, in press]

Comparative study of the energetics of monsoon western boundary currents. As an extension of the above study on the energetics of the global ocean, an analysis was conducted of the energetics of the Vietnam current in the output of OFES run at 0.1°× 0.1° resolution. The analysis focused on the vertical mixing of momentum by mesoscale eddies (based on the formulation of Aiki and Yamagata, 2006). To examine the effect of bottom topography, a 4dVar barotropic ocean model has been developed to as-

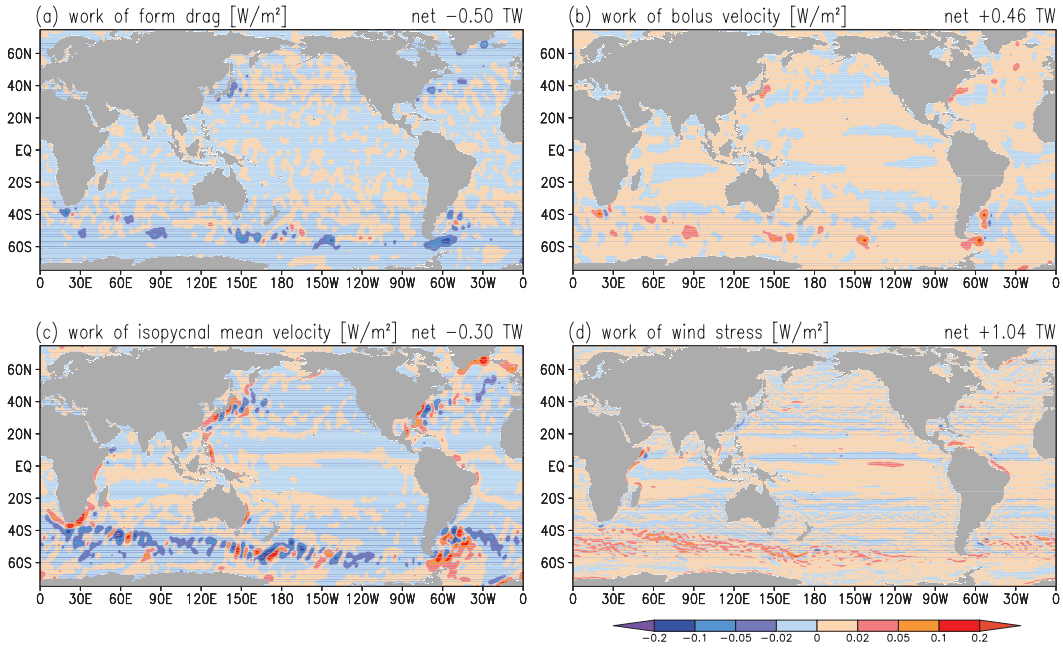

Figure 2.4. Depth integral of the work (energy conversion rate, W/m^2) caused by (a) layer-thickness form drag (momentum redistribution), (b) bolus velocity (eddy-induced overturning circulations), (c) isopycnal mean velocity (Ekman transport), and (d) wind stress. The sign is relative to the budget of mean kinetic energy. The net value over the global ocean is calculated for each quantity with 1 TW (a terawatt) = 10^{12} W.

similate the joint effect of baroclinicity and relief (JEBR) in and around the South China Sea. [H. Aiki and J. P. McCreary (IPRC); T. Yamagata (JAMSTEC-FRCGC)]

Eddy formation in the lee of the Hawaiian Islands. The study of eddy formation and propagation in the Hawaiian region is relevant because mesoscale cyclonic eddies bring nutrient-rich water at depth to the euphotic zone and enhance primary production in a region of generally low productivity in the subtropical gyre. As the northeasterly trade winds flow around the high mountains of the Hawaiian Islands, they create regions of weak wind leeward of the islands and strong wind funnels between the islands. These local wind variations are a major forcing mechanisms for the generation of the lee Hawaiian cyclonic and anticyclonic ocean eddies.

To investigate how the trade winds generate these eddies, experiments were conducted with the Regional Ocean Modeling System (ROMS) using wind products of different spatial and temporal resolutions as follows: a 3-day running mean of the QuikSCAT product at daily intervals for 2005, and monthly averages of (1) COADS wind at 0.5° resolution, (2) gridded QuikSCAT product at 0.25° resolution, and (3) a blend of the QuikSCAT product for the open-ocean region, and the output of a mesoscale atmospheric model, MM5 (whose domain is the state of Hawai‘i at 9-km resolution), for the near-shore region. The monthly averages were compiled with data for 2004–2006. Each product was used repeatedly for 8 model years in the experiments.

The experiments show that higher spatial and temporal resolutions of wind forcing substantially affect the vorticity and deformation field in the immediate lee of the Hawaiian Islands and produce patterns of eddy kinetic energy similar to observations (Figure 2.5 upper panel), whereas lower spatial climatological forcing usually results in low eddy kinetic energy (Figure 2.5 lower panel). This suggests that the surface eddy field in the region is mostly due to the local surface momentum forcing. Of interest for biological production, the modeled cyclonic eddies resemble well the observations in both spatial structure and intensity. As in observations, the model cyclonic and anticyclonic eddies forming in the lee of the Hawaiian Islands have different propagation patterns: the cyclones tend to stay near the island chain and are broken down into filaments of positive vorticity by the exterior deformation field and local wind anomalies; the anticyclones propagate in a predominately westward direction and stay coherent

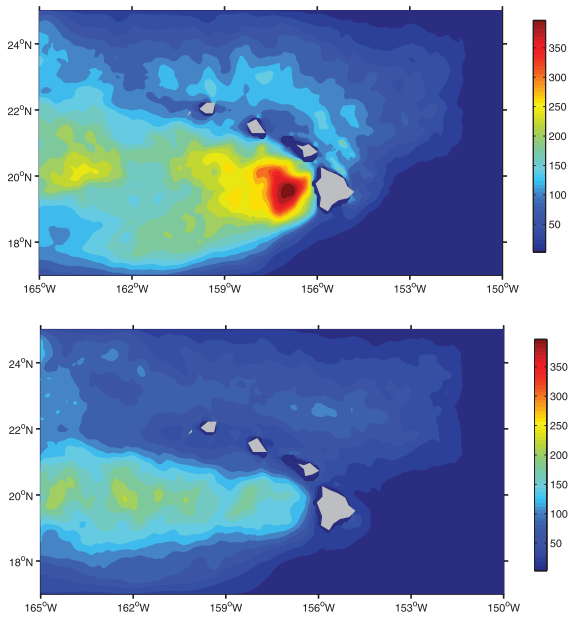

Figure 2.5. Eddy kinetic energy from the experiment forced with the blended wind of QuikSCAT and MM5 (upper panel) and with COADS winds (lower panel).

for a long distance. The local wind anomalies are a necessary but not sufficient factor for generating the Hawaiian lee eddies. For example, during summer months the trade winds tend to be stronger over Hawai‘i, giving rise to stronger local wind anomalies; yet there is no conclusive evidence that eddies are generated more frequently during summer. Future efforts will investigate the physical mechanisms generating the lee Hawaiian eddies. [P.H.R. Calil (U. of Hawai‘i); K. J. Richards, and Y. Jia (IPRC); and R.R. Bidigare (U. of Hawai‘i); P.H.R. Calil et al.: Eddy activity in the lee of the Hawaiian Islands. *Deep-Sea Research Deep-Sea Res. II*, in press]

Impact of weak and strong lateral mixing on Kuroshio Path trigger. Study of the Kuroshio paths and the trigger for its large meander continues. Detailed analysis of the underlying potential vorticity variations found that quasigeostrophic scaling is inappropriate because the horizontal component of relative vorticity impacts the current itself and contributes as much to potential vorticity as the curvature of the undulating Kuroshio path. Given this finding, the low frequency dynamics of the Kuroshio are tied to the anticyclonic recirculation gyres, the latter impacting both shear vorticity and vortex stretching through divergence of the ageostrophic flow. Overall, the study concludes that with sufficiently strong mixing, the system of the Kuroshio and its recirculation gyres is in a steady state and that upstream perturbations are the primary trigger for changing the Kuroshio path. With weak lateral mixing, as in OFES, the Kuroshio and eddies supply the low potential vorticity that leads to the growth of the anticyclonic recirculation gyres and the timescale of the latter determines the Kuroshio path fluctuations. [N. Schneider (IPRC), B. Qiu (UH), and H. Sasaki (JAMSTEC-ESC)]

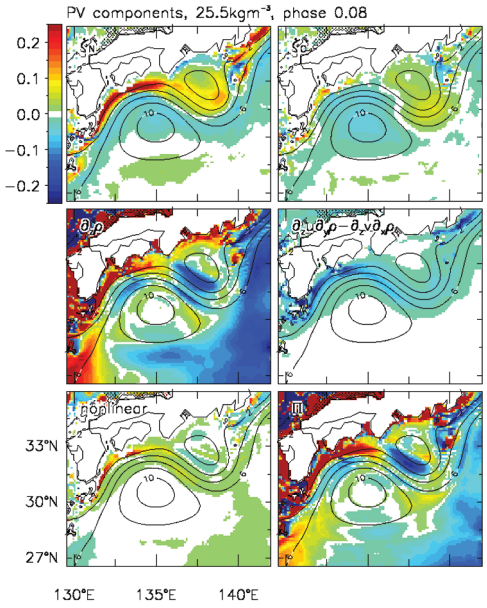

Figure 2.6. Potential vorticity components on the 25.5 σ_θ isopycnal surface for a particular phase of the Kuroshio Large Meander. Shown are the relative vorticity in flow-following coordinates due to lateral velocity shear (top left) and the curvature of the flow (top right), due to vortex thickness (middle left) and vortex tilt (middle right), and due to nonlinear terms (bottom left). Total potential vorticity is shown in the bottom right. All terms are normalized by typical values of the Coriolis frequency and stream-function-dependent buoyancy frequency. The Montgomery stream function is shown as contours on all plots.

Heat flux and cloud formation over the Kuroshio Extension. Heat flux measurements taken during the atmospheric soundings of the 2005 summer cruise in the Kuroshio Extension reveal cloud-regime shifts associated with changes in wind direction. When the winds blow from the south, sea fog tends to form over the Kuroshio Extension as the near-surface atmosphere becomes stable; when the winds blow from the north, stratocumulus tends to form. The Kuroshio Extension front amplifies the atmospheric thermal advection. [Y. Tanimoto (Hokkaido University), and S.-P. Xie (IPRC)]

ASIAN-AUSTRALIAN MONSOON SYSTEM (THEME 3)

Asia-Pacific climate is defined largely by the Asian-Australian monsoon system, the most energetic monsoon system on Earth. This system is driven by complex interactions among air, sea, and land processes over a vast area extending from Africa to the western Pacific and from Australia to Siberia. Research under this theme aims to determine the processes responsible for the variability and predictability of this climate system and its hydrological cycle. The section below summarizes the major IPRC research achievements under this theme during the past year.

Monsoon Diurnal Cycle

The monsoon diurnal cycle is an important component of Earth's climate system. At IPRC, scientists have been analyzing satellite and other data sets to study and quantify these basic cycles in order to understand better their impact on climate and climate variability and to establish metrics for assessing how well these cycles are being simulated in numerical weather and climate models.

Global regimes of the daily tropical rainfall cycle. To provide a unified view of the daily tropical rainfall cycle and a standard for evaluating the performance of computer climate models, IPRC scientists analyzed the 24-hour cycle of rainfall in the tropics using two complementary TRMM datasets (3B42 and 3G68) for the 1998–2006 period. The first two principal EOF modes (Figure 3.1, left panels), which account for about 90% of the daily rainfall variance, reveal three diurnal patterns of peak rainfall times and the propagation characteristics: (1) the oceanic pattern depicted by negative EOF_1 shows an early morning peak in rainfall (6~9 local standard time, LST); (2) the continental pattern, depicted by the combination of positive EOF_1 and EOF_2, shows an afternoon peak (15~18 LST); and (3) the coastal pattern, depicted by a complex combination of EOF_1 and EOF_2, shows strong rainfall movements, either onshore or offshore.

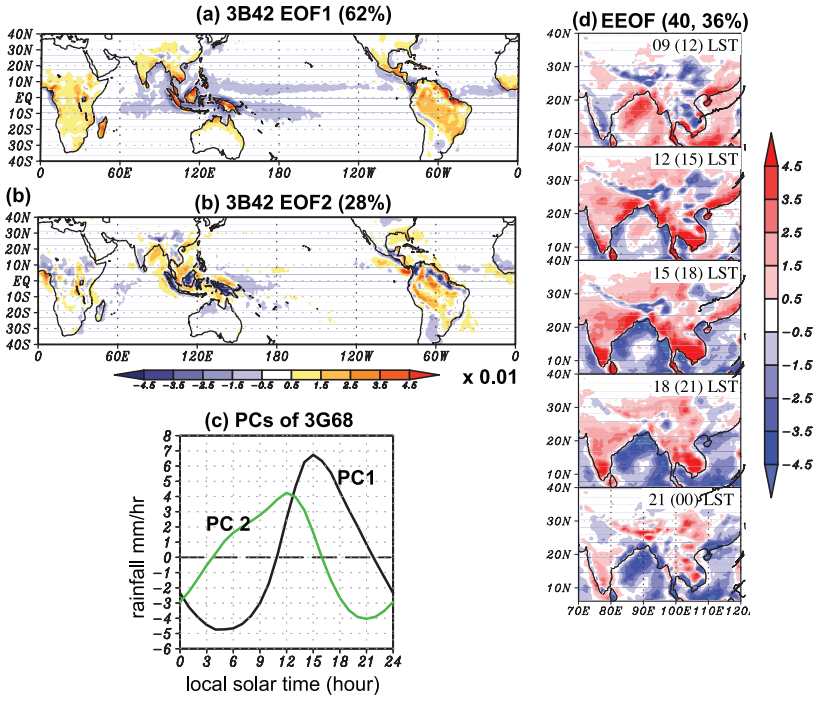

Figure 3.1. EOF analysis of the annual mean diurnal cycle derived from the precipitation TRMM 3B42 data set for the period of 1998–2006, (a) horizontal distribution of EOF_1, (b) EOF_2, (c) time series of the PC1 and PC2. The horizontal resolution of the data from which the EOFs are calculated is 1.5° x 1.5°; (d) evolution of precipitation represented by the combination of an extended EOF_1 and extended EOF_2 for South Asia. The corresponding modified (unmodified) local standard times are shown at the right corner of each subpanel.

In the coastal onshore cycle (shown in Figure 3.1d), a drizzle, for example, sets in along the coastline of India and Indochina at 9 LST and then becomes stronger and moves inland around noon (12–15 LST), peaking around 15 LST. Finally, the rain stops farther inland around 21 LST. In the coastal offshore cycle, rain tends to start near the coast around midnight, expand over the ocean to 12 LST, and then disappear between 12 and 15 LST. [K. Kikuchi and B. Wang (IPRC); K. Kikuchi and B. Wang: Diurnal precipitation regimes in the global tropics. *J. Climate*, in press]

Monsoon Intraseasonal Variation

The summer monsoon over Asia is characterized by alternate wet and dry phases called the *intraseasonal oscillation* (ISO). These phases impact life, particularly agriculture. Understanding the processes that produce such an oscillation in rainfall has been a research focus at the IPRC. Several satellite data analyses and modeling studies were conducted this past year to understand and predict the phases of the ISO better.

Air-sea interaction and the summer monsoon oscillation. The effect of air-sea interaction on the propagation and variance of the 30-to-50-day intraseasonal oscillation was studied by comparing the wavenumber frequency analyses from two parallel 70-year integrations with the SINTEX-F model. In the *control* run, the Indian, Pacific, and Atlantic oceans were coupled to the global atmosphere. In the *sensitivity* run, the atmosphere was decoupled from the tropical Indian Ocean and the model driven with climatological sea surface temperature from the control run. Compared with the uncoupled Indian Ocean run, air-sea coupling over the Indian Ocean in the control run enhanced rainfall variance in the northward-propagating disturbance, while it reduced rainfall variance in the southward-propagating disturbance and in the stationary wave (Figure 3.2). The findings are consistent with observations: the northward moving disturbance is the strongest and the southward moving disturbance is the weakest. [X. Fu and T. Li (IPRC); J. J. Luo and T. Yamagata (FRCGC-JAMSTEC)]

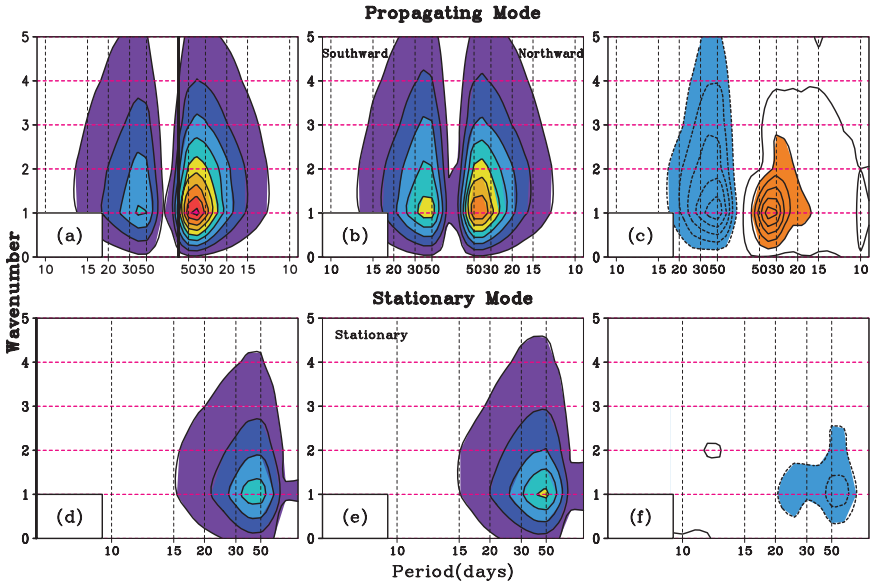

Figure 3.2. The wavenumber-frequency spectra from SINTEX-F: top panels show the meridional propagating ISO mode: (a) control run, (b) decoupled Indian Ocean run and (c) difference (a minus b); bottom panels show the stationary ISO mode: (d) control, (e) decoupled, and (f) difference (d minus e). The contour interval is 2 $(mm/day)^2$ for the left and middle panels and 0.5 $(mm/day)^2$ for the right panels.

Ocean influence on summer monsoon rainfall. The summer monsoon rainfall oscillation with a 30-to-50-day period has been thought to be due to internal atmospheric dynamics. IPRC scientists, however, have analyzed satellite data – QuikSCAT wind and TRMM Microwave Imager sea surface temperature and rainfall – and noted that the southwest summer monsoon induces upwelling filaments off the South Vietnamese coast (Figure 3.3), leading to a basin-wide cooling of the South China Sea. This cooling, in turn, affects the atmosphere. Locally, the cooling weakens the southwesterly winds, possibly through vertical mixing. Regionally, it suppresses atmospheric convection. Of much higher spatial resolution than traditional climate data, these new observations reveal much larger ocean temperature variability than previously thought and suggest that the ocean modulates the intraseasonal rainfall variability over the South China Sea during summer. The findings once more point out that taking into account the ocean's impact on the atmosphere may improve summer rainfall forecasts over the monsoon regions. [S.-P. Xie (IPRC); C.-H. Chang (U. of Hawai'i); Q. Xie and D. Wang (South China Sea Institute of Oceanology); S.-P. Xie et al., 2007: Intraseasonal variability in the summer South China Sea: The wind jet, cold filament, and recirculations. *J. Geophys. Res.-Oceans*, **112**, C10008]

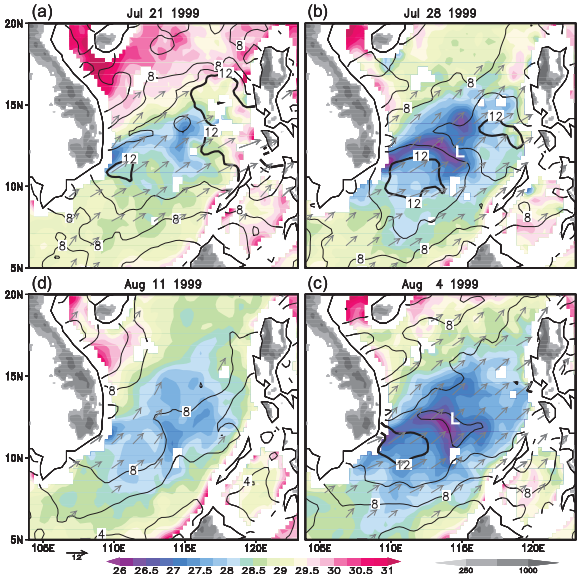

Figure 3.3. A summer intraseasonal event from 21 July to 11 August, 1999. The evolution of the cold filament (SST in °C, color shading), and surface wind speed (m/s, contour). The gray shading indicates mountains 250 m and taller. The vector indicates surface wind greater than 4 m/s. Local wind-speed minimum over the cold filament is marked with a white *L*.

Intraseasonal teleconnection between the Indian summer monsoon and midlatitude wavetrain. IPRC scientists noted in NCEP–NCAR reanalysis data that a Rossby wave train moving at midlatitude across the Eurasian continent during summer is associated with the monsoon convection over northwestern India and Pakistan (referred to here as Indian summer monsoon). During strong convection and rainfall over the Indian summer monsoon region, anomalous high pressure is seen over central Asia and over northeastern Asia (Figure 3.4a). These high pressure regions are accompanied by increased rainfall over the western Siberian plain and northern China and decreased rainfall over the eastern Mediterranean Sea and southern Japan. Further analysis shows that this wave train originates over the northeastern Atlantic and traverses Europe to central Asia (Figure 3.4b). The wave train enhances upper-level high pressure and reinforces Indian summer monsoon convection; meanwhile, it propagates toward East Asia along the westerly jet waveguide. The southeastward propagation of the European wave train is thought to contribute to the Indian summer monsoon intraseasonal rainfall variability by changing the intensity of the monsoonal easterly vertical shear and the associated moist dynamic instability. These changes, in turn, are thought to affect the central Asian high through the "monsoon–desert" mechanism, thus reenergizing during strong convection the downstream propagation of the wave train. Taking this

hypothesized coupling between the Eurasian wave train and the Indian summer monsoon into account may improve prediction of intraseasonal rainfall variations during both the Indian and the East Asian summer monsoon. [Q. Ding and B. Wang (IPRC); Q. Ding and B. Wang: Intraseasonal interaction between the Eurasian wavetrain and the Indian summer monsoon. *J. Climate*, **20**, 3751–3767]

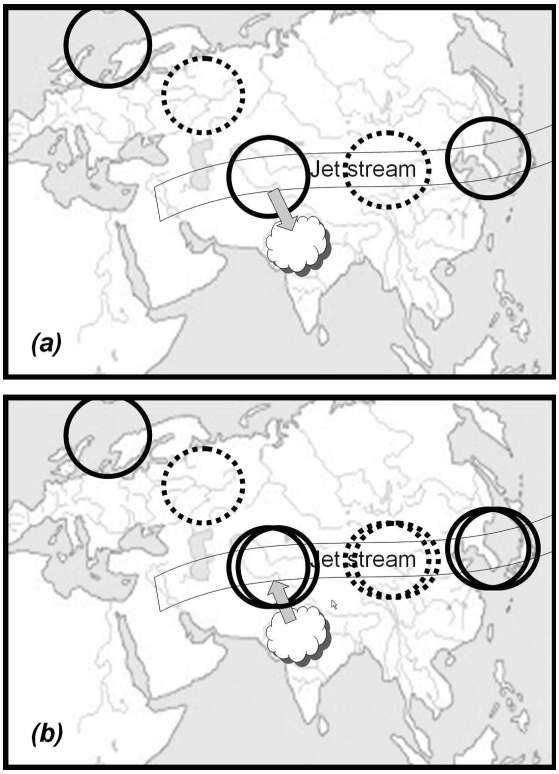

Figure 3.4. The schematic illustrates the hypothesized positive feedback between the Eurasian wave train and the Indian summer monsoon. The cloud denotes strong convection and the circles the Eurasian wave train in the upper troposphere. The solid and dashed circles represent respectively high- and low-pressure regions. The anomalous central Asian high within the wave train triggers the strong convection over the northern Indian summer monsoon region (a), which excites a Rossby wave response that strengthens the central Asian high and downstream wave train (b).

Studies of the Madden–Julian Oscillation. The Madden–Julian Oscillation (MJO) is a tropical convective disturbance of the large-scale circulation that impacts weather around world. Because the MJO recurs with a period of 30 to 60 days, predicting accurately its phases would extend conventional weather forecast beyond the usual one week. Atmospheric general circulation models (AGCMs), however, have had difficulty simulating the MJO. Higher model resolution was thought to be needed to improve the simulation. The Japan Meteorological Research Institute has recently produced a high-resolution version of its AGCM that can be run at 20-km horizontal resolution and with 60 vertical levels. An analysis at the IPRC calculated the characteristics of the mean states, power spectra, propagation features, leading EOF modes, vertical structure, and seasonality associated with the MJO in the model. Using the well-known Arakawa-Schubert convection scheme, the model produces long-term-mean winds that compare well to a reanalysis product. The model, however, does not yield a realistic MJO. At the 30-to-60-day band, the simulated MJO has low amplitude and an almost standing structure (Figure 3.5 bottom right) compared to the observed eastward propagation (top right). Further analysis shows that the weak and standing MJO is attributable to convection biases. The vertical structure of the increased moisture does not show the observed westward tilt, which indicates that increased boundary-layer moisture does not lead convection in order to induce eastward propagation. These results suggest that increasing the resolution of an AGCM does not guarantee realistic simulation of the MJO. [P. Liu, Y. Kajikawa, B. Wang (IPRC); A. Kitoh (Japan Meteorological Research Institute); T. Yasunari (Nagoya University), T. Li (IPRC), and others]

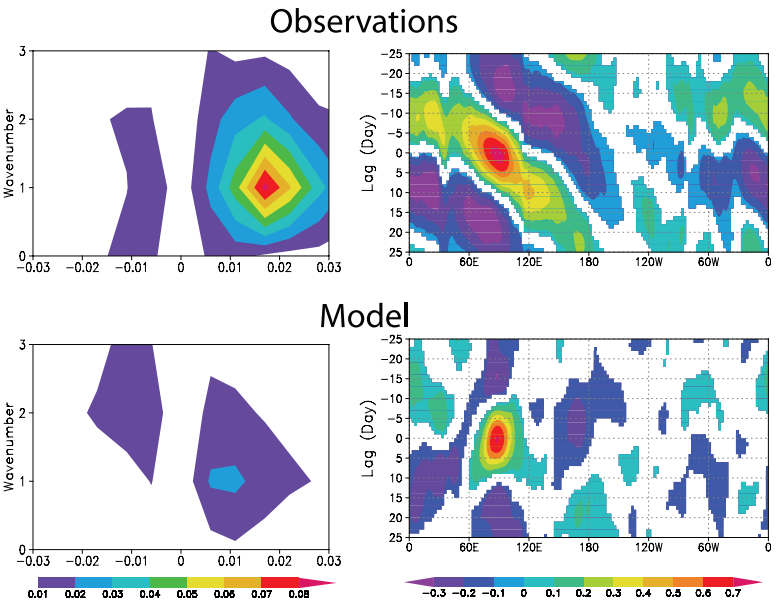

Figure 3.5. Comparison of MJO characteristics in observations (top panels) and in the high-resolution version of the AGCM of the Japan Meteorological Research Institute (bottom panel). Left panels show power spectra in 850-hPa zonal wind, and right panels lag regression of OLR onto 90°E, 0°N during boreal winter.

Taking a different approach to understanding and predicting the MJO, IPRC scientists developed the IPRC Hybrid-coupled General Circulation Model and have applied the model to "forecast" observations taken during the 4 months of TOGA-COARE in 1992–1993. The model was initialized with observations taken on January 1, 1993, and then let run for two months without any further input. A comparison between daily observed rainfall (Figure 3.6, left) and the daily rainfall of a 100-ensemble-mean (right) reveals that the model was able to "forecast" beyond one month fairly accurately the eastward movement and associated rainfall of the MJO. [X. Fu, B. Wang, B. Qing, P. Liu, and B. Yang (IPRC)]

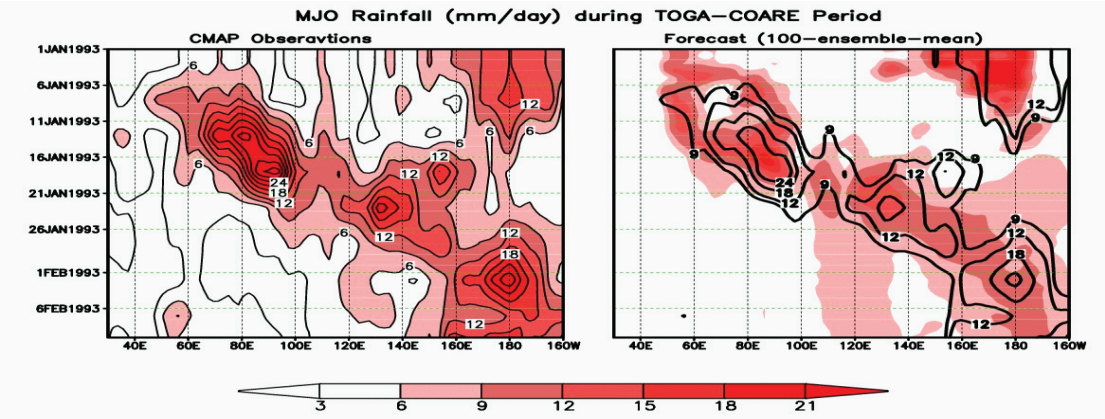

Figure 3.6. Observed (left) and forecast (right) rainfall (mm/day) averaged over 10ºS–10ºN. Selected observational contours have been overlaid on the forecast in the right panel.

In another MJO study, IPRC scientists used TRMM satellite data (2A23) to map the "storm height population" (the percentage of cloud-tops at different heights) for regions where the MJO has been shown to impact rainfall. The mapping revealed that convective clouds of the MJO differ depending upon where they form (Figure 3.7). Over the open Indian Ocean and the western Pacific, two sets of clouds form as the MJO develops (before day 0 in the figure). The lower clouds are most likely stratocumulus and the higher ones congestus. This finding is consistent with previous studies. Over the maritime

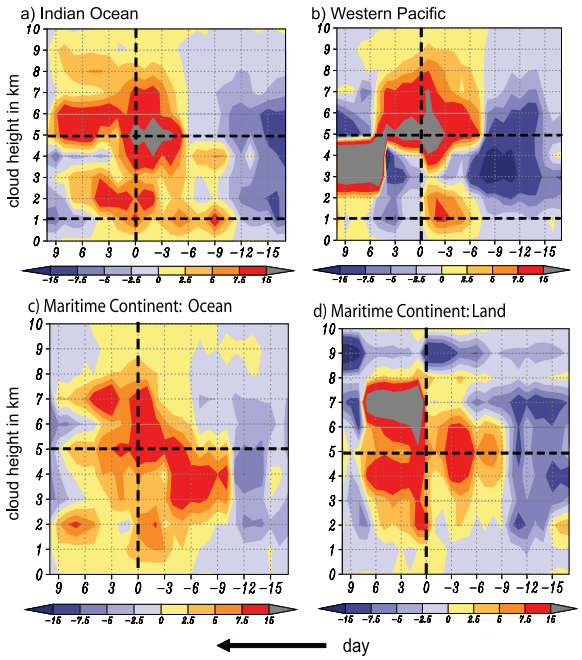

Figure 3.7. Percentage of cloud pixels as a function of height in a 1x1° reference area taken from TRMM precipitation data for (a) Indian Ocean, (b) western Pacific, (c) Maritime Continent Ocean, (d) Maritime Continent Land.

continent land, however, no low clouds seem to form during this stage. This lack may hold the clue to such baffling questions as to why convection associated with the MJO is weaker and its phase speed faster over the maritime continent than over the open ocean. [K. Kikuchi and B. Wang (IPRC)]

Effect of Land Processes on the Monsoon

Tibetan Plateau snow and East Asia summer monsoon rainfall. Recent studies have shown that the Eurasian snow amount in spring can significantly affect the following East Asia summer monsoon (EASM) rainfall. The initial Eurasian spring snow amount in numerical climate model simulations may therefore be critical to their successful seasonal prediction of EASM rainfall. Because of the lack of direct measurement of snow amount on the Tibetan Plateau, IPRC scientists used satellite-derived snow-water-equivalent data (SWE) to initialize the snow amount in a simulation with the IPRC Regional Atmospheric Model (iRAM) in order to assess its impact on EASM rainfall. They carried out two ensemble simulations for the March–August 2005 period: for the *SAT* ensemble runs, they initialized iRAM with the March SWE derived from AQUA AMSR-E; for the *SPN* ensemble runs, they spun up iRAM from November 2004 to March 2005. The amount and spatial distribution of the simulated rainfall resembled satellite observations more closely in the *SAT* run than in the *SPN* run, the latter greatly underestimating the March SWE over the Tibetan Plateau. A detailed analysis of the two ensemble runs showed that the higher initial SWE in the *SAT* run increased surface albedo. The increase in albedo reduced surface heating over the Tibetan Plateau, cooled the near surface air (Figure 3.8a), raised 700-hpa geopotential height (Figure 3.8b), and lowered 200-hpa geopotential height (Figure 3.8c). The result was that the *SAT* ensemble runs simulated less rainfall in most of China than the *SPN* ensemble runs, except in southern China, where more rainfall occurred (Figure 3.8d). Variations in snow coverage over the Tibetan Plateau, therefore, can contribute to variations in monsoon rainfall over China and intializing models with satellite-derived SWE is likely to improve the rainfall simulation of the East Asia summer monsoon. The terrible flooding in southern China in that summer of 2005 can be linked, according to this study, to the large amount of spring snow on the Tibetan Plateau. [K. Souma and Y. Wang (IPRC)]

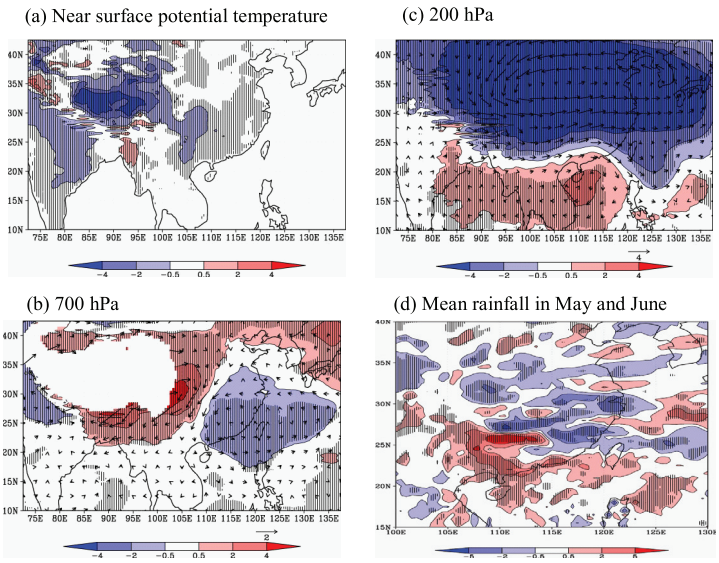

Figure 3.8. May–June mean differences between SAT and SPN ensemble runs: (a) near surface potential temperature in K, (b) 700-hPa wiFigure 3.8. May–June mean differences between SAT and SPN ensemble runs: (a) near surface potential temperature in K, (b) 700-hPa wind vector (m/s) and geopotential height (gpm), (c) 200-hPa wind vector (m/s) and geopotential height (gpm), and (d) mean rainfall (mm/d). Hatching indicates regions significantly different at the 90% confidence level.

Tibetan Plateau topography and summer rainfall in China. Observational and modeling studies show that thermal and mechanical processes arising from the presence of the Tibetan Plateau impact the onset and evolution of the Asian and East Asian monsoons and their moisture transport and rainfall over China. Observational studies, furthermore, show that mesoscale convective cloud systems form over the Tibetan Plateau and move eastward and may contribute greatly to rainfall over the Yangtze River Valley. IPRC scientists and colleagues at the Chinese Academy of Meteorological Sciences examined whether the convective cloud systems are triggered by the heterogeneous topography and associated increase in sensible heat flux over the Tibetan Plateau. They simulated the 1998 summer monsoon season in China by running the Community Regional Climate Model version 3 under two conditions: in the *control* ensemble runs, the standard model settings were used with a 30-km-resolution; in the *smoothed* ensemble runs, the mesoscale topographical features of Tibetan Plateau were smoothed by using a

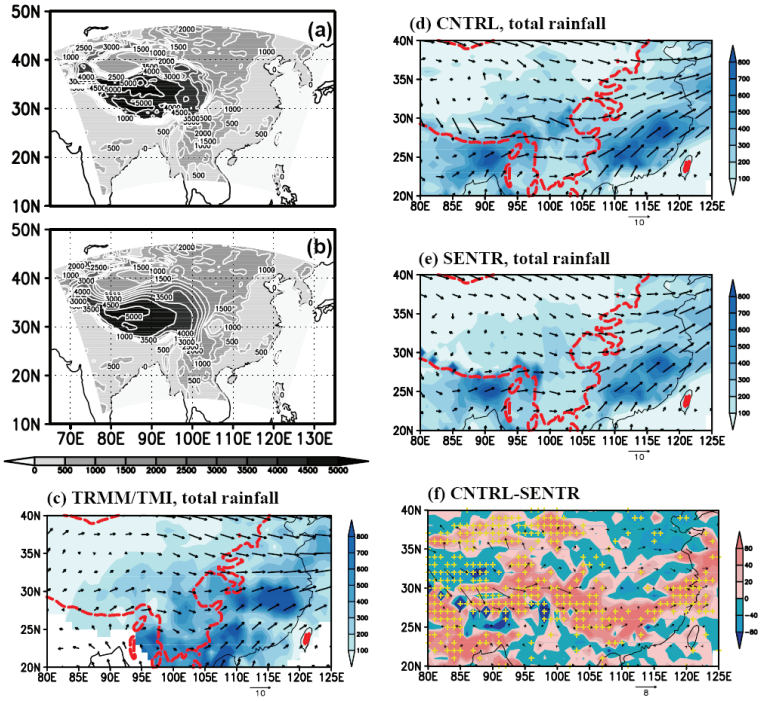

Figure 3.9. The model domain and orography in (a) control and (b) smoothed topography runs (contours: orography at 500-m intervals); spatial distribution of total rainfall in mm (shades) and 500-hPa wind in m/s (vectors) for June 12–July 31, 1998 in (c) observed (d) control run and (e) smoothed run; (f) the difference in total rainfall and 500-hPa winds between control and smoothed topography. The t dashed red curve shows the contours of 1000-m topography in (c) to (e). The "+"s in (f) indicate areas where total rainfall in the control and smoothed runs differs significantly at the 90% confidence level.

120-km resolution topography over the Plateau at elevations over 2000 km (Figure 3.9b). The control runs reproduced reasonably well the observed amount of rainfall in the Yangtze River Valley, while the smoothed runs considerably underestimated it (Figure 3.9c and d). Further analysis showed that the varied topography of the Tibetan Plateau triggered atmospheric disturbances, which over the Plateau increased surface sensible heat flux that moved eastward to trigger and increase convection and rainfall over the Yangtze River Valley (Figure 3.9e and f). The results point out that realistic simulation of the East Asian summer climate requires high-resolution general circulation models that resolve the Tibetan Plateau topography well. [X.-Y. Shi (CAMS), Y. Wang (IPRC), and X.-D. Xu (CAMS)]

Tibetan Plateau warming trend and increased rainfall in East Asia. An analysis of records from 90 weather stations shows that surface air temperatures averaged over the Tibetan Plateau have increased by about 1.8ºC between 1961 and 2007 (Figure 3.10). This represents a significantly larger increase than that reported in the Fourth Assessment Report of the Intergovernmental Panel on Climate Change. East Asian subtropical front rainfall has also been observed to increase significantly during this same period. In simulations with a numerical climate model, an increase in rainfall and a rainfall pattern similar to the one observed in East Asia emerged in response to warming on the Tibetan Plateau. In the model, the linking mechanism consists of two distinct Rossby wave trains and the isentropic uplift east of the Tibetan Plateau, which together deform the western Pacific Subtropical High and increase moisture transport toward the East Asian subtropical front (Figure 3.11). The model calculations suggest that the rise in Tibetan Plateau temperatures and in East Asian summer rainfall is linked, and that as Tibetan Plateau temperatures increase so will East Asian summer rainfall. [B. Wang (IPRC); Q. Bao (LASG); B. Hoskins (University of Reading); G. Wu and Y. Liu (LASG)]

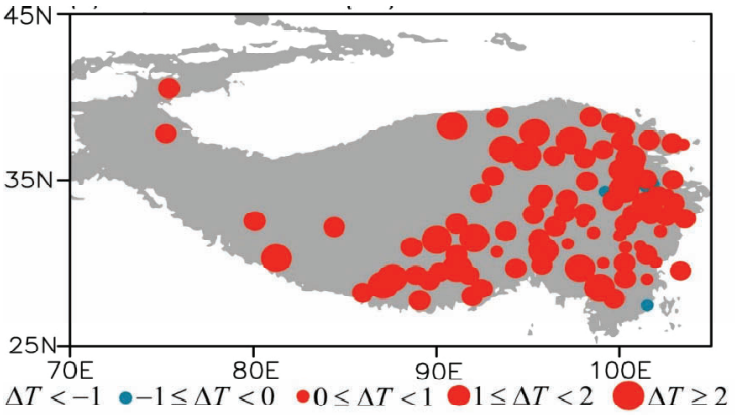

Figure 3.10. The linear trends in surface air temperature for the period 1961–2007 observed over 90 Tibet weather stations. The solid circles indicate the station locations and the shaded regions denote the areas with elevations over 2,500 m. The size of the circles represents the magnitude of the warming in ºC.

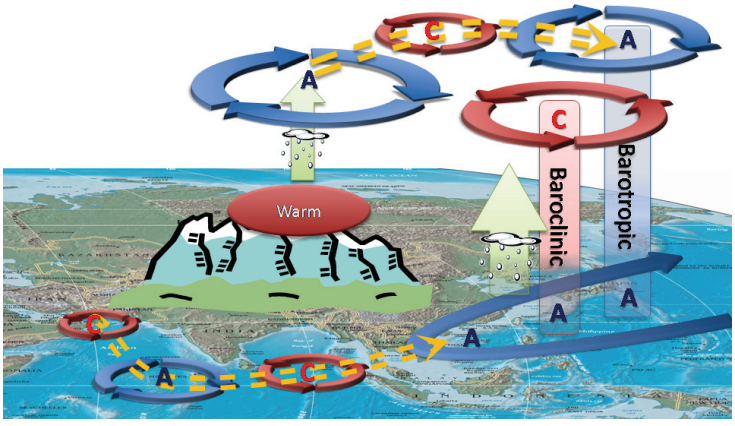

Figure 3.11. Schematic of the atmospheric response to the Tibetan Plateau warming and its impacts on East Asian summer monsoon rainfall through the generation of two Rossby wave trains. The letters A and C denote anticyclonic and cyclonic circulation centers, respectively.

Monsoon Year-to-Year Fluctuations

A unified index of East Asian summer monsoon strength. Basic to monsoon studies is the need for a clear definition of monsoon strength. Arriving at a definition that researchers agree upon, however, has been difficult for the East Asian summer monsoon (EASM). Therefore, in collaboration with the scientists at the Chinese Academy of Science Institute of Atmospheric Physics and Institute of Geography and Limnology, the Naval Postgraduate School, and the Chinese Climate Center, IPRC's Bin Wang, has proposed an index that represents the principal component of the leading mode of the interannual variance of the EASM. Figure 3.12 shows the spatial pattern and time evolution of this principal mode, which is associated with a decaying El Niño. The index highlights variations in the amount of Meiyu/Baiu/Changma rainfall. This represents an important change from the traditional Chinese meaning of a strong EASM, which refers to less Meiyu rainfall and more rainfall in northern China when southerly winds extensively penetrate northern China. The new definition, however, is consistent with those used for other monsoon regions, in which a strong monsoon is defined as significantly more rain than the mean monsoon rainfall of the major local rain-bearing monsoon system. [B. Wang (IPRC); Z. Wu, J. Li, and G. Wu (LASG); J. Liu (Nanjing Institute of Geography and Limnology); C.-P. Chang (Naval Postgraduate School); and Y. Ding (China National Climate Center); B. Wang et al.: How to measure the strength of the East Asian summer monsoon. *J. Climate*, in press]

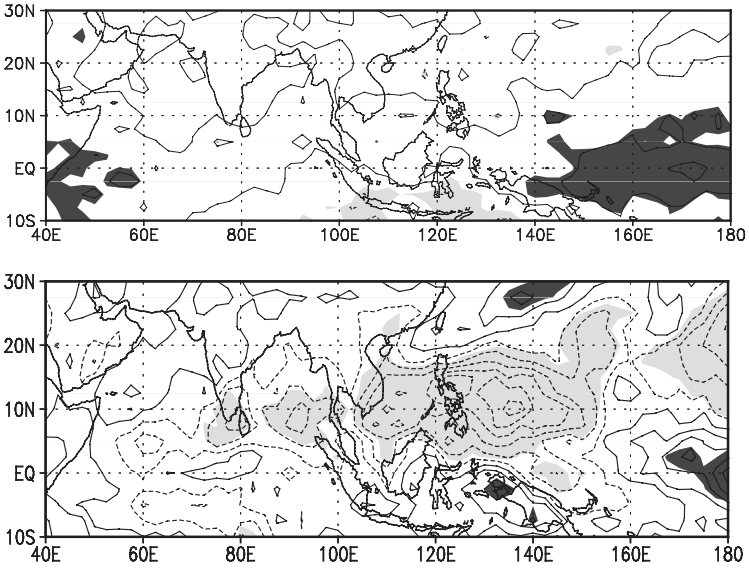

Figure 3.12. Composite differences in the intensity of the boreal summer intraseasonal oscillation (represented by the standard deviation of the filtered outgoing longwave radiation time series, in W/m^2) between (top) El Niño and La Niña developing summers and (bottom) El Niño and La Niña decaying summers. Shading indicates 95% confidence level.

Interannual and decadal variations in the summer western North Pacific Subtropical High. A power-spectral analysis of 48 years of monthly NCEP reanalysis of 500-hPa geopotential height showed that during summer the western North Pacific Subtropical High (WNPSH) has two dominant peaks—at 2.5 years and 3.6 years. In the 2-to-3-year oscillation, most evident after 1990, an enhanced WNPSH is associated in the maritime continent with unusually high sea surface temperature (SST) and strong convection that connects the local ascending motion to the descending motion in the subtropical Western North Pacific through an anomalous Hadley circulation. This oscillation is also associated with a shift from warm SST to unusually cold SST in the central to eastern equatorial Pacific that occurs from the preceding winter to the summer. In the 3-to-5-year oscillation, most evident during the 1980s, an enhanced WNPSH is associated over the maritime continent with anomalous descending motion and in the central-eastern equatorial Pacific with unusually high SST. These conditions persist from the preceding winter to

the summer. The complementary cooling and descending motion in the western Pacific are related to the anomalous east-west circulation associated with ENSO. [C.-H. Sui, P.-H. Chung (Taiwan National Central University); and T. Li (IPRC); C.-H. Sui et al., 2007: Interannual and interdecadal variability of the summertime western North Pacific subtropical high. *Geophys. Res. Lett.*, **34**, L11701]

Strength of the summer intraseasonal oscillation in relation to El Niño and La Niña phases. Analysis of outgoing longwave radiation shows that the boreal summer monsoon intraseasonal oscillation (ISO) differs significantly depending upon whether El Niño or La Niña is developing or decaying (Figure 3.12). During the summer of a developing El Niño, not only does the eastward propagation of the disturbance at the equator grow stronger than usual, but also its northward propagation over the western Pacific (East of 140°E). During the summer of a developing La Niña, the opposite takes place: the ISO equatorial eastward and the northward propagations both become weaker than usual. In contrast, during a decaying El Niño summer, the eastward propagation at the equator weakens, as do the westward propagation off the equator and the northward propagation over the South China Sea and the western Pacific. These movements grow stronger than usual during a decaying la Niña. [A. Lin and T. Li (IPRC)]

Moist teleconnection between the equatorial Indian Ocean and the South Asian monsoon trough. Over most of India, the June–September mean rainfall associated with the summer monsoon accounts for 70-80% of the total annual rainfall. During the rainiest months, July–August, regions along and slightly south of the monsoon trough (a low-pressure region whose axis runs through central India, Bay of Bengal, and the South China Sea) experience intense rainfall. An IPRC study investigated the moist

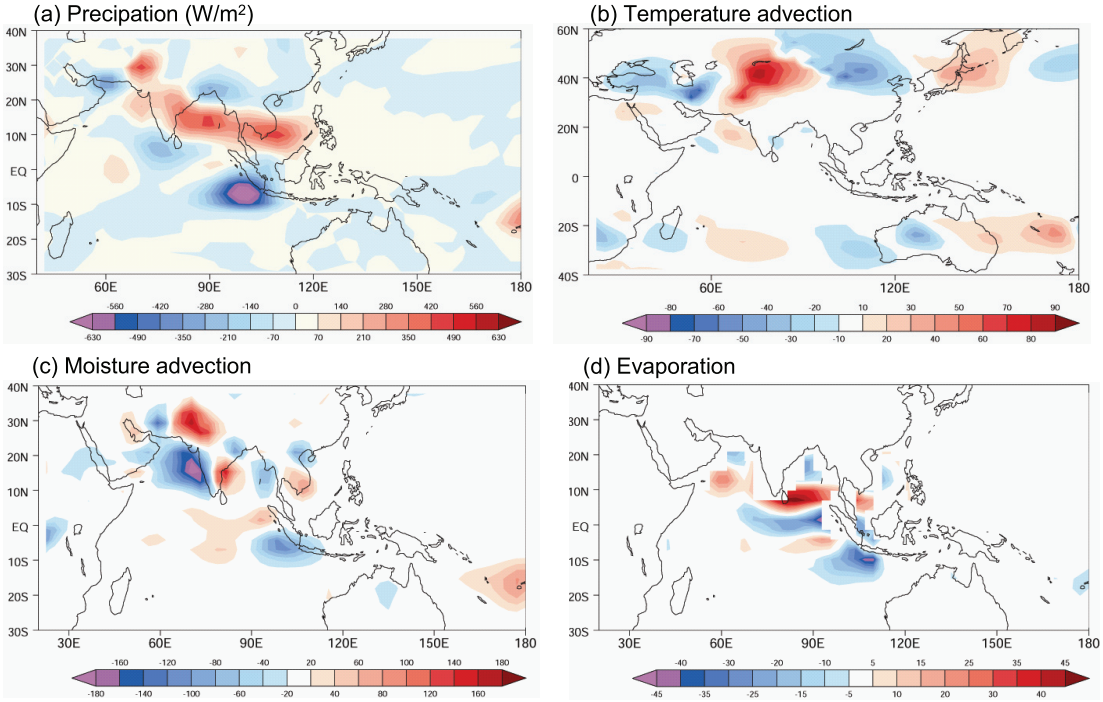

Figure 3.13. (a) The precipitation response to equatorial Indian Ocean SST forcing that corresponds to cold IODZM events illustrates the strengthening of rainfall along the monsoon trough in terms of the MSE budget; (b) temperature advection; (c) moisture advection, and (d) evaporation. The figures show that over the equatorial Indian Ocean and along the monsoon trough, advection of moisture dominates the MSE budget. All units are in W/m^2, but the scaling differs.

teleconnections through which variations in equatorial Indian Ocean sea surface temperature (SST) in July–August determine the anomalous rainfall along the monsoon trough. Because three dimensional moisture observations over the monsoon area are lacking and the moisture budget is not balanced in the NCEP-NCAR reanalysis, answers were sought in a set of solutions from climate models.

The 20th century integrations of the GFDL_CM2.1 coupled model during Indian Ocean Dipole Zonal Mode (IODZM) occurrences were analyzed so that the moist processes in the monsoon teleconnection forced by SST anomalies in the Indian Ocean could be determined without appreciable influence from Pacific SST. The obtained composite SST pattern during IODZM events was then used to force a linear baroclinic (LB) model, and the moisture and moist static energy (MSE) budget in the LB model solutions were analyzed. The moist static energy budget was also calculated for the GFDL composites. Both LB model and CM2.1 coupled model solutions show that (1) advection of moisture, in particular advection of the climatological moisture gradient by the anomalous winds, dominates the MSE budget over the equatorial Indian Ocean and along the monsoon trough and (2) these two regions are connected by a thermally direct over-turning mass circulation. Sensitivity experiments with the LB model demonstrate that the rainfall fluctuations along the monsoon trough are more closely related to SST variations over the equatorial Indian Ocean than to local SST anomalies over the Bay of Bengal and the South China Sea. The results imply that the processes identified operate at any time-scale, from seasonal to possible future climate changes, and that three-dimensional moisture observations over the monsoon area are necessary to monitor and predict variations in monsoon rainfall. [H. Annamalai (IPRC)]

Long-term Changes in the Monsoon

Variations in global monsoon precipitation over the last 1000 years. Last year's annual report described the emerging concept of *global monsoon*, a response of the coupled atmosphere-land-ocean-creosphere-biosphere system to annual variations in solar radiative forcing. Viewed in this way, the global monsoon can be quantitatively defined by the first two principal empirical orthogonal modes of the annual variation of global precipitation and low-level (850 hPa) winds, which, together, account for 84% of the annual variance. Applying this concept, IPRC scientists collaborated with scientists from the Nanjing Institute of Geography and Limnology, the Institute for Coastal Research, the GKSS Research Center, and the Harvard-Smithsonian Center for Astrophysics, in a study of centennial-to-millennial variations in the global monsoon precipitation in the ECGO-G coupled model. During the past 1000 years, the simulated global monsoon precipitation was weak during the Little Ice Age (1450–1850), the three weakest periods occurring around 1460, 1685, and 1800 (Figure 3.14e), which respectively fell into the Spörer, Maunder, and Dalton Minimum periods of solar activity (Figure 3.14a). Periods of strong global monsoon precipitation occurred during the model Medieval Warm Period (1030–1240). The sharp upward trend in the last century, particularly the notable strengthening of the global monsoon in the last 30 years (1961–1990), appears unprecedented and partly due to higher atmospheric carbon dioxide concentrations (Figure 3.14d). The millennium-scale variation and the quasi-bi-centennial oscillation in global monsoon precipitation is coherent with the thermal contrast between the Northern and Southern Hemispheres (Figure 3.14g), which also varies with solar radiative forcing (Figure 3.14c).

The integrated properties of the global monsoon precipitation can serve to link studies of paleo, modern, and future monsoons. Further research is required to understand the fundamental dynamics of the global monsoon system better and the similarities and differences among regional monsoons. [B. Wang and Q. Ding (IPRC); and J. Liu (Nanjing Institute of Geography and Limnology, CAS)]

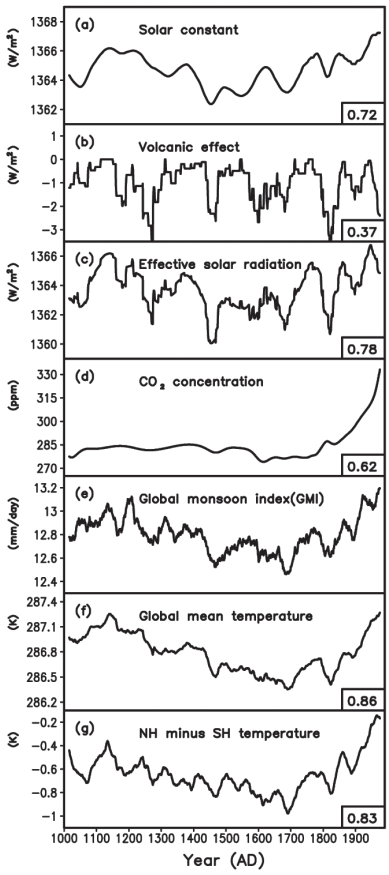

Figure 3.14. (a) Time series of solar radiative forcing (W/m^2), (b) volcanic effect (W/m^2), (c) effective solar radiation (W/m^2), (d) CO2 concentration (ppm), (e) global monsoon index (mm/day), (f) global mean temperature (K), and (g) inter-hemispheric temperature difference (K). All time series are 31-year running means from 1000 to 1990 AD simulated by ECHO-G model. The numbers shown in the lower-right corners indicate correlation coefficients of GMI with the four external forcing factors and two temperature indices, respectively.

The Asian-Australian monsoon system and its relation to ENSO. An empirical orthogonal function analysis that reveals seasonally dependent climate modes isolated two such modes in the NCEP–NCAR reanalysis 1956–2004 data set: (1) a prominent biennial tendency that concurs with the turnabout of the El Niño–Southern Oscillation (ENSO) and provides a new perspective on the seasonally evolving spatiotemporal structure of the tropospheric biennial oscillation; and (2) a mode that leads ENSO by one year. From 1956 to 1979, the first mode shows a strong biennial tendency, and the second mode does not lead ENSO. After 1980, the biennial tendency of the first mode weakens, and the second mode becomes a strong precursory signal for ENSO. Moreover, since the late 1970s the relationships between the western North Pacific, East Asian, and the Indonesian monsoons and ESNO have all become stronger during El Niño's developing, mature, and decaying phases, whereas the anticorrelation between a developing El Niño and the Indian monsoon has weakened. These interdecadal changes are attributed to increased magnitude and periodicity of ENSO and a stronger monsoon–ocean interaction in the later period. [B. Wang and J. Yang (IPRC); T. Zhou and B. Wang (LASG); B. Wang et al.: Interdecadal changes in the major modes of Asian-Australian monsoon variability: Strengthening relationship with ENSO since later 1970s. *J. Climate*, in press]

New Australian monsoon index shows no decreasing trend in Australian monsoon rainfall. A new Australian monsoon index (AUSMI), using 850-hPa zonal wind averaged over the area 110°E–130°E, 5°S–15°S (box in Figure 3.15 top), captures well variations in monsoon rainfall over Australia and the maritime continent at intraseasonal, seasonal, interannual, and interdecadal time scales. The year-to-year variations in rainfall measured at Darwin agree well with the December–February-averaged 850-hpa zonal wind variations (r = 0.6; Figure 3.15 top) and with the monsoon onset date determined by the index.

The index has already shown its usefulness in monitoring Australian monsoon synoptic and climate variations. Among other things, it has revealed that the monsoon onset date varies from year to year much more than the withdrawal; the onset date is related to the mean seasonal amount of monsoon rainfall: the earlier the onset, the more rainfall.

A time series from 1948 to 2006 shows the Australian monsoon varies greatly over the years, but no decreasing trend is detectable (Figure 3.15 bottom). This result is consistent with rain-gauge data and differs from previous findings with another index that showed a decreasing monsoon rainfall trend for Australia. [Y. Kajikawa, B. Wang, and J. Yang (IPRC)]

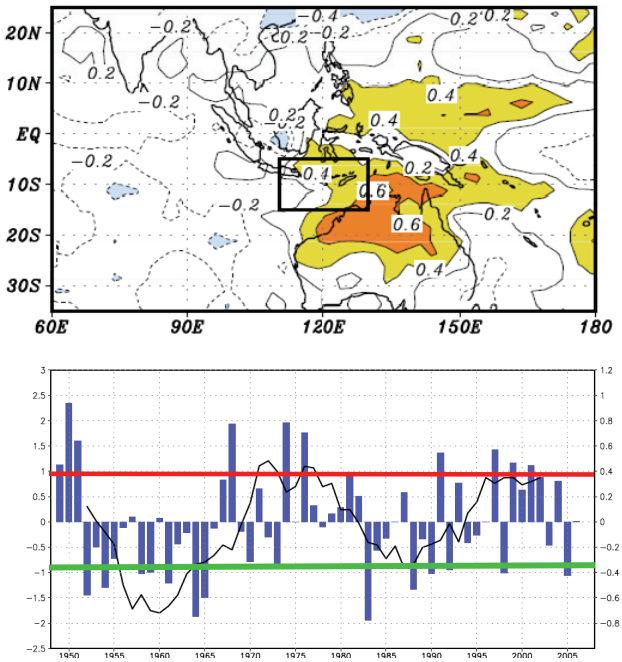

Figure 3.15. Correlation coefficients between December–February mean 850-hPa zonal wind averaged over box and GPCP rainfall anomalies at each grid (top panel); Australian summer monsoon index from 1948 to 2006 (bottom panel). There are 10 strong (above the red line) and 12 weak (below the green line) monsoon seasons.

Monsoon Predictability

How accurately do coupled climate models predict Asian-Australian Monsoon rainfall variability? Accurate prediction of Asian-Australian monsoon (A-AM) seasonal rainfall variation is one of the most important tasks in climate prediction. Yet, numerical climate models still do poorly with this prediction. The APCC/CliPAS team, of which IPRC's Bin Wang is a principle investigator, is analyzing whether simulations of 10 state-of-the-art coupled atmosphere-ocean-land climate models and their multi-model ensemble (MME) can capture the two major modes of A-AM rainfall variations observed in the data of the Global Precipitation Climatology Project. These modes account for 43% of the total interannual variance during 1981–2001. The first mode shows the strong biennial tendency in the strength of the monsoon, the Tropical Biennial Oscillation; the second mode leads the warming/cooling related to ENSO by about one year.

One-month MME seasonal precipitation predictions capture the first two leading modes of variability in terms of seasonally evolving spatial patterns and year-to-year temporal variations, as well as their relationships with ENSO (Figure 3.16). The second mode in the MME may be able to capture the precursors of a strong El Niño about five seasons before the mature El Niño. However, the

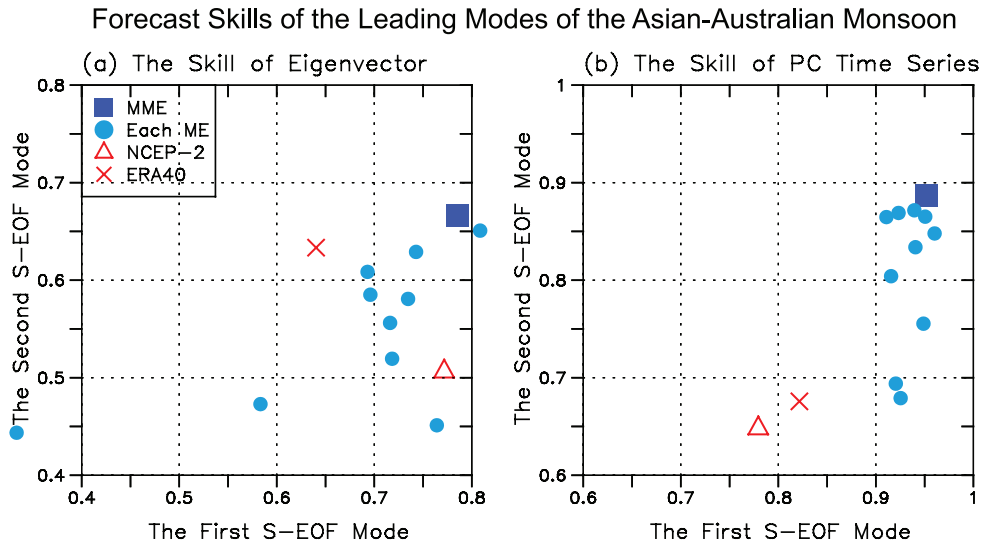

Figure 3.16. Performances of the Multi-model Ensemble (MME) and individual model predictions compared with observation (GPCP) and two (NCEP-2 and ERA-40) reanalyses against the two observed (CMAP) dominant S-EOF modes of seasonal mean precipitation anomalies. The abscissa and ordinate represent, respectively, correlation coefficients between the observed and predicted (reanalyzed) anomalies. The left panel is for the spatial correlation skill, and the right panel is for the temporal correlation skill.

MME underestimates the variances of the two modes and the biennial tendency of the first mode; it has difficulty capturing precipitation over the maritime continent and the Walker-type teleconnection during the decay of El Niño. Nevertheless, the MME predictions of the two leading precipitation modes are closer to the observed variances in the CPC Merged Analysis of Precipitation (CMAP) than the ERA-40 and NCEP-2 reanalysis datasets. This indicates that air–sea coupling is necessary in simulating summer monsoon rainfall variations accurately in regions with heavy rainfall and that *future reanalysis should be carried out with coupled numerical climate models*. [B. Wang and J.-Y. Lee (IPRC); I.-S. Kang (Seoul National University); J. Shukla (George Mason University); J.-S. Kug (Seoul National University); A. Kumar and J. Schemm (NOAA, Climate Prediction Center); J.-J. Luo and T. Yamagata (FRCGC-JAMSTEC); C.-K. Park (APEC Climate Center); B. Wang et al.: How accurately do coupled climate models predict the leading modes of the Asian-Australian monsoon interannual variability? *Clim. Dyn.*, in press]

Tropical Cyclone Research

High-resolution modeling of tropical cyclone formation. The first global cloud-resolving model, the Nonhydrostatic ICosahedral Atmospheric Model (NICAM), has been developed at JAMSTEC. Run with horizontal resolutions of a few km, NICAM can simultaneously simulate cloud clusters and organized mesoscale convective systems. IPRC analysis of a NICAM integration at a horizontal resolution of 7 km and initialized with observed atmospheric data and sea surface temperature on December 15, 2006. The analysis showed that NICAM successfully reproduced an MJO event that actually occurred during the next month. It reproduced not only the large-scale organized cloud systems in the MJO, but also the life-cycles of multi-scale cloud clusters, including tropical cyclones (Figure 3.17). [H. Fudeyasu and Y. Wang (IPRC); M. Satoh, T. Nasuno, W. Yanase, and H. Miura (JAMSTEC-FRCGC)]

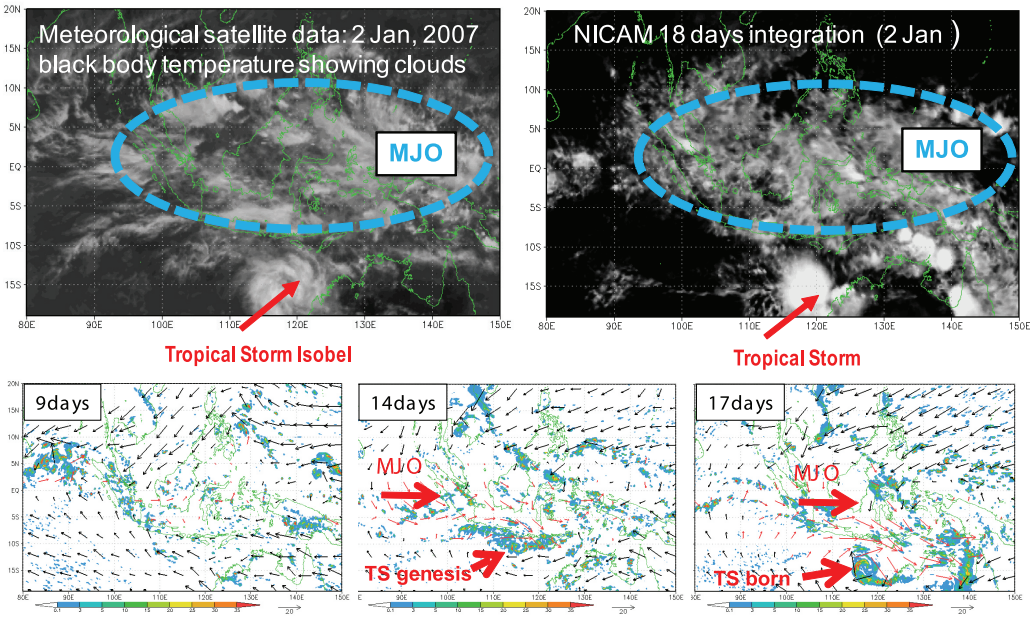

Figure 3.17. Results from the NICAM simulation showed that strong westerly wind bursts associated with the MJO near the equator increased cyclonic vorticity south of the Equator, generating a tropical storm. Top panels show cloud features in satellite data (left) and in NICAM (right); bottom panels show the surface rain rate in mm/h (color bar) and wind (vectors) during evolution of the tropical storm.

The IPRC analysis of the same NICAM integration that successfully simulated a MJO event also showed that NICAM successfully simulated the lifecycles of two tropical storms that occurred over the Indian Ocean in the winter of 2006 (Figure 3.18). The success was found to be due to the realistic simulations of not only the large-scale circulation, such as the MJO and the cross-equatorial flow, but also of the embedded mesoscale convective systems, such as vortical hot towers and their subsequent merging and axisymmetrization. The NICAM simulation also provides a high temporal/spatial resolution dataset

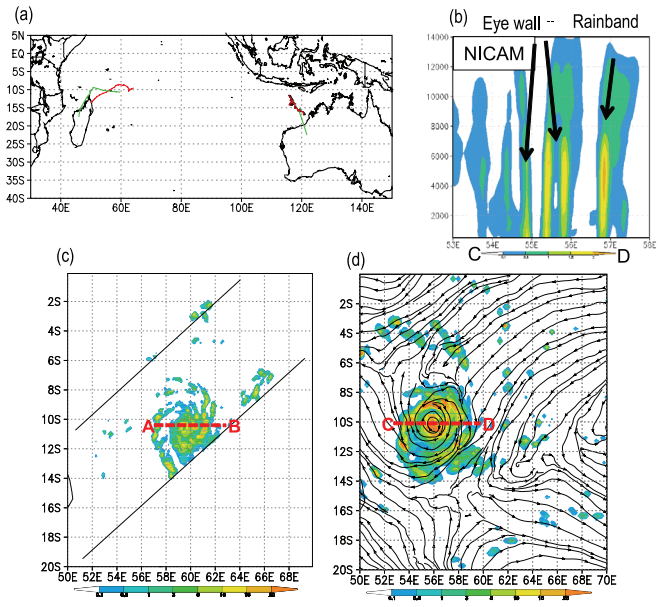

Figure 3.18. (a) A comparison of tracks and locations of the simulated tropical cyclones (red) and Joint Typhoon Warning Center best track data (green) for TC Bondo and TC Isobel; (b) vertical cross-section of the mixing ratio of total hydrometeors (cloud water, precipitation water, cloud ice, and precipitation ice; g/kg) in NICAM simulation at 0600 UTC 20 December 2006; location of cross-section is marked as the line CD in (d); surface rain rate (mm/h) from (c)TRMM-TMI at 0537 UTC 19 Decenber; and (d) NICAM simulation at 0600 UTC 20 December.

that will allow IPRC scientists to study the details of tropical cyclone formation in a global context. For example, the two simulated storms developed in quite different ways, probably because the large-scale environment in which they developed differed as well as the internal dynamics of the convection and the mesoscale cloud features. [H. Fudeyasu and Y. Wang (IPRC); M. Satoh, T. Nasuno, W. Yanase, and H. Miura (FRCGC)].

Relative humidity impacts tropical cyclone size. IPRC researchers have developed a regional cloud-resolving model named TCM4 – a quadruply nested, fully compressible, nonhydrostatic model. They have run the model at 2.5-km resolution in the finest, innermost mesh in order to obtain further insight into tropical cyclone dynamics. In the most recent study, they found that environmental relative humidity is a critical parameter in determining cyclone size: a low relative humidity environment generally favors small tropical cyclones and a high relative humidity environment, large ones. This could explain the observed variations in mean tropical cyclone size seen with ocean basins. For example, the relatively small size of tropical cyclones (TCs) that affect the Hawaiian region could be due to the shallow moist layer in the trade wind regime of the subtropical central Pacific, the smaller TCs in the North Atlantic could be partly due to the dry Saharan Air Layer, while the generally large Northwest Pacific TCs could be due to the moisture-rich western Pacific monsoon environment. Furthermore, given that tropical cyclones transport significant momentum, heat, and moisture polewards, they contribute to both the mean climate and climate variability. Since the poleward transports are a function of the horizontal extent of the tropical cyclone circulation, high-resolution climate models need to simulate realistically the large-scale environmental moisture fields in order to achieve realistic simulation of tropical cyclone size and their contribution to the mean climate and variability. [Y. Wang (IPRC)]

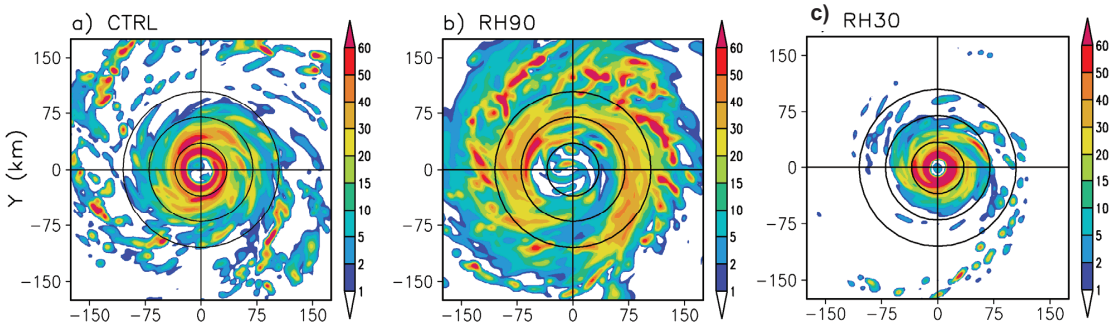

Figure 3.19. Surface rain rate (mm/h) in three idealized simulations of tropical cyclones in TCM4, showing the dependence of tropical cyclone size on the environmental relative humidity (RH), (a) control simulation with mean tropical oceanic RH condition, (b) simulation with a high environmental RH, (c) simulation with low environmental RH.

Vertical wind shear impacts Rossby wave train and tropical cyclone formation. IPRC scientists also studied in a baroclinic model the tropical cyclone Rossby wave energy dispersion under easterly and westerly vertical shears. In a resting environment, the model simulates a Rossby wave train that has a baroclinic structure with alternating cyclonic-anticyclonic-cyclonic circulations in the lower troposphere and anticyclonic-cyclonic-anticyclonic circulations in the upper troposphere (left panel Figure, 3.20). A significant difference appears in the wave train development under easterly and westerly vertical shears: an easterly shear confines the maximum amplitude of the wave train mostly to the lower troposphere (middle panel) while a westerly shear confines the maximum amplitude to the upper troposphere (right panel). The vertical wind shear therefore very likely impacts the Rossby wave train development through barotropic-baroclinic coupling and by modulating the group velocity of the mean

flow through a "Doppler-shift effect." Further experiments with uniform westerly and easterly mean flows support this hypothesis. The effect of easterly wind shear on the Rossby wave train development at lower levels may help to explain tropical cyclogenesis and the origin of the synoptic wave trains in the western North Pacific. [X. Ge and T. Li (IPRC); X. Zhou (U. of Hawai'i)]

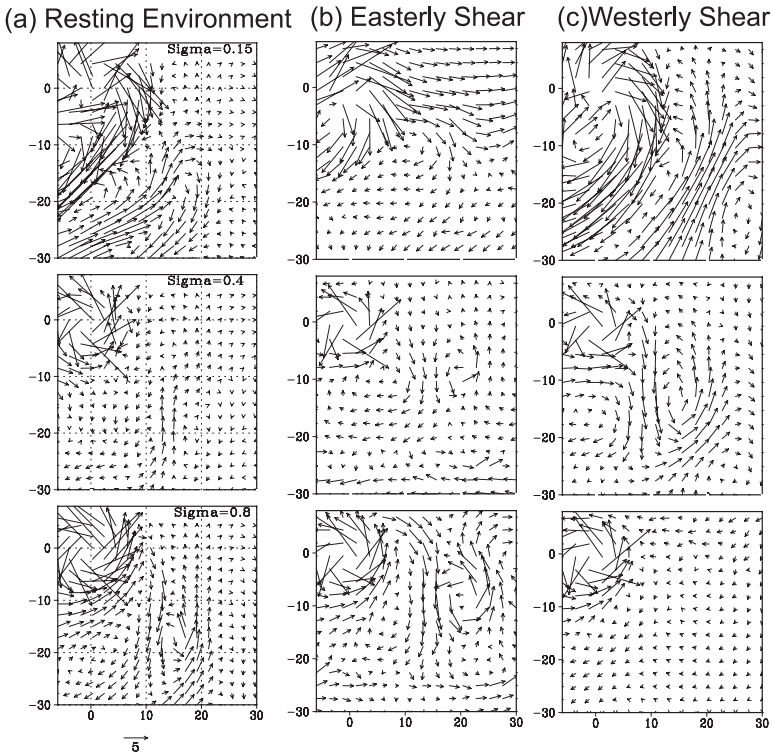

Figure 3.20. Simulated wind fields in the resting environment (left panel), easterly shear (middle panel) and westerly shear (right panel) cases at different sigma levels at day 7. The domain averaged mean flows at each level have been removed. (0, 0) represents the TC center, horizontal distance in units of 100 km.

IMPACTS OF GLOBAL ENVIRONMENTAL CHANGE (THEME 4)

Research in this theme aims to determine impacts of global environmental change on Asia-Pacific climate, to understand processes that shaped past climates and shape present climates, and to improve the numerical modeling of climate change. Several studies conducted during the past year are highlighted in the section below.

Issues in Current Climate Modeling

Fine-resolution global atmospheric modeling. Analysis of very fine-resolution global atmospheric model simulations has continued in collaboration with Japanese colleagues at the JASTEC-ESC. Specifically the results from various versions of the Atmospheric Model for the Earth Simulator (AFES) were analyzed to characterize the horizontal kinetic energy spectrum. The control version of AFES run at T639 horizontal spectral resolution (roughly equivalent to 20-km horizontal grid spacing) was found to simulate a kinetic energy spectrum that compares well at large scales with global observational reanalyses and at smaller scales with available aircraft observations at near-tropopause levels. Specifically there is a roughly –3 power-law dependence on horizontal wavenumber for wavelengths between about 5000 and 500 km, transitioning to a shallower mesoscale regime at smaller wavelengths. This is seen for both one-dimensional spectra and for the two-dimensional total wavenumber spectrum based on a spherical harmonic analysis. The simulated spectrum at mid-tropospheric levels is similar to that near the tropopause in that there is a transition to a shallower mesoscale regime, but the spectrum in the mesoscale is clearly steeper at mid-troposphere than near the tropopause.

A number of experiments with the AFES model T639 version were performed to identify the dominant sources of the mesoscale energy responsible for the shallow spectral slope. The *control* simulation was run in the full AFES mode. In the *aquaplanet* run, the realistic geography was replaced by an all-ocean surface with prescribed zonally-symmetric surface temperatures. In the *dry run*, there was no hydrological cycle and no topography, and the full radiation code was replaced by a simple relaxation of the temperature to a prescribed distribution. For the aquaplanet and dry versions the governing parameters were chosen so that the energy spectrum over the synoptic scales (~500–5000-km wavelengths) was similar to that in the control model simulation.

Figure 4.1 shows a physical space view that contrasts the mesoscale behavior of the three versions of the model. Each panel shows a snapshot of the horizontal wind divergence at the 200-hPa level. The control simulation (top panel) shows the effect of topography in generating small-scale motions. The aquaplanet simulation (middle panel) has no topographic waves but the effects of organized wave sources in both the tropics and extratropics are evident. By contrast, the dry model (bottom panel) has much reduced eddy activity in the tropics, but the organized modulation of the wave activity in the extratropical baroclinic zones is evident.

Figure 4.2 shows the kinetic energy spectra at the 200-hPa level computed from the simulations with the full AFES, the aquaplanet version and the dry version. Also shown are results for a dry model run with twice the horizontal resolution (T1279 or about 10-km equivalent grid spacing). The spectrum is plotted as a function of total spherical wavenumber and the equivalent horizontal wavelength is roughly 40,000 km divided by the spherical wavenumber. The transition to a shallow mesoscale regime around wavenumber 80 (wavelength ~500 km) is apparent in the kinetic energy spectra in all three versions. However, the energy levels in the mesoscale are higher in the aquaplanet than in the dry version and

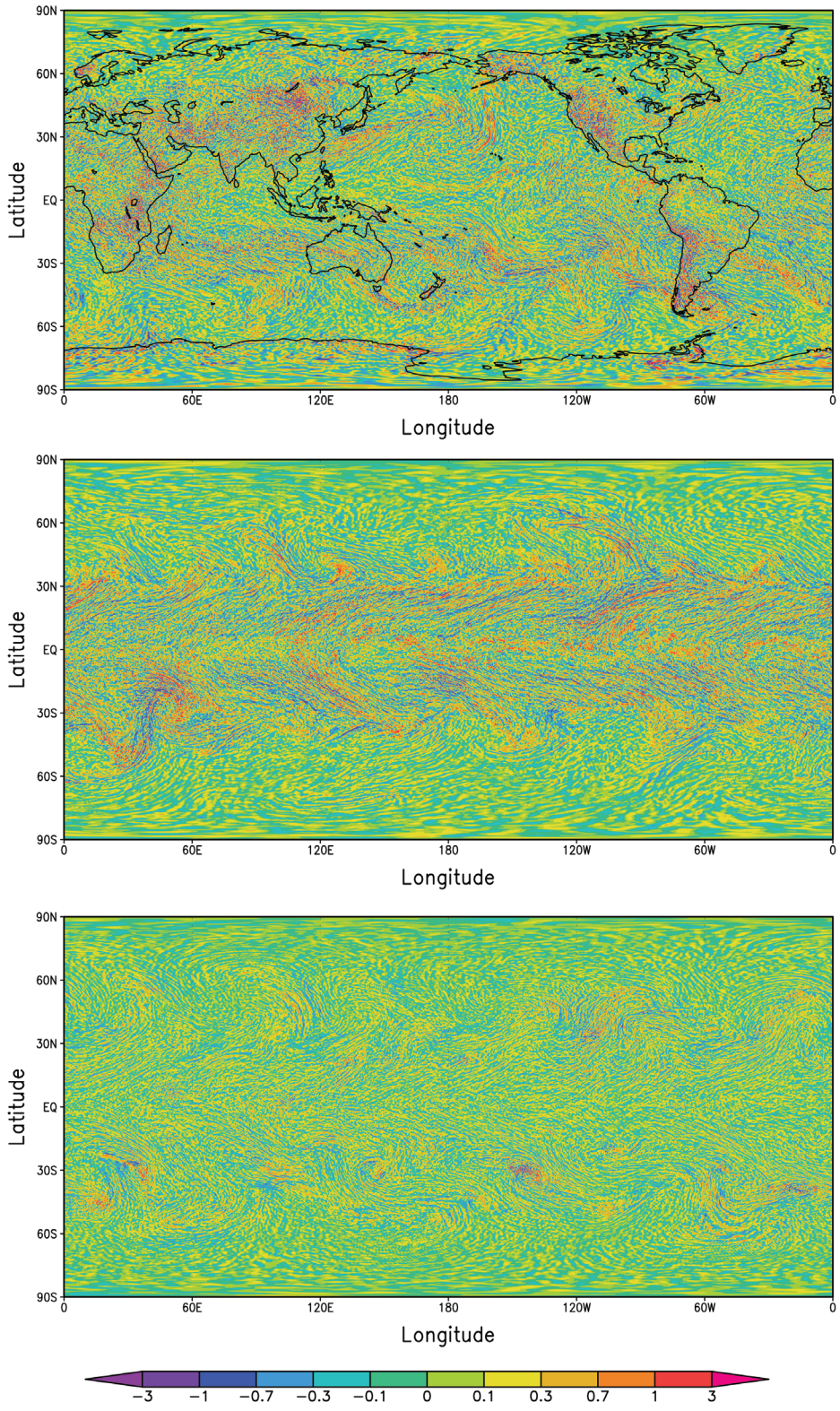

Figure 4.1. Snapshot of the simulated 200 hPa horizontal wind divergence from versions of the T639 AFES model. The color bar is labelled in 10^{-4}/s. Note the non-constant increment in the color bar. Results from (top) full model, (middle) aquaplanet version, and dry version (bottom).

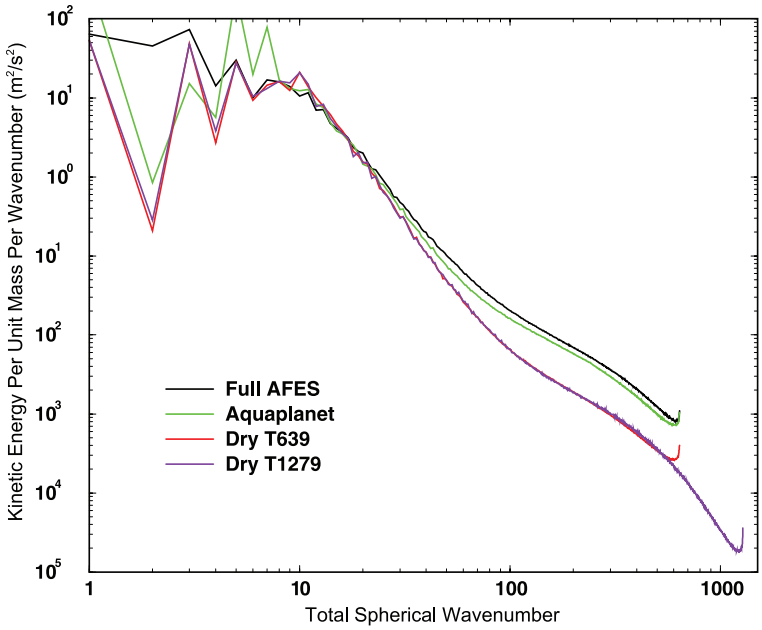

Figure 4.2. Total wavenumber kinetic energy spectrum at 200 hPa from various AFES experiments. The black curve is from the full T639 AFES model. The green curve is from the same model, but run with an aquaplanet lower boundary; the red, for T639 dry version; and the purple, from a T1279 version of the dry model.

highest in the full model. This suggests that both moist convection and topography play a significant role in energizing the mesoscale flow in the atmosphere. [K. Hamilton (IPRC), W. Ohfuchi (JAMSTEC-ESC), Y. Takahashi (Kobe University)]

Hawai'i climate change simulations. Limitations of computational power have meant that the very long integrations of global models needed for climate change predictions have generally been performed with atmospheric component models at effective horizontal grid spacings of ~200 –500 km. This low resolution is problematical for representing many aspects of the atmospheric circulation, but particularly so for Hawai'i. Hawaiian weather is strongly affected by the steep topography present on the islands. Typical global climate models represent all the Hawaiian Islands as a single land grid-box or even ignore Hawai'i entirely!

As part of the model intercomparison conducted for the Intergovernmental Panel on Climate Change (IPCC) Fourth Assessment Report (AR4), the Climate Research Department of the Japan Meteorological Research Institute (MRI) performed 21st century projections using a version of their coupled ocean-atmosphere model run at spectral horizontal resolution T42, which corresponds to a grid spacing of about 300 km. The MRI group supplemented the standard runs with two special 20-year integrations of their global atmospheric model run at much higher resolution (TL959, corresponding to horizontal grid spacing of about 20 km). The sea surface temperatures used as boundary conditions for this high-resolution atmospheric model were taken from the late 20th century and late 21st century coupled T42 integrations. This run provides, for the first time, a global warming forecast with a global model that has a somewhat realistic representation of the coastlines and topography of the main Hawaiian Islands.

The late 20th century and late 21st century simulations in a variety of AR4 models and in the special MRI TL959 model simulations have been analyzed at the IPRC. The low-resolution models produce unrealistically low mean rainfall over the Hawaiian region, and the response of the rainfall to global warming varies markedly among models, with some models predicting increased and others decreased rainfall. The T42 MRI model predicts significantly (~20%) less total annual rainfall over the Hawaiian region in the late 21st century relative to the 20th century. The high resolution TL959 model, by contrast, produces somewhat realistic present-day rainfall, particularly for the Big Island, and forecasts increased

total rainfall in the late 21st century for the land areas of Hawai'i. This increase in mean rainfall would be welcome, as the populace of Hawai'i is already straining its fresh water resources. The increased rainfall in the model, however, is accompanied by more frequent extreme daily rainfall events (Figure 4.3), which would presumably lead to more frequent flooding of low-lying areas, and exacerbate problems expected from rising global sea level. [K. Hamilton (IPRC)]

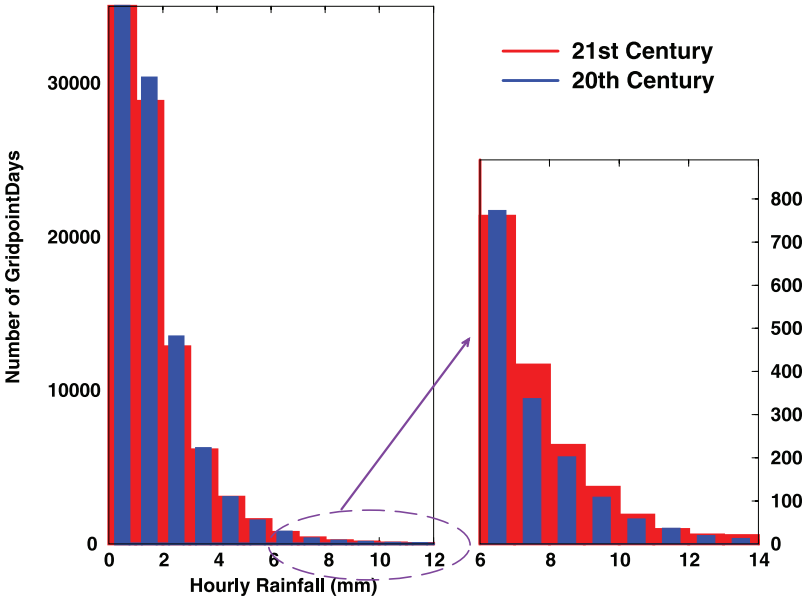

Figure 4.3. Histogram of the occurrence of maximum hourly rainfall accumulation over land in the MRI TL959 model. The accumulation is calculated each hour for each of the 87 land grid points that represent the land mass of the Hawaiian Islands in the model. Results for 20 years of late 20th century simulation are in blue and for the late 21st century simulation in red. The right panel shows a blowup of the figure for the most extreme rainfall amounts.

Understanding trends in atmospheric upwelling. Modeling and diagnostic studies were conducted related to the issue of variability and trends in the tropical upwelling of air into the stratosphere. A simple axisymmetric model of the global atmospheric circulation was constructed and used to establish relationships between the simulated upwelling through the tropical tropopause and the strength and pattern of stratospheric wave drag, which drive the mean circulation. Analysis of the stratospheric wave drag as represented in global reanalyses shows that through the 1980s and 1990s there was a trend of increasing poleward displacement in the pattern of wave drag. The axisymmetric model results suggest that such a trend in wave drag would be accompanied by a reduction in the tropical upwelling into the stratosphere. This, in turn, would be consistent with a trend in increasing stratospheric water vapor concentrations, a trend that was actually observed in this period. This work thus suggests that the considerable (~20%) moistening of the stratosphere observed over the 1980s and 1990s could have been due to changes in the large-scale dynamics of the troposphere that led to changes in the wave driving of the stratosphere. [K. Hamilton (IPRC); M. Geller (Stony Brook University); T. Zhou (NASA GISS); M. Geller et al.: *J. Atmos. Sci.*, in press]

New cloud microphysics for the IPRC Regional Atmospheric Model. The stratocumulus decks over the eastern Pacific off the coasts of North and South America have a net cooling effect by efficiently reflecting incoming solar radiation, and thereby they greatly impact Earth's radiation budget and climate. Most current global and regional numerical climate models have difficulties in reproducing the observed properties of these maritime stratocumulus decks because the tight coupling among atmosphere, ocean, and land surfaces is a challenge to model as well as the many spatial and temporal scales of this complex system. Cloud formation depends on condensation nuclei provided by the atmospheric aerosol. Changes in atmospheric aerosol due to such anthropogenic activities as biomass burning, fossil fuel combustion or changes in land use are known to be able to alter such cloud properties as reflectivity or precipitation

formation efficiency. This so-called indirect aerosol effect is still poorly understood and is considered by the Intergovernmental Panel on Climate Change to be one of the largest uncertainties in predicting future climate change.

In order to assess the impact of anthropogenic aerosol emissions on microphysical and optical properties of stratocumulus clouds over the eastern Pacific, IPRC scientists and their colleagues at other institutions implemented a new cloud microphysics scheme into the IPRC Regional Atmospheric Model (iRAM). In addition to the calculation of the mass mixing ratios of cloud and precipitation particles, this scheme allows calculation of cloud droplet and ice crystal numbers from predicted aerosol properties, which are essential to assess the indirect aerosol effect. The new scheme is now being evaluated against observations. As an example, Figure 4.4 compares a 3-month average of effective cloud droplet radii calculated by iRAM with the old (single-moment, which has no information about droplet number) and the new (double-moment) cloud microphysics scheme, and satellite data from the International Cloud Climatology Project. The effective droplet radius is important because it affects how much light can be reflected by a cloud. Smaller cloud droplets are more effective in scattering solar radiation than larger droplets. Results obtained with the new cloud scheme are closer to satellite observations than those with the old scheme.

Once the new cloud microphysics system has been carefully evaluated, this tool will allow IPRC scientists to investigate how the stratocumulus decks over the eastern Pacific will respond to climate change, particularly to the increase in anthropogenic aerosol, and how, in turn, changes in these cloud decks will impact global climate. [A. Lauer (IPRC); V. Phillips (UH); Y. Wang and K. Hamilton (IPRC)]

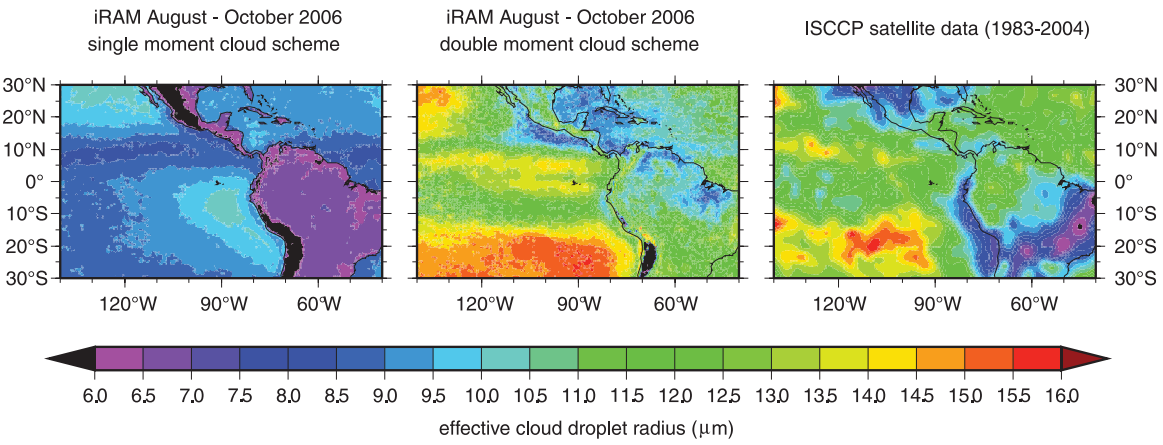

Figure 4.4. August–October 2006 average of the cloud droplet effective radius (μm): (left) iRAM model (year 2006) with original cloud scheme; (middle) iRAM model (year 2006) with new double-moment cloud microphysics; (right) ISCCP (International Cloud Climatology Project) satellite observations (Rossow et al., 1996) for the years 1983–2004.

Paleoclimate Modeling

The climates of the past hold important clues to the processes driving the climate system—clues that may point to the nature of future climate change with rising global temperatures. IPRC research in paleoclimate modeling is mainly on the last glacial period (100,000–11,000 years ago), the relatively stable Holocene (11,000 years ago to the present), and the Anthropocene (from the late 1800s to the present).

Changes in the Atlantic Meridional Overturning Circulation and North Pacific climate-I. The period from 18 to 14.6 thousand years ago, the so-called Mystery Interval, was characterized by major reorganizations of the global ocean circulation and a rapid drop in atmospheric radiocarbon, suggesting a gas exchange between very old waters and the atmosphere, and a rapid warming of the Southern Hemisphere. Analysis of sediment cores from the northern North Pacific suggests that during this period, oxygen concentrations at intermediate depths (1000 – 2000 m) rose significantly. Changes in ventilation-age estimates from benthic samples and stable carbon isotope analyses support the notion that changes in the North Pacific circulation must have contributed to ventilation of the intermediate-to-deep waters during this period.

IPRC scientists in partnership with JAMSTEC colleagues identified a mechanism that could have led to these major reorganizations in the North Pacific circulation. The team conducted simulations with the LOVECLIM and CCSM2 models that were driven with a 1 Sv freshwater infusion into the North Atlantic, mimicking Heinrich 1 events. The models showed that the collapse of the Atlantic Meridional Overturning Circulation between 17 thousand and 15 thousand years ago may have led to a substantial drop in temperature and increase in surface-salinity in the North Pacific Ocean. The resulting higher surface density triggered deep winter-time mixing in the Gulf of Alaska, the Sea of Okhotsk, and the Bering Sea, and helped to establish an intermediate-to-deep Pacific meridional overturning circulation (see Figure 4.5). The simulated high oxygen concentration in LOVECLIM is consistent with an observed increase in the abundance of North Pacific benthic formanifera that thrive in oxygenated waters, and the simulated low phosphate concentration is consistent with stable carbon isotope values in the benthic species Uvigerina. [A. Timmermann (IPRC), N. Harada (JAMSTEC-IORGC), A. Abe-Ouchi (U. of Tokyo)]

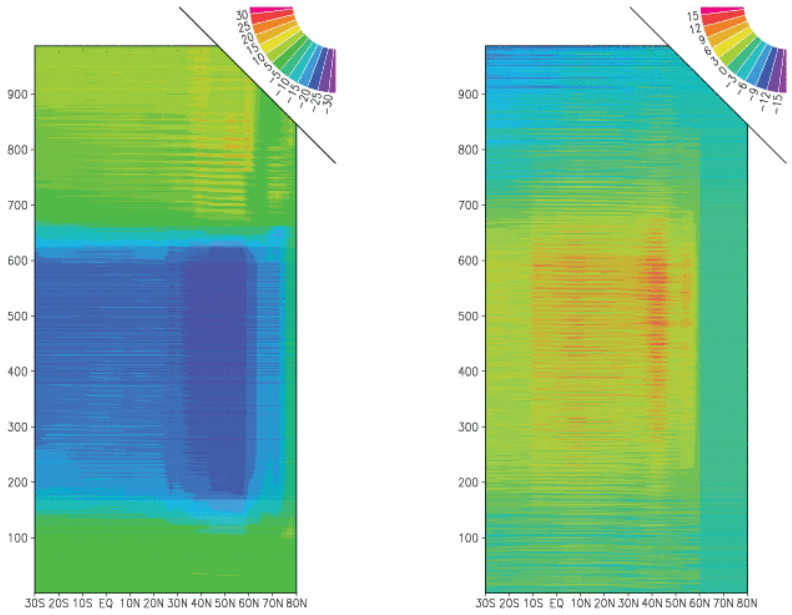

Figure 4.5. (Left panel) Meridional streamfunction anomaly at 1000-m-depth in the Atlantic from 30°S to 80°N during the waterhosing experiment conducted with the LOVECLIM earth system model; (right panel) same as left but for the Pacific. The waterhosing phase begins in year 100 and by year 200, the Atlantic Meridional Overturning Circulation has collapsed.

Changes in the Atlantic Meridional Overturning Circulation and North Pacific climate-II. The impacts on North Pacific atmospheric circulation of changes in the Atlantic Meridional Overturning Circulation (AMOC) that stem from infusing 1 Sv freshwater for 100 years into the extratropical North Atlantic were studied further in collaboration with colleagues from NCAR. A series of experiments with four different coupled general circulation models was analyzed that simulated a shutdown of the

AMOC, mimicking glacial Heinrich events. In all the models, the North Pacific cools, especially along the oceanic frontal zone, and the wintertime Aleutian Low deepens, results that are consistent with paleoclimate records. Additional experiments with atmospheric general circulation models demonstrated that the Aleutian Low intensification can be primarily attributed to the cooling of the Caribbean that results from the weakened AMOC state (Figure 4.6). A new atmospheric teleconnection pathway was identified that links the tropical Atlantic climate conditions with the North Pacific. Whether this teleconnection is responsible for significant variations in the Aleutian Low at interannual-to-multidecadal timescales is still unclear. [Y. Okumura, C. Deser and A. Hu (NCAR); A. Timmermann and S.-P. Xie (IPRC)]

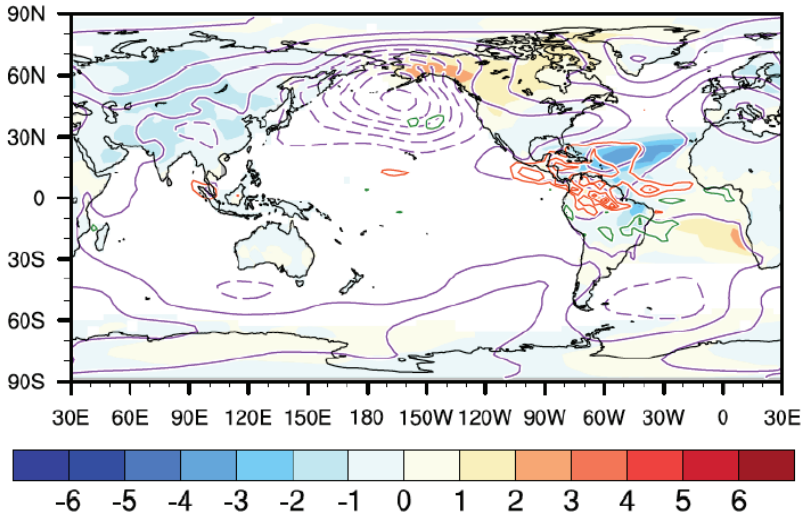

Figure 4.6. Atmospheric anomalies simulated by CAM2 forced with prescribed observed SST and tropical Atlantic (25°S–30°N) SST anomalies representing a shutdown of the Atlantic Meridional Overturning Circulation. In the tropical Atlantic the SST anomalies are added to the observed climatological SST forcing. Surface temperature (shading, °C), sea-level pressure (purple contours at intervals of 1 hPa, negative contours dashed), and precipitation (green contours > 1 mm/day, orange contours < –1 mm/day at intervals of 1 mm/day) anomalies are averaged over October–March.

Evidence for wintertime weakening of the equatorial Pacific cold-tongue during the Holocene. Proxy data that provide evidence for past climate change in the vast central tropical and subtropical Pacific are sparse. Now a University of Hawai‘i analysis of biomarkers (n-alkanes) from the leaf wax of terrestrial plants deposited in sediments in a sinkhole on the leeward coast of the Hawaiian Island of Oahu shows drying occurred in the region during the Holocene period. From about 10 thousand years ago to 4.8 thousand years ago, the $\delta^{13}C$ values of n-alkanes increased steadily from –31‰ to –24‰, and then remained constant at about –28‰ until the arrival of the Polynesians. These changes in the biomarker suggest during those 5 thousand years the local vegetation shifted to flora adapted better to a dryer climate (C_4 plants).

A transient climate model simulation conducted with the coupled general circulation model ECHO-G showed that changes in Earth’s orbital path between 10 and 5 thousand years ago may have been responsible for the reconstructed drying trend in Hawai‘i. Earth’s path around the sun 10 thousand years ago was such that the equatorial Pacific received most solar radiation from April through August. By 5 thousand years ago the maximum solar radiation period had changed to September through March. This shift in the heating of the equatorial Pacific raised the boreal winter sea surface temperature in the eastern equatorial Pacific from a cold state, similar to La Niña today, to a warm state, similar to El Niño condi-

tions today. This shift from a predominantly cool to a predominantly warm equatorial eastern Pacific during wintertime strengthened the Hadley Circulation, which in turn weakened the moisture transport from the tropics to Hawai‘i, particularly to the leeward coasts of the Hawaiian Isles. [Joji Uchikawa, Brian N. Popp, and Jane E. Schoonmaker (U. of Hawai‘i); A. Timmermann (IPRC); S. J. Lorenz (Max Planck Institute of Meteorology)]

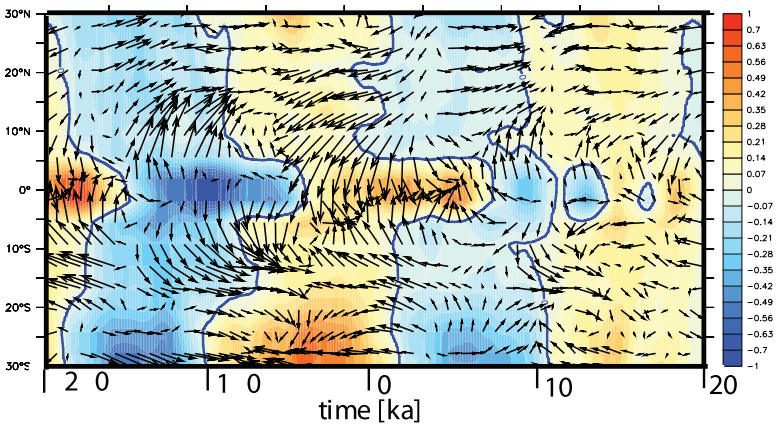

Figure 4.7. Holocene intensification of the winter Hadley Circulation: Simulated boreal winter (DJF) zonally averaged (180 –120˚W) eastern Pacific SST (˚C) and 10-m wind anomalies. Anomaly refers to the difference between the zonally averaged estimates at any given time and the zonally averaged mean from 20 thousand before present to 20 thousand after present.

Future Climate

Equatorial corals most vulnerable to climate change. Corals bleach when temperature, salinity, or light availability change to such an extent that the symbiosis between the dinoflagellate algae *Symbiodinium* and the coral animal breaks down. When such harmful conditions prevail over some time, the coral polyp can die. Corals bleach when sea surface temperature (SST) rises for several weeks by more than 1ºC above the corals' accustomed temperature range. Since temperatures in the western equatorial Pacific vary by only about 0.5ºC during the year (Figure 4.8a), a projected rise in temperature due to greenhouse warming greater than 1.5ºC will likely lead to bleaching there. The SST in the off-equatorial tropical South Pacific has a wider range during the year, and temperature can rise by 2.5ºC over the yearly average before bleaching the corals.

To identify which coral reef regions are more likely to experience thermal stress and coral mortality, a study spearheaded by IPRC scientists analyzed simulations from a model ensemble consisting of 20 state-of-the art climate models that were forced by doubling atmospheric CO_2 until 2100, at which time concentrations reach 700 ppmv in the model. The projected future warming in the ensemble was largest around the equator; in the off-equatorial regions, stronger winds, changes in the air–sea specific humidity gradient, and increased low-level clouds promoted latent cooling, thereby damping the effect of CO_2. This outcome suggests that corals in the equatorial warm pool (the Coral Triangle and parts of Melanesia) are most vulnerable to global warming not only because they are already more sensitive to temperature fluctuations but also because the predicted temperature rise is greatest around the equator. The models predict that by 2050 temperatures in the warm pool will permanently exceed present-day estimates of the bleaching threshold, a phenomenon that then spreads poleward, reaching the Hawaiian Islands by about 2080.

These results are important for marine management aiming to protect biodiversity hotspots in such regions as the Coral Triangle and for adaptation and mitigation strategies by western tropical Pacific island nations. So far, there is no evidence that coral reefs can adapt as quickly as the rate at which these changes are likely to occur. Since this study did not consider such coral bleaching agents as pollution,

sea level rise, and ocean acidification, the situation for corals might be even more ominous than the study suggests. [A. Timmermann (IPRC), L. Menviel (U. of Hawai‘i), L. McLeod (The Nature Conservancy), and Z. Liu (U. of Wisconsin)]

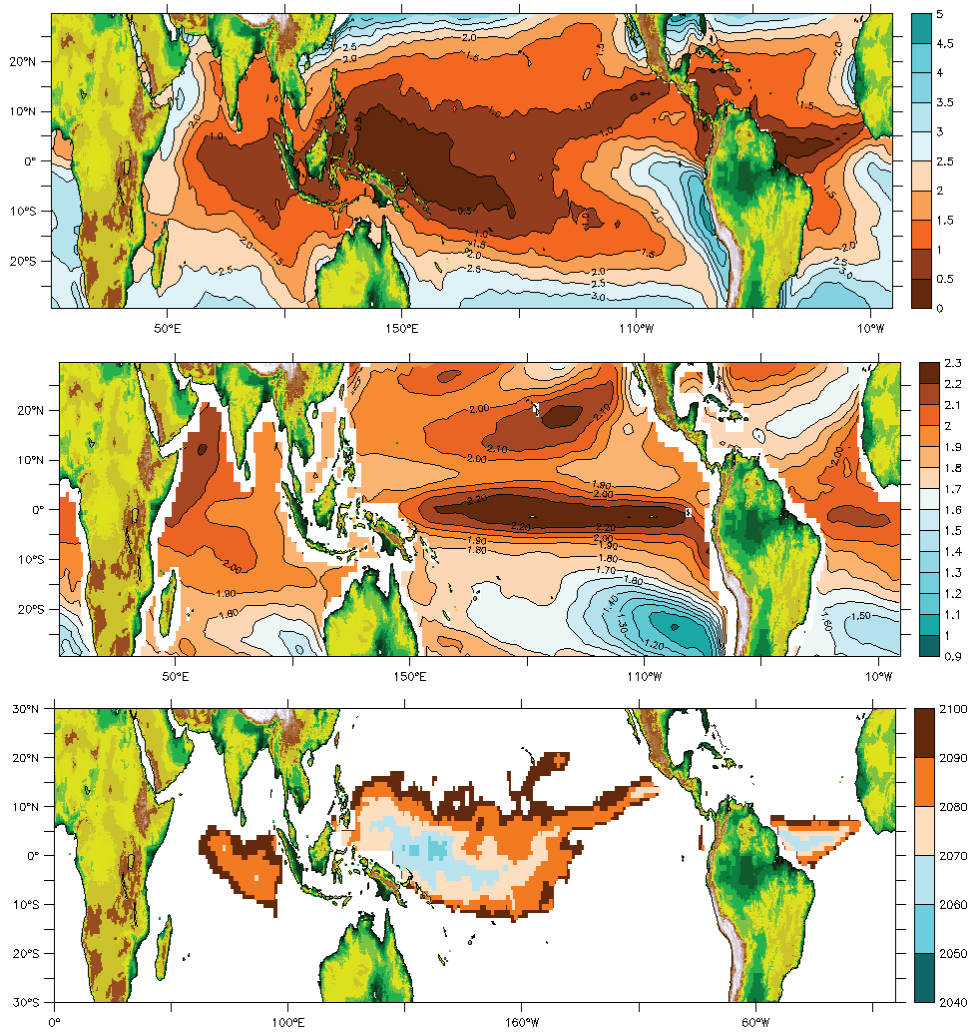

Figure 4.8. (top) Difference between maximum and mean of SST climatology in ºC (from HadSST, average computed from 1985 –1995); (middle) Multi-model ensemble mean rise in SST from 2000–2007 to 2090–2100 based upon 20 state-of-the-art climate model simulations forced by increasing greenhouse gas concentrations following IPCC scenario A1B; (bottom) temporal horizon for simulated multi-model ensemble SST to permanently exceed observed maximum climatological temperature by 1ºC. If the simulated monthly mean SST in 10-year intervals exceeds the hotspot thermal threshold permanently, massive coral bleaching and mortality are very likely to occur.

ASIA-PACIFIC DATA-RESEARCH CENTER (THEME 5)

The APDRC vision is to establish an efficient, distributed yet integrated, data management and data server system infrastructure for Indo-Pacific climate research and to generate and serve products needed for a wide range of research and applications. The mission is to provide "one-stop shopping" for climate data and products to IPRC researchers and their research partners, the national climate research community, and the general public. Activities focus on three major themes: data server system operation and development; data management; and applied research that leads to product development and delivery aimed at a wide range of users including researchers, decision makers and the general public.

The Data Server System

APDRC staff, together with their national and international partners, continued to operate and upgrade the data server system, which consists of LAS, EPIC, TSANA, and OPeNDAP servers, together with two new OPeNDAP servers, THREDDS for data aggregation, and DAPPER/DChart for in situ data. DCHART will serve as a future replacement for the EPIC server and will also allow for the downloading of larger netcdf files than the LAS server. LAS version 7.0, which is now Java-based and allows web services, was installed and is operated in a test mode. The new version offers such output formats as animations and Google Earth files.

Further upgrades to the server system were also made to handle the large new data sets that will be served in the near future, and to handle paleoclimate data, which required restructuring the time sequence to include a "before present" calendar and dates greater than 10,000 years.

Data Management

APDRC staff continued to build the data archive in support of applications and research with a focus on atmospheric, oceanic, air-sea flux, and model- and satellite-derived products. New data sets and products have been identified for research in Themes 1 to 4 and have been added to APDRC servers since April 2007. They include the following: (1) AMSR-E daily surface soil moisture, (2) TRMM monthly 3A12, (3) QuikSCAT winds at daily resolution, (4) GHRSST (aggregated from NASA/JPL), (5) Indian Ocean bathymetry, (6) ADCP data added to DAPPER/DChart, (7) the full terms from the NCEP run (daily intervals) for heat flux studies, (8) paleoclimate-model runs (SIM2BL), (9) IPRC Regional Ocean Atmosphere Model (iROAM) runs, (10) ECCO-JPL Kalman Filter assimilation runs (1993–present), (11) NRL NCOM nowcasts, (12) JRA-25, and (13) Hawaiian Island region tidal currents.

The APDRC also continued to provide easy access to the operational and delayed-mode ocean products prepared in the context of the Global Ocean Data Assimilation Experiment (GODAE) and the Integrated Ocean Observing System (IOOS). The APDRC serves the global Navy Research Laboratory (NRL) Layered Ocean Model (NLOM) surface layer fields (both hindcasts and forecasts), the multi-layer NRL NCOM (Navy Coastal Ocean Model) output for the Hawaiian Islands region, and the global real-time Hybrid Coordinate Ocean Model (HYCOM) output in the Hawaiian Islands region since June 2007 (see Figure 5.1).

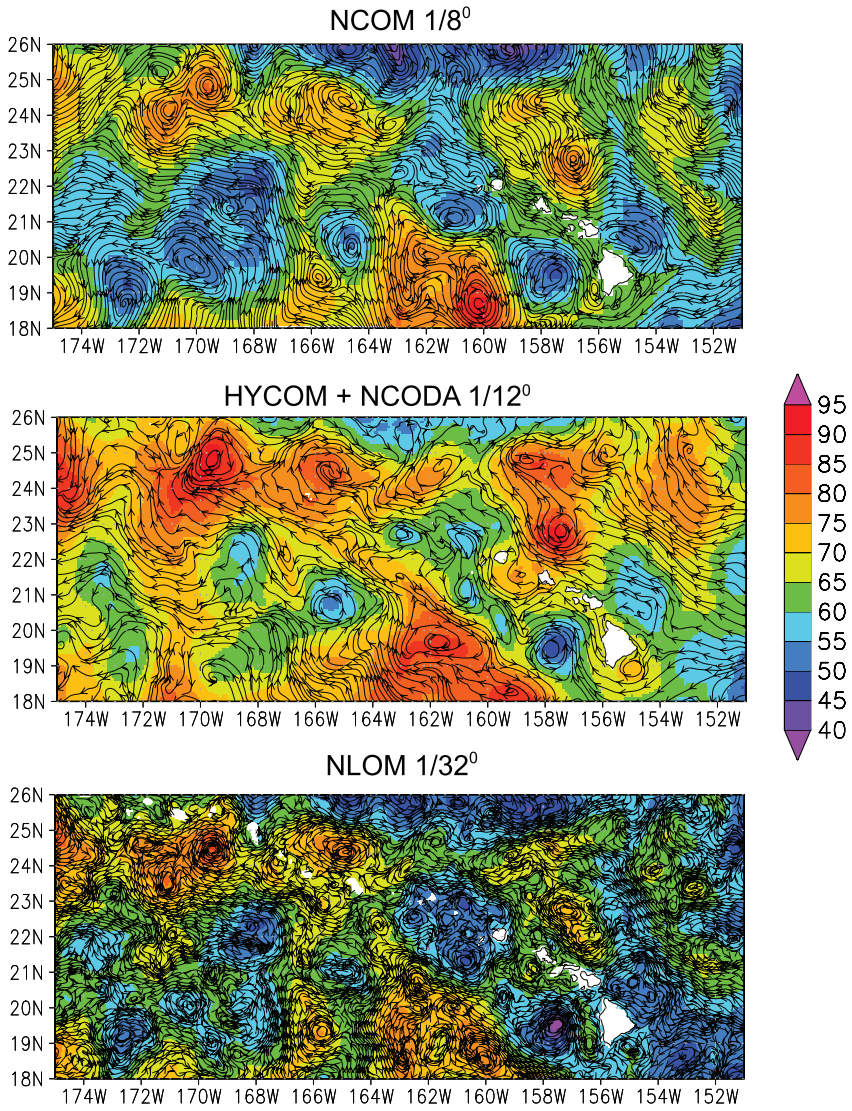

Figure 5.1. Sea surface height and upper-layer (0–100 m) circulation pathways from the NCOM, HYCOM, and NLOM nowcast products on December 30, 2007, for the Hawaiian Islands region. Note the strong eddy features northeast of the island of Oahu and west of the island of Hawai‘i. Products are available at http://apdrc.soest.hawaii.edu.

IPRC scientists, moreover, are working with JAMSTEC scientists on a variety of projects that involve large data sets: the analysis of high-resolution atmospheric model output from NICAM; the daily, full-resolution climatological run for 8 years (24 TB) of the Ocean General Circulation Model for the Earth Simulator (OFES); several OFES runs for the South China Sea region at 0.1°, 3-day, QuikSCAT-forced, for the 2001–2004 period. New assimilation-based products produced this year and the various OFES runs take up much of the storage available.

The APDRC has assisted in setting up the following websites: the IPRC Asian-Australian monsoon monitoring web page, which provides real-time and forecast information about the status of the monsoon; the IPRC Regional Ocean–Atmosphere model (iROAM) web page; an ENSO expert's prediction web site; and paleoclimate model results.

Applied Research: Product Development and Distribution

Atmospheric modeling for the Hawai'i region. The three-dimensional variable data assimilation system of the Weather Research and Forecasting Model (WRF) has been adapted to assimilate high-quality and fine-resolution satellite and radiosonde data to create atmospheric surface forcing fields at a resolution of about 18 km for the Hawaiian Archipelago Islands (Figure 5.2). The background is taken from the NCEP final analysis of the NCEP global forecast. The observations assimilated include radiosondes (TTAA, TTBB, PPBB, etc.), surface observations (SYNOPS, METARS, AWS, ships, buoys, CMAN), satellite winds (QuikSCAT, GOES, METSAT, MODIS, AVHRR), Satellite Remote Upper Soundings, aircraft measurements (PIREPS, AIREPS, AMDAR, ACARS), dropsondes and "hurricane hunter" observations, and ground-based GPS and COSMIC GPS refractivity. Figure 5.2 shows a snapshot of the forcing fields that can now be used to drive the Hybrid Coordinate Ocean Model (HYCOM) implemented for the Hawaiian Island region.

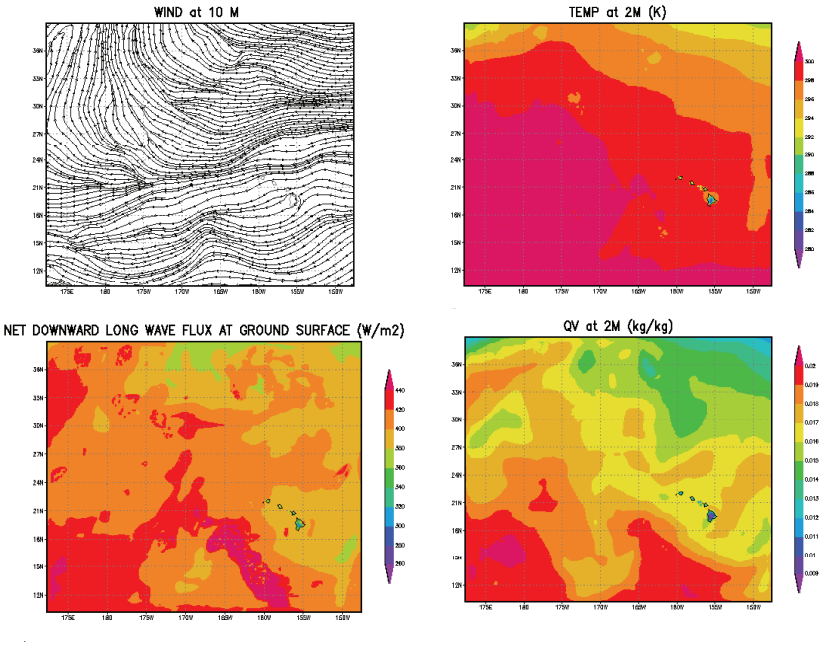

Figure 5.2. Atmospheric surface forcing fields (175°E–150°W) created through data assimilation into the WRF model for the domain surrounding the Hawaiian Islands. These forcing fields can now be used to drive HYCOM downscaled for the Hawaiian Island region. The panels show a snapshot of assimilated 10-m wind (top left), 2-m temperature (top right), net downward longwave radiative flux (bottom left), and 2-m specific humidity (bottom right) fields at hour 18:00 on 8/10/2007.

Ocean modeling for the Hawai'i region. HYCOM has been implemented for the waters surrounding the Hawaiian Islands at various domain sizes and horizontal resolutions, ranging from a region encompassing the major Hawaiian Islands at a resolution of 0.04° to the south shore of the island of Oahu at a resolution of 0.01°. The goal of this activity is to establish a downscaled regional ocean prediction system comprising multiple nested sub-regions by using results from the coarser global ocean prediction system such as the real-time HYCOM (Figure 5.1 middle panel) for initial and lateral boundary conditions. As an example, we show in Figure 5.3 the sea surface height (SSH) on December 30, 2007, from a simulation performed with a configuration for the region encompassing the major Hawaiian Islands. It was initialized with the ocean state on June 23, 2007, and forced with velocity, temperature and salinity fields at the lateral boundaries taken from the global real-time HYCOM. The surface forcing comes from a high-resolution regional atmospheric system, WRF, as discussed above (Figure 5.2). A regional atmospheric model is expected to be running in real-time soon and will provide the surface forcing fields needed to drive the regional HYCOM. Data assimilation is not implemented in the regional configurations at present, but will become a major focus in future efforts.

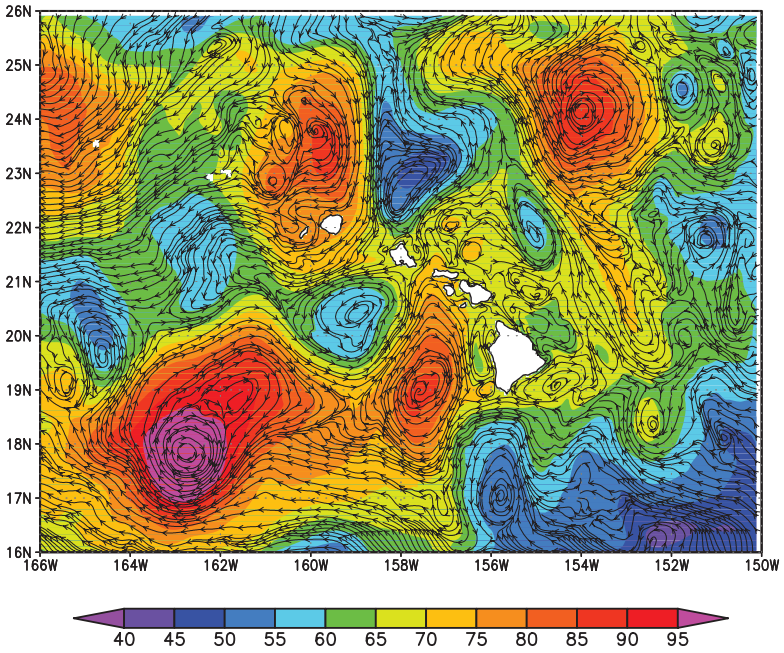

Figure 5.3. Sea surface height on December 30, 2007 in the HYCOM simulation for the region of the Hawaiian Islands that used the global real-time HYCOM output (Figure 5.1 middle panel) for initial and lateral boundary conditions and was forced at the surface by output from the regional atmospheric model WRF (Figure 5.2). The eddy characteristics are different from those in Figure 5.1 (middle panel) because the model was driven with different atmospheric forcing and was run without data assimilation, except via the boundary forcing.

Shallow bay modeling. A high-resolution, σ-coordinate model, the Princeton Ocean Model (POM), has been implemented for Kaneohe Bay on the island of Oahu (denoted by X in Figure 5.4a). Its horizontal grid covers 10.8 km by 14.4 km with a resolution of 123 m by 132 m; depths in the bay vary from 1–100 m with 11 vertical levels ranging from 0.05 m to 11 m. The model uses lateral boundary conditions and an initial state provided by a regional configuration of HYCOM for the island of Oahu at 1-km resolution. Figure 5.4b shows the surface currents and sea surface height response after one day of forcing by a uniform easterly wind with a speed of 34 m/s (strong trades) and a 3-m swell; Figure 5.4c shows the wave height response. The model was used as a test case for potential use as part of the SOEST model-based forecasting system to enable researchers to simulate and study the impacts of stream runoff, sewage spills,

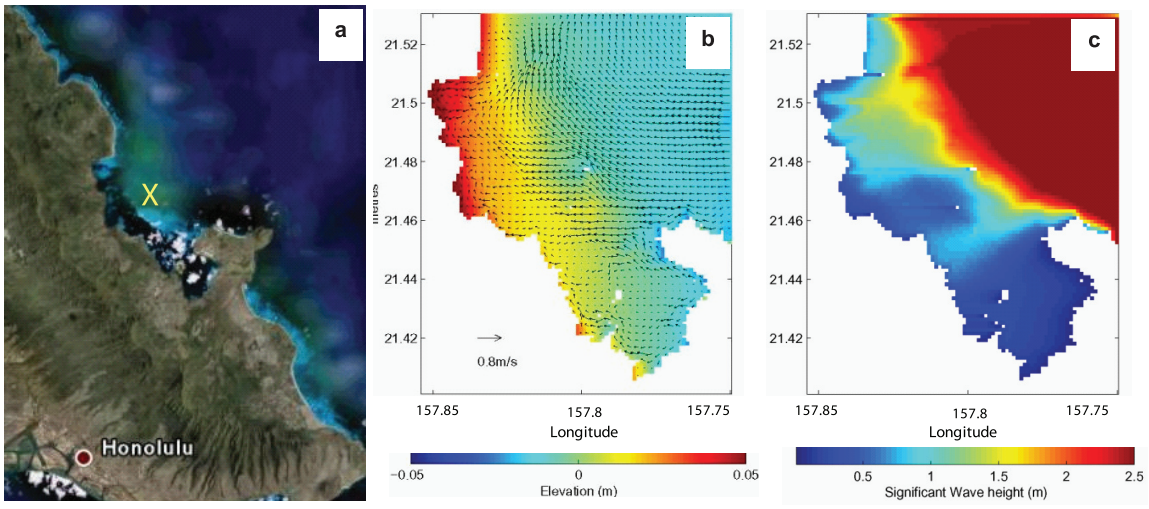

Figure 5.4. Kaneohe Bay (a), sea surface height (b), and wave height (c) after one day of forcing POM with lateral boundary conditions and an initial state provided by the regional configuration of HYCOM for the island of Oahu at 1-km resolution, and with a wind speed of 34 m/s and a 3-m swell.

and flow characteristics (turbulence, temperature, salinity, etc.) on marine habitats, including their effects on larval dispersion and coral health.

Argo products. The APDRC has made significant progress on Argo products, which support the Pacific Argo Regional Center in partnership with JAMSTEC. Codes have been unified and combined into a quasi-automated system. A secure public website has been started and is being filled with new data and products, which include in situ, Argo-based velocity estimates (YoMaHa'07), mixed-layer and isothermal-layer depths, hydrographic variables on standard levels and on isopycnals, and statistics and various gridded climatologies both in numerical and graphical forms (e.g., Figure 5.5). Products are currently being updated monthly and are available at http://apdrc.soest.hawaii.edu/projects/argo/. Work on a new global, three-dimensional velocity- and profile-product based on altimeter data and Argo velocity estimates and profile data has begun. Plans for the coming year include development of an efficient system for the quality control and mapping of the data at 10-day, near-real time intervals, and improving interfaces to communicate with Data Assembly Centers (DACs) and users. The dataset will be announced in *EOS*, on Argo mailing lists, and at scientific conferences.

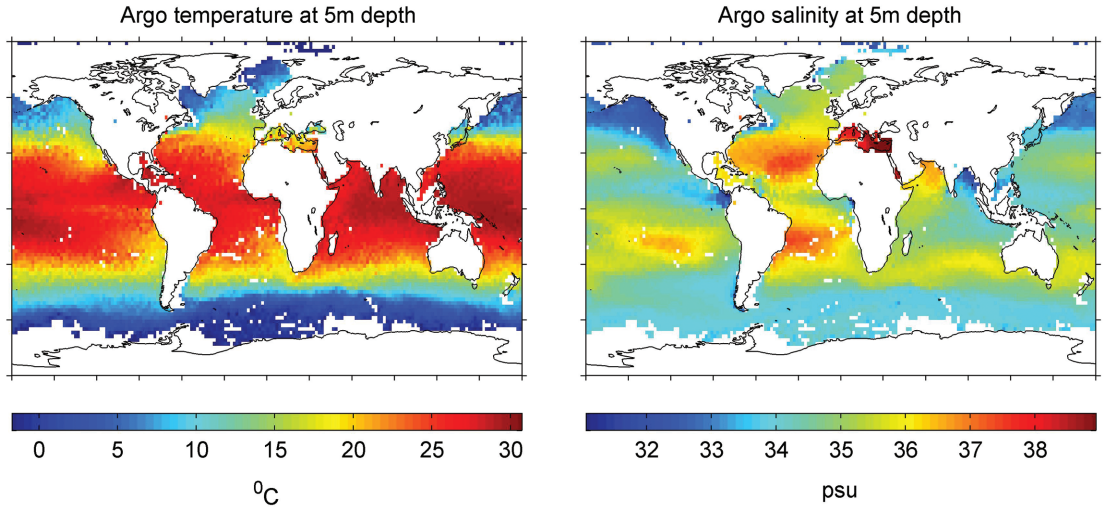

Figure 5.5. Multi-year mean (1997–2008) temperature and salinity at 5-m depth averaged in 2 x 2 degree boxes from Argo profile data. These fields and other Argo products are available at: http://apdrc.soest.hawaii.edu/projects/argo/index.html.

PUBLICATIONS

Published Papers

Annamalai, H., H. Okajima, and M. Watanabe, 2007: Possible impact of the Indian Ocean SST on the Northern Hemisphere circulation during El Niño. *J. Climate*, **20**, 3164–3189. IPRC-374.

Chambers, C. R. S., and T. Li, 2007: Simulation of formation of a near-equatorial typhoon Vamei (2001), *Meteor. Atmos. Physics*, **97,** DOI: 10.1007/s00703-006-0229-0. IPRC-424.

Chen, J.-M., T. Li, and C.-F. Shih, 2007: Fall persistence barrier of sea surface temperature in the South China Sea associated with ENSO. *J. Climate*, **20**, 158–172. IPRC-414.

Chen, S., B. Qiu, and P. Hacker, 2007: Profiling float measurements of the recirculation gyre south of the Kuroshio Extension in May-November 2004. *J. Geophys. Res.-Oceans*, **112**, C05023, doi:10.1029/2006. IPRC-449.

de Szoeke, S. P., S.-P. Xie, T. Miyama, K. J. Richards, and R. J. Small, 2007: What maintains the SST front north of the eastern Pacific equatorial cold tongue? *J. Climate,* **20**, 2500–2514. IPRC-436.

Di Lorenzo, E., N. Schneider, K. M. Cobb, P. J. S Franks, K. Chhak, A. J. Miller, J. C. McWilliams, S. J. Bograd , H. Arango, E. Curchitser, T. M. Powell, and P. Riviere, 2008: North Pacific Gyre Oscillation links ocean climate and ecosystem change. *Geophys. Res. Lett.*, **35**, L08607, doi:10.1029/2007GL032838. IPRC-507.

Ding, Q., and B. Wang, 2007: Intraseasonal interaction between the Eurasian wavetrain and the Indian summer monsoon. *J. Climate*, **20**, 3751–3767. IPRC-427.

Drbohlav, H.-K., and B. Wang, 2007: Horizontal and vertical structures of the northward propagating intraseasonal oscillation in the South Asian monsoon region simulated by an intermediate model. *J. Climate*, **20**, 4278–4286. IPRC-451.

Fu, B., T. Li, M. S. Peng, and F. Weng, 2007: Analysis of tropical cyclogenesis in the western North Pacific for 2000 and 2001. *Weather and Forecasting*, **22**, 763–780. DOI: 10.1175/WAF1013.1. IPRC-440.

Fu, X., B. Wang, D. E. Waliser, and L. Tao, 2007: Impact of atmosphere-ocean coupling on the predictability of monsoon intraseasonal oscillations. *J. Atmos. Sci.*, **64**, 157–174. IPRC-422.

Gan, J., and T. Qu, 2008: Coastal jet separation and associated flow variability in the Southwest South China Sea. *Deep-Sea Research I*, **55,** 1–19. IPRC-475.

Ge, X., T. Li, and X. Zhou, 2007: Tropical cyclone energy dispersion under vertical shears. *Geophys. Res. Lett.*, **34**, doi:10.1029/2007GL031867. IPRC-485.

Huang, H.-P., A. Kaplan, E. N. Curchitser, and N. A. Maximenko, 2007: The degree of anisotropy for mid-ocean currents from satellite observations and an eddy-resolving model simulation. *J. Geophys. Res.-Oceans*, **112**, C09005, doi:10.1029/2007JC004105. IPRC-459.

Jensen, T. G., 2007: Introduction: Special Issue on Indian Ocean Climate. *J. Climate*, **20**, 2869–2871. IPRC-430.

Jensen, T. G., 2007: Wind-driven response of the northern Indian Ocean to climate extremes. *J. Climate*, **20**, 2978–2993. IPRC-443.

Krebs, U., and A. Timmermann, 2007: Fast advective recovery of the Atlantic meridional overturning circulation after a Heinrich event. *Paleoceanography*, **2**, PA1220/doi 10.1029/2005PA001259. IPRC-466.

Krebs, U., and A. Timmermann, 2007: Tropical air-sea interactions accelerate the recovery of the Atlantic Meridional Overturning Circulation after a major shutdown. *J. Climate*, **20**, 4940-4956. IPRC-444.

Lamy, F., J. Kaiser, H. Arz, U. Ninnemann, O. Timm, A. Timmermann, and D. Hebbeln, 2007: Modulation of the bipolar seesaw in the Southeast Pacific during Termination 1. *Earth Planetary Science Letters*, **259**, 400–413. IPRC-464.

Li, L., B. Wang, Y. Wang, and H. Wan, 2007: Improvements in climate simulation with modifications to the Tiedtke Convective Parameterization in the Grid-point Atmospheric Model of IAP/LASG (GAMIL), *Advances in Atmospheric Sciences*, **24,** 323–335. IPRC-410.

Ma, S.-H., A.-X. Qu, and Y. Wang, 2007: The performance of the new tropical cyclone track prediction system of the China National Meteorological Center. *Meteor. Atmos. Phys.,* **97,** 29–39. IPRC-409.

Maximenko, N. A., O. V. Melnichenko, P. P. Niiler, and H. Sasaki, 2008: http://iprc.soest.hawaii.edu/~nikolai/Papers/2008GL033267.pdf. Stationary mesoscale jet-like features in the ocean. *Geophys. Res. Lett.*, **35**, L08603, doi:10.1029/2008GL033267. IPRC-516.

McCreary, J. P., T. Miyama, R. Furue, T. Jensen, H.-W. Kang, B. Bang, and T. Qu, 2007: Interactions between the Indonesian Throughflow and circulations in the Indian and Pacific Oceans. *Progr. in Oceanography,* **75** (1)**,** 70–114. IPRC-454.

Melnichenko, O. V., and N. A. Maximenko, 2007: Stationary alternating zonal jets in hydrographic data of the eastern North Pacific. *Proceedings of PACON 2007: Ocean Observing Systems and Marine Environment*, 55–63. IPRC-463.

Menviel, L., A. Timmermann, A. Mouchet, and O. Timm, 2008: Meridional reorganizations of marine and terrestrial productivity during glacial Heinrich events. *Paleoceanography*, **23**, doi:10.1029/2007PA001445. IPRC-484.

Minobe, S., A. Kuwano-Yoshida, N. Komori, S.-P. Xie, and R. J. Small, 2008: Influence of the Gulf Stream on the troposphere. *Nature,* **452,** 206–209. IPRC 505.

Natarov, A., K. Richards, and J. P. McCreary, 2008: Two-dimensional instabilities of time-dependent zonal flows: Linear shear. *J. Fluid Mech.*, **599**, 29–50. IPRC-468.

Okajima, H., and S.-P. Xie, 2007: Orographic effects on the northwestern Pacific monsoon: Role of air-sea interaction. *Geophys. Res. Lett.,* **34**, L21708, doi:10.1029/2007GL032206. IPRC-477.

Pahnke, K., J. Sachs, L. Keigwin, A. Timmermann, and S.-P. Xie, 2007: Eastern tropical Pacific hydrological changes during the past 27,000 years from D/H ratios in alkenones. *Paleoceanography*, **22**, PA4214, doi:10.1029/2007PA001468. IPRC-483.

Pan, L.-L., and T. Li, 2007: Interactions between the Tropical ISO and midlatitude low-frequency flow. *Climate Dynamics*, doi: 10.1007/s00382-007-0272-7. IPRC-453.

Potemra, J. T., and N. Schneider, 2007: Influence of low-frequency Indonesian throughflow transport on temperatures in the Indian Ocean in a coupled model. *J. Climate*, **20**, 1339–1352. IPRC-431.

Qiu, B., N. Schneider, and S. Chen, 2007: Coupled decadal variability in the North Pacific: An observationally-constrained idealized model. *J. Climate*, **20**, 6302-6320. IPRC-437.

Qiu, B., S. Chen, and P. Hacker, 2007: Effect of mesoscale eddies on Subtropical Mode Water variability from the Kuroshio Extension System Study (KESS). *J. Phys. Oceanogr.*, **37**, 982–1000. IPRC-448.

Qu, T., S. Gao, I. Fukumori, R. A. Fine, and E. J. Lindstrom, 2008: Subduction of South Pacific Waters. *Geophys. Res. Lett.*, **35,** L02610, doi:10.1029/2007GL032605. IPRC-495.

Qu, T., Y. Du, J. Gan, and D. Wang, 2007: Mean seasonal cycle of isothermal depth in the South China Sea. *J. Geophys. Res.-Oceans*, **112**, C02020, doi:10.1029/2006JC003583. IPRC-416.

Qu, T., Y. Du, J. P. McCreary, G. Meyers, and T. Yamagata, 2008: Buffering effect and its related ocean dynamics in the Indonesian Throughflow region. *J. Phys. Oceanogr.*, **38** (2) 503–516. IPRC-455.

Raible, C., M. Yoshimori, T. F. Stocker, and C. Casty, 2007: Extreme midlatitude cyclones and their implications for precipitation and wind speed extremes in simulations of the Maunder Minimum versus present day conditions. *Climate Dynamics,* **28**, 409–423, doi:10.1007/s00382-006-0188-7. IPRC-389.

Sampe, T., and S.-P. Xie, 2007: Mapping high sea winds from space: A global climatology. *Bull. Amer. Meteor. Soc.*, **88** (12), 1965–1978. IPRC-469.

Sentchev, A., and M. Yaremchuk, 2007: VHF radar observations of surface currents off the Northern Opal coast in the eastern English Channel. *Cont. Shelf Res.*, **27**, 2449–2464. IPRC-461.

Small, R. J., S. P. deSzoeke, and S.-P. Xie, 2007: The Central American Mid-summer Drought: regional aspects and large scale forcing. *J. Climate*, **20**, 4853–4873. IPRC-441.

Stocker, T. F., A. Timmermann, M. Renold, and O. Timm, 2007: Effects of salt compensation on the climate model response in simulations of large changes of the Atlantic meridional overturning circulation. *J. Climate*, **20**, 5912–1928. IPRC-452.

Stott, L., A. Timmermann, and R. Thunell, 2007: Southern Hemisphere and deep sea warming led deglacial atmospheric CO_2 rise and tropical warming. *Science*, DOI: 10.1126/1143791. IPRC-471.

Sui, C.-H., P.-H. Chung, and T. Li, 2007: Interannual and interdecadal variability of the summertime western North Pacific subtropical high. *Geophys. Res. Lett.,* **34**, L11701, doi:10.1029/2006GL029204. IPRC-490.

Timm, O., and A. Timmermann, 2007: Simulation of the last 21,000 years using accelerated transient boundary conditions, *J. Climate*, **20**, 4377–4401. IPRC-439.

Timmermann, A., S. Lorenz, S.-I. An, A. Clement, and S.-P. Xie, 2007: The effect of orbital forcing on the mean climate and variability of the tropical Pacific. *J. Climate,* **20**, 4147–4149. IPRC-450.

Timmermann, A., Y. Okumura, S.-I. An, A. Clement, B. Dong, E. Guilyardi, A. Hu, J. H. Jungclaus, M. Renold, T. F. Stocker, R. J. Stouffer, R. Sutton, S.-P. Xie, and J. Yin, 2007: The influence of a shutdown of the Atlantic meridional overturning circulation on ENSO. *J. Climate*, **20**, 4899–4919. IPRC-442.

Tozuka, T., T. Qu, and T. Yamagata, 2007: Dramatic impact of the South China Sea on the Indonesian Throughflow. *Geophys. Res. Lett.*, **34,** L12612, doi:10.1029/2007GL030420. IPRC-456.

Ventham, J. D., and B. Wang, 2007: Large scale flow patterns and their influence on the intensification rates of western North Pacific tropical storms. *Mon. Wea. Rev.*, **135**, 1110–1127. IPRC-388.

Wang, B., and X. Zhou, 2008: Climate variation and prediction of rapid intensification in tropical cyclones in the western North Pacific. *Meteorology and Atmospheric Physics*, **99**, 1–16. doi: 10.1007/s00703-006-0238-z. IPRC-428.

Wang, B., J.-G. Jhun, and B.-K. Moon, 2007: Variability and singularity of Seoul rainy season (1778-2004). *J. Climate*, **20**, 2572–2580. IPRC-446.

Wang, Y., 2007: A multiply nested, movable mesh, fully compressible, nonhydrostatic tropical cyclone model - TCM4: Model description and development of asymmetries without explicit asymmetric forcing. *Meteor. Atmos. Phys.*, **97**, 93–116. IPRC-433.

Wang, Z., B. Wang, and C.-P. Chang, 2007: Impacts of El Niño and La Niña on the U.S. Climate during Northern Summer. *J. Climate*, **20**, 2165–2177. IPRC-447.

Watanabe, Y. W., H. Yoshinari, A. Sakamoto, Y. Nakano, N. Kasamatsu, T. Midorikawa, and T. Ono, 2007: Reconstruction of sea surface dimethylsulfide in the North Pacific during 1970s to 2000s. *Marine Chemistry*, **103**, 347–358. IPRC-421.

Wilson, C., T. A. Villareal, N. Maximenko, S. J. Bograd, J. P. Montoya, and C. A. Schoenbaechler, 2008: Biological and physical forcings of late summer chlorophyll blooms at 30°N in the oligotrophic Pacific. *J. Mar. Sys.,* **69**, 164–176. IPRC-350.

Xie, S.-P., C.-S. Chang, Q. Xie, and D. Wang, 2007: Intraseasonal variability in the summer South China Sea: The wind jet, cold filament, and recirculations. *J. Geophys. Res.-Oceans*, **112**, doi:10.1029/2007JC004238. IPRC-470.

Xie, S.-P., T. Miyama, Y. Wang, H. Xu, S. P. de Szoeke, R. J. Small, K. J. Richards, T. Mochizuki, and T. Awaji, 2007: A regional ocean-atmosphere model for eastern Pacific climate: Towards reducing tropical biases. *J. Climate*, **20**, 1504–1522. IPRC-413.

Yang, B., Y. Wang, and B. Wang, 2007: The Effect of internally generated inner-core asymmetries on tropical cyclone potential intensity. *J. Atmos. Sci.*, **64**, 1165–1188. IPRC-435.

Yang, Y., and Y.-L. Chen, 2008: Effects of terrain heights and sizes on island-scale circulations and rainfall for the island of Hawaii during HaRP. *Mon. Wea. Rev.,* **136,** 120–126, doi: 10.1175/2007MWR1984.1. IPRC-457.

Yu, Z., J. P. McCreary, M. Yaremchuk, and R. Furue, 2008: Subsurface salinity balance in the South China Sea. *J. Phys. Oceanogr.*, **38** (2), 527–539. IPRC-460.

Zhang, X., T. Li, F. Weng, C.-C. Wu, and L. Xu, 2007: Reanalysis of western Pacific typhoons in 2004 with multi-satellite observations. *Met. and Atmos. Phys.*, **97**, 3–18. IPRC-434.

Zhao, Y., B. Wang, and Y. Wang, 2007: Initialization and simulation of a landfalling typhoon using a variational bogus mapped data assimilation (BMDA). *Meteor. Atmos. Phys.,* **98** (3-4), 269-282. IPRC- 472.

Zhou, X., and B. Wang, 2007: Transition from an Eastern Pacific upper-level mixed Rossby-gravity wave to a Western Pacific tropical cyclone. *Geophys. Res. Lett.,* **34**, L24801, doi:10.1029/2007GL031831, IPRC-486.

Papers in Press

For up-to-date listing of IPRC publications see our website http://iprc.soest.hawaii.edu/publications/publications.html

Aiki, H., and K. J. Richards: Energetics of the global ocean: The role of layer-thickness form drag. *J. Phys. Oceanogr.*, IPRC-504.

Boer, G. J., and K. Hamilton: QBO influence on extratropical predictive skill. *Climate Dynamics*, IPRC-506.

Cahyarini, S. Y., M. Pfeiffer, O. Timm, W.-C. Dullo, and D. G. Schönberg: Reconstructing seawater $\delta^{18}O$ from paired coral $\delta^{18}O$ and Sr/Ca ratios: Methods, error analysis and problems, with examples from Tahiti (French Polynesia) and Timor (Indonesia). *Geochimica et Cosmochimica Acta*, IPRC-520.

Calil, P. H. R., K. J. Richards, Y. Jia, and R. R. Bidigare: Eddy activity in the lee of the Hawaiian Islands. *Deep-Sea Research II*, IPRC-462.

de Szoeke, S.P., and S.-P. Xie: The tropical eastern Pacific seasonal cycle: Assessment of errors and mechanisms in IPCC AR4 coupled ocean-atmosphere general circulation models. *J. Climate*, IPRC-480.

Du, Y., T. Qu, and G. Meyers: Interannual variability of the sea surface temperature off Java and Sumatra in a global GCM. *J. Climate*, IPRC-487.

Du, Y., and S.-P. Xie: Role of atmospheric adjustments in the tropical Indian Ocean warming during the 20th century in climate models. *Geophys. Res. Lett.*, IPRC-517.

Fu, X., B. Yang, Q. Bao, and B. Wang: Sea surface temperature feedback extends the predictability of tropical intraseasonal oscillation. *Mon. Wea. Rev.*, IPRC-482.

Ge, X., T. Li, Y. Wang, and M.S. Peng: Tropical cyclone energy dispersion in a three-dimensional primitive equation model: Upper tropospheric influence. *J. Atmos. Sci.*, IPRC-489.

Geller, M., T. Zhou, and K. Hamilton: Morphology of tropical upwelling in the Lower Stratosphere. *J. Atmos. Sci.*, IPRC-476.

Hong, C.-C., T. Li, LinHo, and J.-S. Kug: Asymmetry of the Indian Ocean dipole. Part I: Observational analysis. *J. Climate*, IPRC-499.

Hong, C.-C., T. Li, and J.-J. Luo: Asymmetry of the Indian Ocean Dipole. Part II: Model Diagnosis. *J. Climate*, IPRC-500.

Kikuchi, K., and B. Wang: Diurnal precipitation regimes in the global tropics. *J. Climate*, IPRC-491.

Maximenko, N. A., P. P. Niiler, and O. V. Melnichenko: Global mean dynamic ocean topography reveals new coherent features of surface circulation. *Proceedings of the 2007 International Conference Fluxes and Structures in Fluid*, Moscow, Russia, IPRC-488.

Richter, I., and S.-P. Xie: On the origin of equatorial Atlantic biases in coupled general circulation models. *Climate Dynamics*, IPRC-498.

Sasaki, Y. N., S. Minobe, N. Schneider, T. Kagimoto, M. Nonaka, and H. Sasaki: Decadal sea level variability in the South Pacific in a global eddy-resolving ocean model hindcast. *J. Phys. Oceanogr.*, IPRC-508.

Small, R. J., S. P. de Szoeke, S.-P. Xie, L. O'Neill, H. Seo, Q. Song, P. Cornillon, M. Spall, and S. Minobe: Air-sea interaction over ocean fronts and eddies. *Dynamics of Atmospheres and Oceans*, IPRC-501.

Solomon, A., S.-I. Shin, M. A. Alexander, and J. P. McCreary: The relative importance of tropical variability forced from the North Pacific through ocean pathways. *Climate Dynamics*, IPRC-496.

Sperber, K. R., and H. Annamalai: Coupled model simulations of boreal summer intraseasonal (30-50 day) variability, Part I: Systematic errors and caution on use of metrics. *Climate Dynamics*, IPRC-519.

Timm, O., A. Timmermann, A. Abe-Ouchi, F. Saito, and T. Segawa: On the definition of seasons in paleoclimate simulations with orbital forcing. *Paleoceanography*, IPRC-513.

Wang, B., and Q. Ding: Global monsoon: Dominant mode of annual variation in the tropics. *Dynamics of Atmospheres and Oceans*, IPRC-502.

Wang, B., J.-Y. Lee, I.-S. Kang, J. Shukla, J.-S Kug, A. Kumar, J. Schemm, J.-J. Luo, T. Yamagata, and C.-K. Park: How accurately do coupled climate models predict the leading modes of the Asian-Australian monsoon interannual variability? *Climate Dynamics*, IPRC-478.

Wang, B., J. Yang, T. Zhou, and B. Wang: Interdecadal changes in the major modes of Asian-Australian monsoon variability: Strengthening relationship with ENSO since the late 1970s. *J. Climate*, IPRC-481.

Wang, B., Z. Wu, J. Li, J. Liu, C.-P. Chang, Y. Ding, and G.-X. Wu: How to measure the strength of the East Asian summer monsoon. *J. Climate*, IPRC-511.

Wang, B., and H. Yang: Hydrological issues in lateral boundary conditions for regional climate modeling: simulation of East Asian summer monsoon in 1998. *Climate Dynamics*, IPRC-512.

Wang, Y.: Structure and formation of an annular hurricane simulated in a fully-compressible, nonhydrostatic model - TCM4. *J. Atmos. Sci.*, IPRC-474.

Wang, Y.: Rapid filamentation in a numerically simulated tropical cyclone. *J. Atmos. Sci.*, IPRC-479.

Wu, L., C. Li, C. Yang, and S.-P. Xie: Global teleconnections in response to a shutdown of the Atlantic meridional overturning circulation. *J. Climate*, IPRC-492.

Xie, S.-P., Y. Okumura, T. Miyama, and A. Timmermann: Influences of Atlantic climate change on the tropical Pacific via the Central American Isthmus. *J. Climate*, IPRC-503.

Yang, B., X. Fu, and B. Wang: Atmosphere-ocean conditions jointly guide convection of the boreal summer intraseasonal oscillation: satellite observations. *J. Geophys. Res.-Atmos.*, IPRC-510.

Yang Y., J. Ma, and S.-P. Xie: Observations of the trade wind wakes of Kauai and Oahu. *Geophys. Res. Lett.*, IPRC-497.

Yang, Y., S.-P. Xie, and J. Hafner: The thermal wake of Kauai Island: Satellite observations and numerical simulations. *J. Climate,* IPRC-509.

Zhang, C.-X., Q.-H. Zhang, and Y. Wang: Climatology of hail in China: 1961-2005. *J. Appl. Meteor. Climatol.*, IPRC-473.

Zhang, Y., and T. Li: Influence of the sea surface temperature in the Indian Ocean on the in-phase transition between the South Asian and North Australian summer monsoons. *Terr. Atmos. Ocean. Sci.* , IPRC-515.

Zhu, W., and K. Hamilton: Empirical estimates of global climate sensitivity: An assessment of strategies using a coupled GCM. *Advances in Atmospheric Sciences*, IPRC-514.

Books and Book Chapters

Hamilton, K., and W. Ohfuchi (Eds.), 2008: *High Resolution Numerical Modelling of the Atmosphere and Ocean*, Springer Publishers, New York, New York, 296 pp.

Hamilton, K., 2008: Numerical resolution and modelling of the global atmospheric circulation: A review of our current understanding and outstanding issues. *High Resolution Numerical Modelling of the Atmosphere and Ocean*, Springer Publishers, New York, New York, pp. 7-28.

Richards, K. J., H. Sasaki, and F. O. Bryan, 2008: Jets and waves in the Pacific Ocean. *High Resolution Numerical Modelling of the Atmosphere and Ocean*, Springer Verlag, New York, New York, pp. 187–196.

WORKSHOPS AND CONFERENCES

Date	Title
February 14–15, 2008	Asian Monsoon Variability and Predictability
February 5, 2008	Mini-workshop on High-Resolution Climate Modeling
January 2–12, 2008	START (Global Change SysTem Analysis for Research Training) Workshop - The Monsoon System: Prediction of Change and Variability Advanced Institute
December 6, 2007	Mini-workshop on Jets and Fronts
November 16–17, 2007	Workshop on the JAMSTEC-PMEL-IPRC Joint Study Program of the Buoy Measurements in the Western North Pacific
November 13–14, 2007	Workshop on Climatic Changes in the Last 1500 Years: Their Impact on Pacific Islands
August 28, 2007	Mini-workshop on Air-sea Interaction at Ocean Fronts
April 17–18, 2007	Seventh Annual IPRC Symposium

THE YEAR'S SEMINARS

Date	Speaker	Affiliation	Title
*** March 27, 2008**	Minoru Kadota	Center for Atmosphere Ocean Science (CAOS), New York University, New York	*The MJO and statistical mid-latitude atmospheric predictability*
**** March 20, 2008**	Niklas Schneider	International Pacific Research Center	*The Kuroshio Large Meander in an eddy resolving ocean model (OFES)*
****** March 18, 2008**	Gerold Siedler	Leibniz-Institute for Marine Sciences, Kiel University, Germany	*Western boundary currents and the subtropical countercurrent in the southern Indian Ocean*
*** March 14, 2008**	Shunya Koseki	IPRC Visiting Scientist	*Effect of the mesoscale SST anomaly on the synoptic scale disturbance in the Kuroshio Extension*
**** February 28, 2008**	Jay McCreary	International Pacific Research Center	*Interactions between the Indonesian Throughflow and circulations in the Indian and Pacific Oceans*
*** February 6, 2008**	Yuqing Wang	International Pacific Research Center	*How do outer spiral rainbands affect tropical cyclone structure and intensity?*
January 16, 2008	Claude Frankignoul	Université Pierre et Marie Curie, Paris, France	*The role of salinity in the decadal variability of the North Atlantic meridional overturning circulation*
January 8, 2008	Ted Durland	Woods Hole Oceanographic Institution, Woods Hole, Massachusetts	*Eddy generation by a poleward outflow*
*** December 7, 2007**	Craig Bishop	Naval Research Laboratory, Monterey, California	*A new adaptive error covariance localization tool for 4-dimensional ensemble data assimilation*
***** December 4, 2007**	Peter B. Rhines	Oceanography and Atmospheric Sciences, University of Washington, Seattle, Washington	*Exploring the subarctic seas from above and below: satellite altimetry and robotic seagliders*
November 15, 2007, Special IPRC Seiminar	Lonnie Thompson	Ohio State University, Columbus, Ohio	*Abrupt climate change: Past, present, and future*
*** October 31, 2007**	Hidenori Aiki	IPRC Visiting Scientist JAMSTEC-FRCGC, Yokohama, Japan	*The Red Sea outflow regulated by the Indian monsoon*
October 30, 2007	Ian Eisenman	Harvard University, Boston, Massachusetts	*Rain driven by ice sheets as a cause of past abrupt climate change*
*** October 10, 2007**	Axel Lauer	International Pacific Research Center	*Global model simulations of the impact of ocean-going ships on aerosols, clouds, and the radiation budget*
*** October 3, 2007**	Eric Guilyardi	Visiting Scholar LOCEAN/ IPSL, University Paris VI, Paris, France	*Understanding El Niño in ocean-atmosphere general circulation models*

Date	Speaker	Affiliation	Title
*** September 19, 2007**	Hisayuki Kubota	JAMSTEC Institute of Observational Research for Global Change, Yokosuka, Japan	*Impact of tropical cyclones on interannual rainfall variability over the western North Pacific*
*** September 12, 2007**	Tim Li	International Pacific Research Center	*Asymmetry of the Indian Ocean Dipole - Observational analysis and model diagnosis*
**** August 30, 2007**	Nikolai Maximenko	International Pacific Research Center	*Improved mean ocean surface circulation: What's new?*
**** August 23, 2007**	Hyodae Seo	International Pacific Research Center	*Ocean-atmosphere interaction in a high-resolution regional coupled model*
July 30, 2007	Audine Laurian	LOCEAN, Université Pierre et Marie Curie, Paris, France	*Surface generation of poleward-propagating spiciness anomalies in the North Atlantic Ocean*
June 28, 2007	Soon-Il An	Atmospheric Sciences, Yonsei University, Seoul, Korea	*How ENSO and its impact on climate may change with increasing greenhouse gases*
May 21, 2007	Johannes Loschnigg	Space and Aeronautics Subcommittee, Washington, DC	*Science, Policy and the U.S. Congress: Current Issues involving NASA, NOAA and climate change*
May 14, 2007	William Kessler	NOAA Pacific Marine Environmental Laboratory, Seattle, Washington	*The annual cycle of circulation in the southwest subtropical Pacific, diagnosed in an OGCM*
May 4, 2007	Zhengyu Liu	Center for Climatic Research, University of Wisconsin, Madison, Wisconsin	*Rethinking tropical SST response to global warming: El Niño-like vs. Enhanced Equatorial Response*
*** April 11, 2007**	Justin Small	International Pacific Research Center	*Intraseasonal variability of rainfall in the eastern Tropical Pacific and Central America*
April 4, 2007	Alexandre Ganachaud	NOAA-PMEL, Joint Institute for the Study of the Atmosphere and the Ocean, Seattle, Washington	*Southwest Pacific Ocean and SPICE: Jets around Vanuatu and New Caledonia from an inverse box model and a high-resolution regional model*

* Joint IPRC UH Mānoa Meteorology Department Seminar
** Joint IPRC UH Mānoa Oceanography Department Seminar
*** Joint IPRC UH Mānoa Meteorology and Oceanography Department Seminar
****Joint IPRC-ICCS Seminar

LUNCHEON DISCUSSIONS

Date	Speaker	Affiliation	Title
March 11, 2008	Kunihiro Aoki	Hokkaido University, Japan	*Midlatitude baroclinic Rossby waves in a high-resolution OGCM simulation*
February 19, 2008	Tomoki Tozuka	Earth and Planetary Science, University of Tokyo	*Impacts of the South China Sea Throughflow on seasonal and interannual variations of the Indonesian Throughflow*
November 9, 2007	Takuji Waseda	University of Tokyo, Tokyo, Japan	*Application oriented oceanography: Freak wave, renewable energy and larval dispersion*
	Hitoshi Tamura	JAMSTEC-FRCGC, Yokohama, Japan	*Numerical study of wave-current interaction using a new scheme of nonlinear energy transfer among wind waves*
September 25, 2007	Ping Liu	International Pacific Research Center	*Tropical intraseasonal variability in the MRI 20km60L AGCM*
September 18, 2007	Kelvin Richards	International Pacific Research Center	*The impact of ocean mixing in the eastern tropical Pacific*
August 8, 2007	Kazuhisa Tsuboki	Hydrospheric Atmospheric Research Center, Nagoya University, Japan	*Numerical simulations of high-impact weather systems using the cloud-resolving model on the Earth Simulator*
May 31, 2007	Oliver Timm	International Pacific Research Center	*The future climate of Hawai'i*
May 30, 2007	Yoichi Tanimoto	Graduate School of Environmental Science, Hokkaido University, Sapporo, Japan	*Modifications of the marine boundary layer over the Kuroshio extension: A study based on ship-board GPS soundings.*
May 4, 2007	Tangdong Qu	International Pacific Research Center	*Origin and pathway of the 13°C water in the Pacific*

IPRC VISITING SCHOLARS

The IPRC has a visiting scholar program. From April 2007 to March 2008, the following scholars visited the IPRC for one week or longer.

Name	Affiliation	Dates
Yoshikazu Sasai	JAMSTEC-FRCGC, Yokohama, Japan	03/31/08–06/27/08
Gerold Siedler	Leibniz-Institute for Marine Sciences, University of Kiel, Kiel, Germany	03/12/08–03/20/08
Kenneth Sperber	Lawrence Livermore National Laboratory, Livermore, California	03/02/08–08/28/08
Kunihiro Aoki	Hokkaido University, Sapporo, Japan	03/01/08–04/15/08
Haiming Xu	Nanjing University of Information Science and Technology, Nanjing, China	02/16/08–04/15/08
Hideharu Sasaki	JAMSTEC-ESC, Yokohama, Japan	02/08/08–02/29/08
Tomoki Tozuka	University of Tokyo, Tokyo, Japan	02/14/08–02/23/08
R.H. Kripalani	Indian Institute of Tropical Meteorology, Pashan, India	01/05/08–01/11/08
Yi Lu	National Taiwan University, Taipei, Taiwan	01/21/08–02/20/08
Peter Niiler	Scripps Institution of Oceanography, La Jolla, California	01/14/08–02/29/0
Shunya Koseki	Hokkaido University, Sapporo, Japan	01/10/08–03/31/08
In-Sik Kang	Seoul National University, Seoul, Korea	12/30/07–02/15/08
Emilia Jin	George Mason University, Fairfax, Virginia	12/26/07–01/09/08
Peter Rhines	University of Washington, Seattle, Washington	12/02/07–12/20/07
Dejun Gu	China Meteorological Administration, Beijing,China	11/01/07–01/31/08
Kohei Takatama	Hokkaido University, Sapporo, Japan	08/27/07–09/07/07
Shoshiro Minobe	Hokkaido University, Sapporo, Japan	08/27/07–08/31/07
Audine Laurian	Université Pierre et Marie Curie, Paris, France	07/27/07–08/06/07
Kazuhisa Tsuboki	Nagoya University, Nagoya, Japan	07/26/07–08/14/07
Soon-Il An	Yonsei University, Seoul, Korea	06/17/07–08/10/07
Johannes Loschnigg	Space and Aeronautics Subcommittee, Washington, DC	05/07/07–05/22/07

IPRC FUNDING

Institutional Support

Title	PI and Co-PIs	Agency	Amount	Period
Enhancement of Data and Research Activities for Climate Studies at the International Pacific Research Center (IPRC)	J.P. McCreary, P. Hacker & J. Potemra	NOAA	$1,005,000	10/01/07–09/30/08
JAMSTEC YR 11, (2007 – 2008)	J. McCreary	JAMSTEC	$2,316,000	04/01/07–03/31/08
Support of Research at the International Pacific Research Center	Not applicable	*University of Hawai'i	$528,670	04/01/07–03/31/08
Data-Intensive Research and Model Development at the International Pacific Research Center	J.P. McCreary, S.P. Xie, & P. Hacker	NASA	$1,050,000	03/01/07–02/29/12

* The University of Hawai'i also provides approximately 16,500 sq. ft. of office space to the IPRC

Individual Grants

Title	PI and Co-PIs	Agency	Amount	Period
Arrangement of historical observation dataset for Philippines meteorological stations II	S.P. Xie	JAMSTEC / IORGC	$4,232	12/01/07–03/31/08
Climate Change and Persistent Droughts: Impacts, Vulnerability and Adaptation in Rice Growing Subdivisions of India	H. Annamalai	Norwegian Embassy	$127,053	12/07/07–11/30/10
Measurements of the velocity field associated with interleaving	K. Richards	NSF	$117,330	08/01/07–01/31/09
An adaptive food web model for the epipelagic and mesopelagic	K. Richards	LSU	$95,531	02/01/06–07/31/08
Arrangement of historical observation dataset for Philippines meteorological stations	S.P. Xie	Tokyo Metropolitan University	$6,000	09/13/07–12/31/07
UH/MHPCC Generation of Submesoscale	K. Richards	MHPCC-Engagement Grant	$35,174	08/25/07–06/30/09
PI-GCOS Server Reimbursement	J. Potemra	Bureau of Meteorology Australia	$20,000	06/01/07–05/31/09
Improving the COAMPS atmospheric variational data assimilation system with direct use of satellite radiances	T. Li & X. Zhang	DOD-PET / ONR	$68,000	06/01/07–05/31/08
Understanding Annual Cycle-ENSO Interactions in Climate Change Simulations	N. Schneider & A. Timmermann	DOE	$142,877	08/15/07–08/14/08
Collaborative Research: Impacts of ocean physics on the Arabian Sea oxygen minimum zone	J. McCreary, K. Richards, & Z. Yu	NSF	$385,570	10/01/07–09/3010
Future Projections of Mean and Variability of the Asian Summer Monsoon and Indian Ocean Climate Systems	H. Annamalai	DOE	$165,836	08/01/07–07/31/08
Understanding climate-biogeochemical feedbacks during the last glacial-interglacial transition: A systematic modeling and paleo-data synthesis approach	A. Timmermann	NSF	$314,100	07/01/07–06/30/10
Inter-annual variability and prediction on eddies in the Gulf of Aden and the Somali Current Region	T. Jensen	ONR	$103,050	05/01/07–12/31/08

Title	PI and Co-PIs	Agency	Amount	Period
APCC Multi-Model Ensemble Seasonal Prediction System Development	B. Wang	APCC	$159,184	05/01/07–03/31/08
Analysis of climate change in Korea and East Asia area and study of the atmospheric and ocean effects	B. Wang	Yonsei University	$121,279	04/01/07–12/31/09
Collaborative Research: Decadal Coupled Ocean-Atmosphere Interactions in the North	N. Schneider	NSF	$72,365	03/01/07–02/28/10
Dynamics of Boreal Summer Intraseasonal Oscillation	B. Wang & J. Fu	NSF	$342,883	03/01/07–02/28/09
Acceleration of the Last Glacial Termination Due to Climate-Carbon Cycle Feedbacks	A. Timmermann	NSF	$42,465	02/01/07–01/31/09
Western Pacific Tropical Cyclone Reanalysis with the NRL Atmospheric Variational Data Assimilation System (NAVDAS)	T. Li & X. Zhang	ONR	$180,957	01/01/07–08/31/10
Using a Digital Filter As a Weak Constraint in WRF 4D-VAR	T. Li & X. Zhang	NCAR	$105,816	11/01/06–07/31/08
Collaborative Research: Origin, Pathway and Fate of Equatorial 13°C Water in the Pacific	T. Qu & I. Fukumori	NSF	$486,210	09/01/06–08/31/09
Dynamics of Tropical Cyclone Intensity Change	T. Li	ONR / NRL	$91,000	09/01/06–08/31/09
Sensitivity of MJO to the CAPE Lapse Time in the NCAR CAM 3	B. Wang & P. Liu	DOE/NSF	$25,000	09/01/06–08/31/07
Using Climate Information to Identify Coral Communities That Are Positioned to Survive Global Climate Change	A. Timmermann	NOAA / Nature Conservancy	$55,000	07/01/06–07/31/07
The Atmospheric Response to Ocean Heat Flux Convergences	N. Schneider	UCSD / Scripps	$51,327	07/01/06–04/30/07
Orographically Induced Ocean-Atmosphere Interaction: Satellite Observations and Numerical Modeling	S.P. Xie	NASA	$248,162	06/15/06–06/24/10
Further Testing and Evaluation of Code Coupling Methodologies and Application of a Leading Coupling Framework to Atmospheric and Oceanic Models	T. Li, X. Zhang & Y. Jia	DOD-PET / MSU	$87,700	07/01/06–05/31/07
Effects of the Stratospheric Quasi-biennial Oscillation on Seasonal Predictability of Tropospheric Circulation in the Northern Hemisphere Extratropics	K. Hamilton	NOAA-CLIVAR	$166,355	06/01/06–05/31/09
APCC Multi-Model Ensemble Seasonal Prediction System Development	B. Wang, I.S. Kang & J. Shukla	APCC	$167,617	05/15/06–09/30/07
Collaborative Research: Eddy Dynamics and Impacts of Low Frequency Variations in the California Current System	N. Schneider	NSF	$193,340	03/01/06–02/28/09
Validation of Alternating Zonal Jets Detected in Satellite Altimetry Using *In-Situ* Observations	N. Maximenko	NSF	$170,147	02/15/06–01/31/09
Tropical Cyclone Genesis and Sudden Changes of Track and Intensity in the Western Pacific	B. Wang, T. Li & Y. Wang	ONR	$643,500	01/01/06–09/30/08
Ship-board Atmospheric Sounding over the Kuroshio Extension: A Supplement to CLIVAR KESS	S.P. Xie & B. Qiu	NSF	$219,707	04/01/05–03/31/09

Title	PI and Co-PIs	Agency	Amount	Period
Roles of Ocean Atmosphere-Interaction in Seasonal and Interannual variation of the Atlantic ITCC	S.P. Xie	NOAA	$244,990	02/01/05–01/31/08
Dynamic Balance of the Oceanic Mixed Layer Observed by *In Situ* Measurements and Remote Sensing	N. Maximenko	NASA / Scripps	$332,614	01/01/05–09/28/08
Analysis of Climate Change in Korea and East Asia Area and Study of the Atmospheric and Ocean Effects	B. Wang	Yonsei University	$149,199	06/01/04–03/31/08
Study of Processes Leading to Tropical Cyclone Intensity Change	Y. Wang	NSF	$278,840	10/15/04–09/30/08
Predictability and Diagnosis of Low Frequency Climate Processes in the Pacific	N. Schneider	Dept of Energy	$150,002	09/15/04–09/14/08
Application of Satellite Data to Improve the Simulation and Prediction of Tropical Intraseasonal Oscillation	J. Fu, B Wang, & X. Xie	NASA	$272,333	06/01/04–05/31/08
Mixing in the Equatorial Pacific: The Role of Interleaving	K. Richards & J.P. McCreary	NSF	$346,315	09/01/03–08/31/07
Development of Tropical Cyclone Ensemble Forecast and Cyclogenesis Modeling and Forecast for the DOD's JTWC	T. Li & B. Wang	DOD / ONR	$499,982	06/01/03–12/31/07
Application of Comprehensive Global Models to Problems in the Dynamics of the Troposphere and Stratosphere	K. Hamilton	NSF	$322,809	09/01/02–05/31/08

IPRC STAFF*

LEADERSHIP TEAM

Julian McCreary, Jr.
Director
Professor of Oceanography, UH

Lorenz Magaard
Executive Associate Director
Director, ICCS
Professor of Oceanography, UH

Saichiro Yoshimura
Liaison Officer
Advisor, FRCGC

RESEARCH TEAMS

Indo-Pacific Ocean Climate

Shang-Ping Xie
Team Co-Leader
Professor of Meteorology, UH
Editor, *Journal of Climate*

Niklas Schneider
Team Co-Leader
Associate Professor, Oceanography, UH

Ryo Furue
Visiting Assistant Researcher

Jan Hafner
Scientific Computer Programmer

Nikolai Maximenko
Associate Researcher
Affiliate Researcher, Oceanography, UH

Oleg Melnichenko
Postdoctoral Fellow

Ingo Richter
Postdoctoral Fellow

Takeaki Sampe
Postdoctoral Fellow

Richard Justin Small
Visiting Assistant Researcher

Hiroki Tokinaga
Postdoctoral Fellow

Yang Yang
Postdoctoral Fellow

Zuojun Yu
Associate Researcher
Affiliate Researcher, Oceanography, UH

Regional Ocean Influences

Kelvin Richards
Team Leader
Professor of Oceanography, UH

Hidenori Aiki
Research Scientist, FRCGC

Yan Du
Postdoctoral Fellow

Shan Gao
Postdoctoral Fellow

Tommy G. Jensen
Associate Researcher
Affiliate Researcher, Oceanography, UH

Shinichiro Kida
Postdoctoral Fellow

Mototaka Nakamura
Visiting Associate Researcher
Research Scientist, FRCGC

Andrei Natarov
Visiting Assistant Research

James T. Potemra
Assistant Researcher
Data Manager, APDRC
Affiliate Researcher, Oceanography, UH

Tangdong Qu
Associate Researcher
Affiliate Researcher, Oceanography, UH

Max Yaremchuk
Associate Researcher
Affiliate Researcher, Oceanography, UH

Asian-Australian Monsoon System

Bin Wang
Team Co-Leader
Professor of Meteorology, UH

Tim Li
Team Co-Leader
Professor of Meteorology, UH

H. Annamalai
Associate Researcher
Affiliate Researcher, Meteorology, UH

Hae-Kyung Lee Drbohlav
Postdoctoral Fellow

Joshua Xiouhua Fu
Associate Researcher
Affiliate Researcher, Meteorology, UH

Hironori Fudeyasu
Postdoctoral Fellow

Yoshiyuki Kajikawa
Postdoctoral Fellow

Kazuyoshi Kikuchi
Postdoctoral Fellow

Hyung-Jin Kim
Postdoctoral Fellow

June-Yi Lee
Postdoctoral Fellow

Ping Liu
Scientific Computer Programmer

Jiayi Peng
Postdoctoral Fellow

Kazuyoshi Soma
Postdoctoral Fellow

Yuqing Wang
Research Scientist
Associate Professor, Meteorology, UH

Bo Yang
Visiting Assistant Researcher

Xin Zhang
Visiting Assistant Researcher

Shengjun Zhang
Visiting Assistant Researcher

Impacts of Global Environmental Change

Kevin Hamilton
Team Co-Leader
Professor and Chair, Meteorology, UH

Axel Timmermann
Team Co-Leader
Associate Professor, Oceanography, UH

Axel Lauer
Postdoctoral Fellow

Oliver Timm
Postdoctoral Fellow

Asia-Pacific Data-Research Center

Peter W. Hacker
Manager
Senior Research Scientist, HIGP, UH

Sharon H. DeCarlo
Computer Systems Engineer

Yanli Jia
Visiting Associate Researcher

Konstantin Lebedev
Data Assimilation Specialist

Yingshuo Shen
Research Systems Specialist

Sachiko Yoshida
Postdoctoral Fellow

Yongsheng Zhang
Atmospheric Data Specialist

TECHNICAL SUPPORT AND SPECIALISTS

Ronald Merrill
Computer Systems Manager

David Burns
Computer Systems Engineer

ADMINISTRATIVE SUPPORT

Aimee Nakajima
Administrative Associate

Jeanie Ho
Administrative Program Assistant

Lori Wakumoto
Administrative Program Assistant

OUTREACH

Gisela E. Speidel
Outreach Specialist

Rieko Armstrong
Administrative Assistant

*April 1, 2007 – March 31, 2008

A publication of the
International Pacific Research Center
School of Ocean and Earth Science and Technology
University of Hawai‘i at Mānoa
1680 East-West Road, POST Bldg., Room 401
Honolulu, Hawai‘i 96822

Tel: (808) 956-5019 Fax: (808) 956-9425
Web: http://iprc.soest.hawaii.edu

For inquiries and address corrections, contact
Gisela Speidel at gspeidel@hawaii.edu.
Should you no longer wish to receive our mailings,
please let us know.

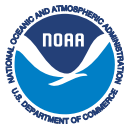

The IPRC is a climate research center funded by governmental agencies in
Japan and the United States and by the University of Hawai‘i.